LA-UR-21-29335
Approved for public release; distribution is unlimited.

Title: Changes in climate and its effect on timing of snowmelt and intensity-duration-frequency curves

Author(s): Wagner, Anna
Hiemstra, Christopher A.
Liston, Glen E.
Bennett, Katrina Eleanor
Cooley, Dan S.
Gelvin, Arthur B.

Intended for: Report

Issued: 2021-10-14 (rev.1)

ERDC/CRREL TR-21-8

US Army Corps of Engineers®
Engineer Research and Development Center

ERDC
ENGINEER RESEARCH & DEVELOPMENT CENTER

Strategic Environmental Research and Development Program (SERDP)

Changes in Climate and Its Effect on Timing of Snowmelt and Intensity-Duration-Frequency Curves

Anna M. Wagner, Christopher A. Hiemstra, Glen E. Liston,
Katrina E. Bennett, Dan S. Cooley, and Arthur B. Gelvin

July 2021

Cold Regions Research and Engineering Laboratory

The U.S. Army Engineer Research and Development Center (ERDC) solves the nation's toughest engineering and environmental challenges. ERDC develops innovative solutions in civil and military engineering, geospatial sciences, water resources, and environmental sciences for the Army, the Department of Defense, civilian agencies, and our nation's public good. Find out more at www.erdc.usace.army.mil.

To search for other technical reports published by ERDC, visit the ERDC online library at https://erdclibrary.on.worldcat.org/discovery.

Strategic Environmental Research and Development Program (SERDP)

ERDC/CRREL TR-21-8
July 2021

Changes in Climate and Its Effect on Timing of Snowmelt and Intensity-Duration-Frequency Curves

Anna M. Wagner, Christopher A. Hiemstra, and Arthur B. Gelvin

U.S. Army Engineer Research and Development Center (ERDC)
Cold Regions Research and Engineering Laboratory (CRREL)
4070 9th, Street
Fort Wainwright, AK 99703

Glen E. Liston

Colorado State University
Cooperative Institute for Research in the Atmosphere
Fort Collins, CO 80523-1375

Katrina E. Bennett

Los Alamos National Laboratory
Earth and Environmental Sciences
Computational Earth Science
MS T003
Los Alamos, NM 87545

Dan S. Cooley

Colorado State University
Department of Statistics
Fort Collins, CO 80523-1877

Final Report

Prepared for Strategic Environmental Research and Development Program (SERDP)
4800 Mark Center Drive, Suite 17D03
Alexandria, VA 22350-3605

Under SERDP Resource Conservation (RC) and Resilience Project RC-2515, "Changes in Climate and its Effect on Timing of Snowmelt and Intensity-Duration-Frequency Curves," MIPR W74RDV60835264

Abstract

Snow is a critical water resource for much of the U.S. and failure to account for changes in climate could deleteriously impact military assets. In this study, we produced historical and future snow trends through modeling at three military sites (in Washington, Colorado, and North Dakota) and the Western U.S. For selected rivers, we performed seasonal trend analysis of discharge extremes. We calculated flood frequency curves and estimated the probability of occurrence of future annual maximum daily rainfall depths. Additionally, we generated intensity-duration-frequency curves (IDF) to find rainfall intensities at several return levels. Generally, our results showed a decreasing trend in historical and future snow duration, rain-on-snow events, and snowmelt runoff. This decreasing trend in snowpack could reduce water resources. A statistically significant increase in maximum streamflow for most rivers at the Washington and North Dakota sites occurred for several months of the year. In Colorado, only a few months indicated such an increase. Future IDF curves for Colorado and North Dakota indicated a slight increase in rainfall intensity whereas the Washington site had about a twofold increase. This increase in rainfall intensity could result in major flood events, demonstrating the importance of accounting for climate changes in infrastructure planning.

Contents

Figures and Tables

Figures

Tables

Preface

This study was conducted for the Strategic Environmental Research and Development Program (SERDP) under SERDP Resource Conservation (RC) and Resilience Project RC-2515, "Changes in Climate and its Effect on Timing of Snowmelt and Intensity-Duration-Frequency Curves," MIPR W74RDV60835264. The technical monitor was Dr. Kurt Preston, SERDP.

The work was performed by the Biogeochemical Sciences Branch (Mr. Nathan Lamie, Branch Chief), the Terrestrial and Cryospheric Sciences Branch (Dr. John Weatherly, Chief), and the Engineering Resources Branch (Dr. Caitlin A. Callaghan, Chief) of the Research and Engineering Division (Dr. George Calfas, Chief), U.S. Army Engineer Research and Development Center, Cold Regions Research and Engineering Laboratory (ERDC-CRREL). At the time of publication, Dr. Douglas Howard was the Technical Director for the Cold Regions Office of the Technical Directors. The Deputy Director of ERDC-CRREL was Mr. David B. Ringelberg, and the Director was Dr. Joseph L. Corriveau.

Work was also performed by Colorado State University and Los Alamos National Laboratory. Further, the authors acknowledge Mr. Peter Nissen, Yakima Training Center; Ms. Kristen Rundquist, Grand Forks Air Force Base; and Ms. Suzanne Rohrs, Fort Carson, for their instrumental support of this project and for providing crucial local perspectives and observation advice.

COL Teresa A. Schlosser was Commander of ERDC, and Dr. David W. Pittman was the Director.

Acronyms and Abbreviations

AFB	Air Force Base
AHTUN	Ahtanum Creek at Union Gap
AME	American River near Nile
AMJ	April, May, June
AP	Airport
CanESM2 (CanRCM4)	Second-Generation Canadian Earth System Regional Climate Model
CL	Confidence Level
CORDEX	Coordinated Regional Downscaling Experiment
CRREL	Cold Regions Research and Engineering Laboratory
CTL	Current-Climate-Lateral
DoD	Department of Defense
ERDC	U.S. Army Engineer Research and Development Center
FCF	Fountain Creek near Fountain
FCP	Fountain Creek near Piñon
FCCS	Fountain Creek at Colorado Springs
FNCS	Fountain Creek near Colorado Springs
FOR	Forest River near Fordville
GCM	Global Climate Model
GEV	Generalized Extreme Values
GFAFB	Grand Forks Air Force Base
GFDL	Geophysical Fluid Dynamics Laboratory
GFDL-ESM2M (RegCM4)	GFDL's Earth System Regional Climate Model
GFDL-ESM2M (WRF)	GFDL's Earth System Weather Research Forecasting Model

HUC	Hydrologic Unit Codes
IDF	Intensity-Duration-Frequency
JAS	July, August, September
JFM	January, February, March
KT	Log Pearson Frequency Factor
LNS	Linear Nonstationary
max	Maximum
MCCS	Monument Creek at Bijou St. at Colorado Springs
MCUSAF	Monument Creek AB North Gate Blvd. at USAF Academy
min	Minimum
MIN	Forest River at Minto
mod	Modeled
MPI-ESM-LR (WRF)	Max Planck Institute for Meteorology's Earth System WRF Model
NLDAS	North American Land Data Assimilation System
obs	Observed
OND	October, November, December
PAR	Park River at Grafton
PGW	Pseudo-Global-Warming
PRRCT	Purgatoire River at Rock Crossing near Timpas
PTLA	Purgatoire River near Las Animas
PURT	Purgatoire River near Thatcher
Q	Discharge Magnitude
Qt	Exceedance Value
RC	Resource Conservation
RCP8.5	Representative Concentration Pathway 8.5

RCM	Regional Climate Model
RCSON	Resource Conservation and Climate Change Statement of Need
ROS	Rain-on-Snow
S	Stationary
SDi	Snow Depth at Cell i
SERDP	Strategic Environmental Research and Development Program
SNOTEL	Snowpack Telemetry
STD	Standardized
SWE	Snow Water Equivalent
T	Return Period
TUR	Turtle River at Turtle River state park near Arvilla
TURK	Turkey Creek above Teller Res near Stone City
UND	University of North Dakota
USAF	United States Air Force
USGS	United States Geological Survey
VIC	Variable Infiltration Capacity
WRF	Weather Research Forecasting
YR	Year
YAKUM	Yakima River at Umtanum
YAKUN	Yakima River above Ahtanum Creek at Union Gap
YTC	Yakima Training Center
μ	Population Mean
σ	Standard Deviation

Executive Summary

Introduction

Snow is a critical precipitation input for much of the U.S., and changes in the amount, timing, and departure of snow impact the hydrological cycle and can result in faster snowmelt rates that may lead to an increase in spring flooding events. For example, the major driver for severe spring flooding in the Western U.S. is snow meltwater (Berghuijs et al. 2016; Li et al. 2019). Therefore, the projected increase in rain-on-snow (ROS) events for higher-elevation snow-dominated areas could complicate flood risk assessment (Musselman et al. 2018; Jeong and Sushama 2018). Model projections show an estimated reduction of persistence of snowpacks across the western contiguous U.S. (e.g., Gleick 1987; Lettenmaier and Gan 1990; Dettinger et al. 2004; Knowles and Cayan 2004; Stewart, Cayan, and Dettinger 2004; Lemke et al. 2007; Elsner et al. 2010; Rupp et al. 2013; Leung et al. 2004; Rhoades, Ullrich, and Zarzycki 2018). Any changes to the snowpack can result in drastic hydrological changes and, as such, result in inadequate reservoir storage capacity to accommodate the shift of the hydrograph.

Objectives

Understanding the nature of the effects of a changing snowpack at appropriate temporal and spatial scales remains a formidable challenge. Our knowledge of snow on the ground is limited, especially at middle-to-lower elevations and in landscapes where snow lingers. With a heterogeneous snowpack, sparsely distributed snow gauges makes it difficult to collect sufficient information about the spatial distribution of snow, particularly in windy environments. The absence or presence of snow can be estimated by remote sensing, but estimates of water equivalent in the snowpack are too coarse or unreliable. Therefore, to estimate anticipated effects of climate change in snow-dominated watersheds, a modeling approach represents an attractive method and also the only possible solution to projecting future snow distribution realistically.

The objectives of this study were (1) to investigate the timing of and intensity of snow accumulation, snowmelt, and runoff for historical and future climate scenarios at regional and watershed scales and (2) to produce historical and future intensity-duration-frequency (IDF) curves for our study sites.

Technical Approach

Our approach centered on observed data synthesis and modeling of snow processes. We focused our snow accumulation and ablation characterization at a regional scale of the Western U.S., Joint Base Lewis McChord Yakima Training Center (YTC), Washington; Fort Carson, Colorado; and Grand Forks Air Force Base (GFAFB), North Dakota. This project relied heavily on field data collection to validate model outputs and weather information. SnowModel (Liston and Elder 2006) was our choice of model for snow simulations. To more accurately characterize snow distribution patterns and the amount of snow on ground, we carried out spatial snow depth and snow water equivalent measurements. We performed historical snow simulations, including 36 years (1 September 1979 to 1 September 2015) for the three local sites and the Western U.S. From our snow-modeling simulations, we produced spatially explicit historical and future snow depth, duration, and snowmelt events. For the hydrological modeling effort, we used the HydroFlow and variable infiltration capacity (VIC; Liang et al. 1994; Liang, Wood, and Lettenmaier 1996) models. We compared modeled and observed streamflow in selected watersheds at each study sites.

We calculated flood frequency curves using a statistical technique for understanding the nature and magnitude of high discharge in a river, for selected subbasins in the study areas. For the selected rivers, a nonstationary generalized extreme value (GEV) analysis allowed us to determine the form of the nonstationarity (if one existed) that fit the streamflow data. These models were generated for each season and averaged over the year.

We calculated rainfall intensity using the Gumbel equation and prepared rainfall IDF curves using Gumbel's method. We used a theoretical extreme value distribution to fit the observations and estimated the rainfall events for selected return periods. Lastly, we used climate models to project maximum annual precipitation and IDF curves at selected sites.

Results and Discussion

The focus of our project was to investigate the timing and intensity of snow accumulation, snowmelt, and runoff at three Department of Defense (DoD) locations experiencing snow-related transitions. We also produced flood frequency curves and estimated the probability of annual maximum daily rainfall depths in addition to current and future IDF curves for our

study sites. Our approach focused on data synthesis and snow and hydrological modeling. We used historical U.S. Geological Survey (USGS) discharge and peak flows and performed seasonal streamflow trend analysis for a select number of gages within each study site. We also calculated flood return levels for the same gages. Additionally, we estimated annual maximum daily precipitation return levels and IDF curves by using historical precipitation and climate model outputs.

In general, the Western U.S. showed a historical decreasing trend in snow duration, ROS events, and snowmelt runoff, which could have a significant effect if it continues. Similar results are found for the three local sites. There is a high spatial variability of snow duration, ROS, and snowmelt runoff trends in the local sites. The Washington and Colorado sites showed a variability of ±40 days/decade with most of the increase simulated in the lower elevations. If this trend continues, there are areas in both sites (to the north) where the snowpack could disappear in the next decade. In the North Dakota site, the majority of the site showed a decreasing trend in snow duration. During the past 36 years, the trend of ROS events was significantly higher in the Washington site (50 days) compared to 10 days in the Colorado site and only one ROS event in the North Dakota site. A decreasing trend of ROS days was seen at all three sites. The greatest 36-average snowmelt runoff was simulated for the Washington site. The snowmelt runoff in this site ranged from 5 to 400 cm with the greatest amount occurring in the western part of this site. The snowmelt runoff trend at this location was also the greatest with up to ±10 cm/decade. At lower elevations, this trend could result in no snowmelt runoff in the next decade. In the North Dakota site, even though a small trend in snowmelt runoff was simulated (±2 cm/decade), this could have a significant effect on the total snowmelt runoff for the site because the snowmelt runoff ranged between 9 and 17 cm. The future projection showed a decreasing trend in snow duration at all three sites.

We calculated maximum and minimum streamflow monthly trends for historical observations in USGS gaged streams. All sites experienced a statistically significant increase in maximum streamflow. Rivers in the Washington and North Dakota sites indicated an increase for several months of the year; and in Colorado, only a limited number of months experienced an increase. Most of the increase occurred in July–September in Fountain Creek (Colorado). At the Turkey Creek at Teller Reservoir near Stone City (Colorado), we found a decrease in maximum streamflow for all months.

During a majority of the months in Colorado, there was a statistically significant increase in minimum streamflow. Further, there was a statistically significant increase in maximum streamflow for three out of four rivers in the North Dakota site during the July–September and October–December time periods. In fact, there was also a statistically significant increase in minimum streamflow for the same three rivers that showed an increase in maximum streamflow.

For all rivers analyzed for streamflow trends, we also performed a GEV analysis of the maximum streamflow. Through this analysis, we explored if the historical streamflow was considered stationary (no change and constant through time) or nonstationary (not constant over time). At all sites (Washington, North Dakota, and Colorado), most rivers showed a stationary model. In fact, only two rivers in the Washington site, Yakima River at Umtanum and American River near Nile, resulted in a linear nonstationary model, and this was only for a shorter time period (January–March and July–September, respectively). A nonstationary model was the best fit for the annual average for some rivers in the Colorado site (Fountain Creek near Fountain and Piñon and the Purgatoire River at Rock Crossing near Tildas and near Las Animas). When looking at 3-month time periods, six of the seven studied rivers resulted in a nonlinear stationary fit and the timing of these varied. The GEV results in North Dakota varied both spatially and temporally in three out of four rivers. Turtle River at River State Park near Arvilla was the only river that did not result in a nonstationary model. The linear nonstationary models in North Dakota were mainly from July to December.

We estimated the maximum rainfall depths using Gumbel's equation and generated IDF curves for different return levels. Because of a great difference in values between lower and higher elevations, where a greater precipitation intensity is evident for higher elevations, care should be taken when using these values for infrastructure-designing purposes. We produced an envelope of projected annual maximum daily rainfall depths and IDF curves by using numerous climate models from the international Coordinated Regional Downscaling Experiment. There was a great variance between the 16 climate models we used for the probability of annual maximum daily rainfall depths. All sites projected highest confidence levels for the second-generation Canadian Earth System Regional Climate Model (CanESM2 [CanRCM4]); and the lowest confidence levels were for the Geophysical Fluid Dynamics Laboratory's Earth System Weather Research

Forecasting Model (GFDL-ESM2M [WRF]), GFDL's Earth System Regional Climate Model (GFDL-ESM2M [RegCM4]), or the Max Planck Institute for Meteorology's Earth System WRF Model (MPI-ESM-LR [WRF]).

The annual maximum daily precipitation projected in the Washington site (Yakima International Airport) is higher than historical. In fact, the highest projected annual maximum daily precipitation at this location is about two times more than historical values at a return period of 100 years. In comparison, the annual maximum precipitation in the Colorado and North Dakota sites indicated similar values for projected annual maximum daily precipitation. Do note that the range between lower- and upper-boundary confidence levels at a return period of 100 years was wide: 160 mm at Colorado and 100 mm at North Dakota. This is about a 70% and 35% increase of the upper-boundary confidence level.

There was further a great difference in both historical and future IDF curves between locations, again requiring caution when using them for designing of infrastructure. For example, at Yakima Airport, the IDF curves showed a rainfall intensity of less than 50 mm for a duration of 1 hour and a return period of 100 years. At Stampede Pass, this value was almost 220 mm. In the Colorado site, there was also a wide difference in IDF curves. The rainfall intensity for the 1-hour duration, 100-year return period at Colorado Springs Municipal Airport was almost double that at Rocky Ford 2 SE. Similarly, at the North Dakota site, the IDF curves ranged for the different locations.

The future IDF curves varied, where the greatest difference was found at YTC, Washington, with a twofold increase at a 1-hour duration for the 100-year return period when compared to the current climate. The future IDF curves at Fort Carson and GFAFB are similar to current climate when comparing to the trend line. Even though the projected trend line indicated similar rainfall intensity as current climate, it should be recognized that the range of rainfall intensity values for this return period varied greatly between models. At Fort Carson, there was about a 2.5 times difference between the model that produced the lowest and highest rainfall intensity. The difference between the models at GFAFB was close to 1.5 times.

Implications for Future Research

Estimating snow distribution and snowmelt runoff over different landscapes remains a formidable challenge. Increasingly, models are used to

identify precipitation patterns; but validation of models through field measurements is labor intensive, and there is a great need to develop more-streamlined methods. To explore this, we investigated several other methods that could be developed further to help with this research gap. We found that remote-sensing imagery, snow-pattern identifications, and photogrammetry analysis have great potential to improve modeling outputs. We therefore recommend that future efforts explore these methods to help close this research gap and to make the process more efficient.

The natural and human-caused fires at YTC is shifting areas of the landscape that is dominated by sagebrush steppe toward annual and perennial grasslands. Deep winter snowpacks are required to recharge local aquifers, replenish soil moisture, and to reestablish native plant communities (including sagebrush) following fires. We recommended further research exploring impacts of snow on sagebrush (*Artemisia tridentata*) and greater sage-grouse (*Centrocercus urophasianus*) and their interactions. Moreover, we identified a need to better understand fire, snow, and loss of sagebrush to help protect the greater sage-grouse on the military range.

This study advances the understanding of a spatial snow and runoff climatology of past and future projections at a regional scale and at selected military installations. Not only are the presented streamflow analysis and precipitation-intensity estimates for our study sites important for infrastructure planning and risk assessments, but our methods are also transferable to a myriad of locations where snowmelt and its subsequent runoff present infrastructure challenges. Additionally, this work provides a new understanding of IDF curves in a changing climate. Overall, the work presented helps DoD define impacts from a changing climate, providing the information necessary to develop mitigation or adaptation strategies and lowering operational costs.

1 Introduction

1.1 Background

Snow is a major component of the hydrological cycle, and any change in timing and duration could lead to a negative outcome for locations that depend on snow for water resources. Long-term analyses of snow accumulation and ablation suggest that substantial shifts in snow amount, characteristics, timing, and duration have been occurring in the Northern Hemisphere (Edwards, Scalenghe, and Freppaz 2007; Stewart 2009; Liston and Hiemstra 2011b; Derksen and Brown 2012; Hall et al. 2015). Some areas have declining snowpacks, while others have increasing snow depths (Räisänen 2008; Liston and Hiemstra 2011a). Most areas have shorter snow duration (Brown and Robinson 2011; Derksen and Brown 2012), yet indications are that a warmer atmosphere laden with water can lead to deeper snowpack quantities or large snowfall events in regions where temperatures remain low enough for precipitation to fall as snow (Groisman et al. 2005; Räisänen 2008). Mote et al. (2005) reported widespread decline in springtime snow water equivalent (SWE) in much of the North American West from 1925 to 2000. An updated study by Mote et al. (2018) found a continuing declining trend across all months, states, and climates, with a decline at 90% of the snow monitoring sites. Since 1915, they estimate that there has been a 21% decrease in the Western U.S. snowpack. Knowles (2015) reported a decline in total snow duration for the Western U.S. and an increase for the Great Plains and southern Rockies for 1950–2010.

Snow will melt at an earlier date in a warmer climate, and this is occurring at many locations (Cayan et al. 2001; Stewart, Cayan, and Dettinger 2004; Mote et al. 2005; Gergel et al. 2017). Since the 1970s, the onset of snowmelt in parts of the Western U.S. has been occurring 6 to 26 days earlier (Hall et al. 2015). It has been projected that climate change will continue to reduce the volume and persistence of snowpacks across the western contiguous U.S. (e.g., Gleick 1987; Lettenmaier and Gan 1990; Dettinger et al. 2004; Knowles and Cayan 2004; Stewart, Cayan, and Dettinger 2004; Lemke et al. 2007; Elsner et al. 2010; Rupp et al. 2013; Leung et al. 2004; Rhoades, Ullrich, and Zarzycki 2018). Lute, Abatzoglou, and Hegewisch (2015) predicted a decline in snowfall days and snowfall water equivalent will occur in the Western U.S. by the mid-twenty-first century. In snowmelt-dominated rivers, there has been a shift in spring runoff of up to 3

weeks earlier over the past 50 years (Stewart, Cayan, and Dettinger 2005). In a warming climate, maximum spring streamflow in the Western U.S. has been predicted to peak approximately 1 month earlier in the year (e.g., Barnett, Adam, and Lettenmaier 2005).

As described, mounting evidence indicates that changes in snowpack have noticeable hydrological impacts in the Northern Hemisphere (Mote et al. 2005; Yang et al. 2007; Stewart 2009; Clow 2010; Pederson et al. 2011; Derksen and Brown 2012; Gan et al. 2013; Li et al. 2017). Snow is heterogeneously distributed, and current methods of calculating snow are too coarse or unreliable to meaningfully assist decision-makers. However, snow is a critical precipitation input for much of the U.S.; and changes in its amount, timing, and departure impact water and energy budgets as well as ecosystems (Barnett, Adam, and Lettenmaier 2005).

Across the Western U.S., snow meltwater is the major driver for severe spring flooding (Berghuijs et al. 2016; Li et al. 2019). Moreover, rain-on-snow (ROS) events during winter can cause peak flow events during what is normally considered a low-flow period (Berghuijs et al. 2016; Villarini 2016). This fact complicates flood risk assessments and requires further research (Musselman et al. 2018; Jeong and Sushama 2018). Importantly, failure to account for these changes in snow could result in deleterious military mission and asset impacts.

Understanding the nature of these impacts at appropriate temporal and spatial scales remains a formidable challenge. Satellite remote sensing does well in determining if snow is absent or present, but estimates of water equivalent in the snowpack are too coarse (e.g., microwave remote sensing with 25 km* horizontal resolution) or unreliable. Specifically in mountainous regions, obtaining reliable SWE estimates is extremely challenging (Bormann et al. 2018). Gauge networks can tell us about precipitation falling out of the sky (Rasmussen et al. 2012), but sufficient information about the actual distribution of snow on the ground is lacking, especially in windy environments. Snowpack Telemetry (SNOTEL) networks can estimate snow on the ground, but they are sparsely distributed and constrained to higher-elevation mountain watersheds. At middle-to-lower

* For a full list of the spelled-out forms of the units of measure used in this document, please refer to U.S. Government Publishing Office Style Manual, 31st ed. (Washington, DC: U.S Government Publishing Office, 2016), 248–252, https://www.govinfo.gov/content/pkg/GPO-STYLEMANUAL-2016/pdf/GPO-STYLEMANUAL-2016.pdf.

elevations and in landscapes where snow lingers, snow is generally not monitored (e.g., the Great Plains), making it difficult to estimate the snowpack. Moreover, there is no way to reasonably extrapolate snow gauge and snow remote-sensing observations into the future. Therefore, a snow-modeling approach, if trained by coincident observations, represents an attractive way forward in estimating anticipated climate change impacts in snow-dominated watersheds.

1.2 Objectives

The objectives of this study were (1) to investigate the timing and intensity of snow accumulation, snowmelt, and runoff for historical and future climate scenarios at regional and watershed scales and (2) to produce historical and future intensity-duration-frequency (IDF) curves for our study sites: Western U.S., the Joint Base Lewis McChord Yakima Training Center (YTC), Washington; Fort Carson, Colorado; and Grand Forks Air Force Base (GFAFB), North Dakota (Figure 1-1). At the Western U.S. site, the Federal Government manages vast tracts of land, ranging from National Parks to military installations and flood control projects (Figure 1-1 show only Department of Defense [DoD], Department of Energy, and Bureau of Reclamation projects). Our study locations (YTC, Fort Carson, and GFAFB) include different climates, vegetation, and snow environments as defined by Sturm, Holmgren, and Liston (1995). Additionally, YTC also experience extreme snowmelt events most often initiated by rain on frozen ground (Wigmosta et al. 2009). Fort Carson and the high plains have experienced a dramatic decline in spring snow cover over the last 50 years (Brown and Robinson 2011), and it is on the southern edge of the 50% snowmelt runoff estimate. The Grand Forks area experiences chronic flooding tied to snowmelt, with notable recent flooding events occurring in 1997, 2009, and 2013.

We had two main research questions addressed during this study: (1) How are snow accumulation and snowmelt changing? (2) How are these changes manifesting at local scales where they may impact landscapes and infrastructure? Snow accumulation and ablation characteristics are changing in most watersheds, and failure to account for these changes could result in expensive military mission and asset impacts.

Figure 1-1. The Western U.S. study area (*green*) spans many western states and includes areas where snow is the primary source of runoff. Three local-scale study areas (*yellow*) are centered on military installations located in three different snow environments.

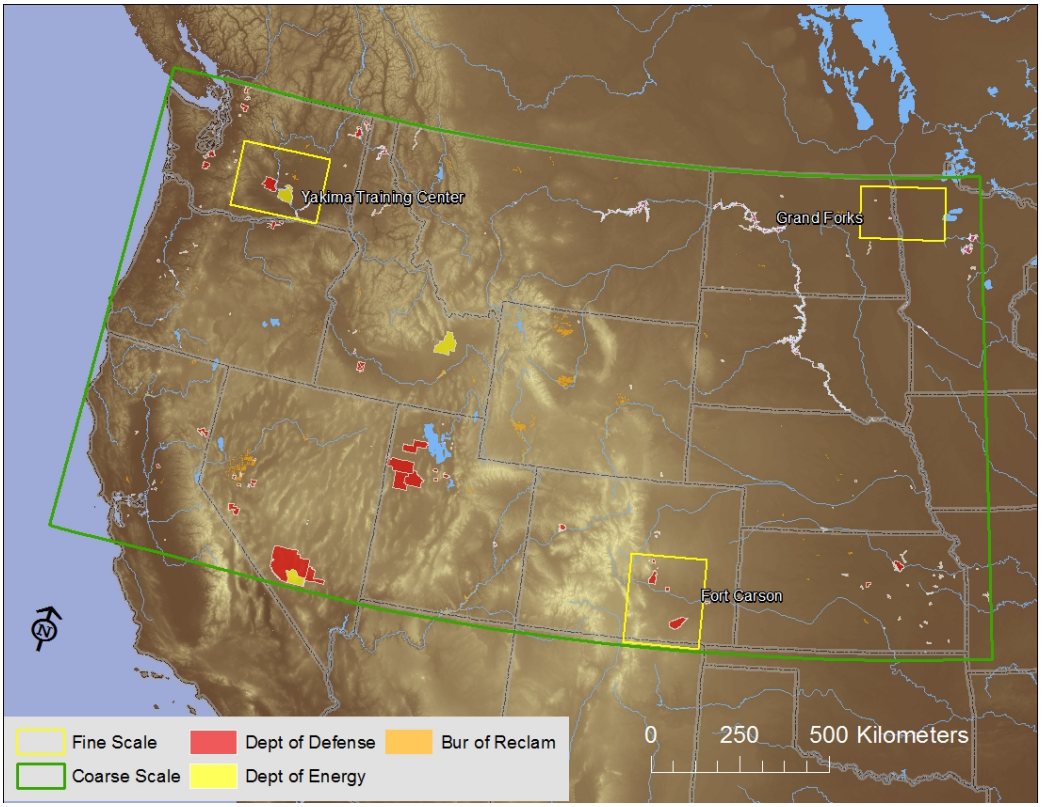

The technical objectives of this study addressed the Strategic Environmental Research and Development Program (SERDP) Resource Conservation (RC) and Climate Change Program area statement of need (SON) (SERDP 2013). Specifically, we are advancing the Department of Defense's ability to manage and adapt to winter and spring runoff events: "developing improved understanding of and responses to changes in the timing and intensity of snowmelt and subsequent run-off events" (SERDP 2013).

The expected benefits of the proposed system also address RCSON 15-02 goals, including generating next-generation IDF curves and changes in snowmelt-driven runoff events associated with specific regions and applications that address future DoD management challenges. In alignment with the background section of RCSON-15-02, this project focuses on how precipitation (rain and snow) may change with time and location in regions of interest to DoD and other Federal and State Agencies (Figure 1-1).

1.3 Approach

This project was performed by the Cold Regions Research and Engineering Laboratory (CRREL), Colorado State University, and Los Alamos National Laboratory; and our approach centered on observed data synthesis and modeling of snow processes. Using distributed, physically based models was an ideal approach to assess snow changes in recent decades and is the only method that yields snow and snowmelt projections for coming decades. This project included snow and hydrological modeling in our areas of interest (Figure 1-1). We produced spatial historical and future snow depth, duration, and snowmelt event trends by performing snow accumulation and ablation simulations for the Western U.S., Washington, Colorado, and North Dakota sites. The North Dakota site also included parts of Minnesota, but we will call this site North Dakota hereafter. We also performed hydrological modeling in the three sites to produce discharge from rivers within the local sites. Additionally, we integrated our snow-model results into the runoff model and performed snow-model verification using observations. We calculated flood frequency curves for river flow at our sites. Changes in hydrological extremes were explored by using trend analysis of flows (minimum and maximum). We also analyzed streamflow using nonstationary generalized extreme value (GEV) theory. Using the Gumbel's method, we calculated maximum rainfall depths for numerous meteorological stations at each site. IDF curves were produced using a theoretical extreme value distribution that was used to fit the rainfall event observations and the theoretical distribution associated with the given exceedance probabilities. Finally, we also made future projections of snow duration, probability occurrence of maximum annual precipitation return levels, and IDF curves.

2 Methods

2.1 Field measurements

Field measurements were needed to validate snow-model outputs (section 2.3). We relied on spatial sampling of different landscapes to more accurately characterize snow distribution patterns and the amount of snow on the ground (as opposed to gauge measurements). Snow observations were a primary focus of our field efforts and largely supported fine-scale snow modeling and informed validation efforts. Observations spanned three consecutive winters (2015–2016, 2016–2017, and 2017–2018) and employed two different approaches. First, a snow-depth time-series approach used time-lapse cameras and incremented stakes to record daily snow depths in a variety of sites at each installation. In addition, a midwinter spatially distributed snow measurement campaign occurred where a number of depths and snow-density profiles were observed over several days.

Three Wingscapes TimelapseCam Pro snow cameras (Dickerson-Lange et al. 2015) were installed at each location (YTC, Washington; GFAFB, North Dakota; and Fort Carson, Colorado) in fall 2015 to collect three daily (11 a.m., 12 p.m., and 1 p.m. local time) field-site photos. The resolution of these battery-operated cameras was 10 megapixels. The cameras pointed toward incremented snow stakes indicating heights above the ground surface in 5 cm marked intervals (Figure 2-1). From these pictures, we noted daily snow depths. At YTC, Washington, we installed a meteorological station with a snow-depth sounder to augment the cameras and to ensure reliable weather data as there were no other nearby stations at similar elevations.

To accurately measure snow and the amount of water present, sampling for snow depth and density must occur (Judson and Doesken 2000). Because snow depths vary more over landscapes than snow density does (Sturm et al. 2010), we weighted our sampling approach to favor extensive snow-depth measurements and a limited density sample. We completed snow-depth and snow-density measurements at multiple sites within each local area during the 2015–2018 snow seasons, working to capture snow variability between landscapes and peak snow accumulation. We used a Magnaprobe to take snow-depth measurements along transects located within different terrain types (Sturm 2009; Sturm and Holmgren 2018).

Figure 2-1. Time-lapse camera and 5 cm incremented snow stakes for measuring snow depths.

The transects included different snow types, topography, and vegetation. SWE measurements were performed in selected snow pits (Figure 2-2) by using density cutters that sampled a volume of snow (250 and 1,000 cm^3) every 10 cm along a vertical snow profile. Samples were weighed to calculate column water content. Temperature data were also collected in the snow pits every 10 cm to assess the thermal state of the snow.

Figure 2-2. Snow-depth and snow-density field measurements.

2.2 Field installations

2.2.1 YTC, Washington

We installed a meteorological station (CRREL station) on a ridge in the Saddle Mountains (1,143 m elev.) at YTC (easting = 0714397; northing = 05193693) on 3 December 2015 (Figure 2-3). Measurements collected include air temperature (at 1.8 m), relative humidity (at 1.8 m), wind speed and direction (at 3 m), and snow depth (sounder mounted at 1.5 m, measuring down to the surface). Minute-level data were stored in 15-minute averages in a data logger (Campbell Scientific CR1000). The tower was powered with two 12 V batteries and a solar panel; data were stored at the tower until they could be downloaded.

At the general location of the meteorological station, three time-lapse cameras were also installed. One camera was on the tower (Tower) of the meteorological station, observing stakes on the windswept ridge (Figure 2-3*a*); a second camera was installed on the north slope (North) of the ridge (Figure 2-3*b*) immediately downhill, observing a large drift that lasted well into spring; and the third camera (Valley overview) gave an overview of the valley north of the meteorological tower.

Figure 2-3. (*a*) Meteorological station (CRREL station) and time-lapse camera (Tower) and (*b*) time-lapse camera north (North) of the meteorological station at YTC, Washington.

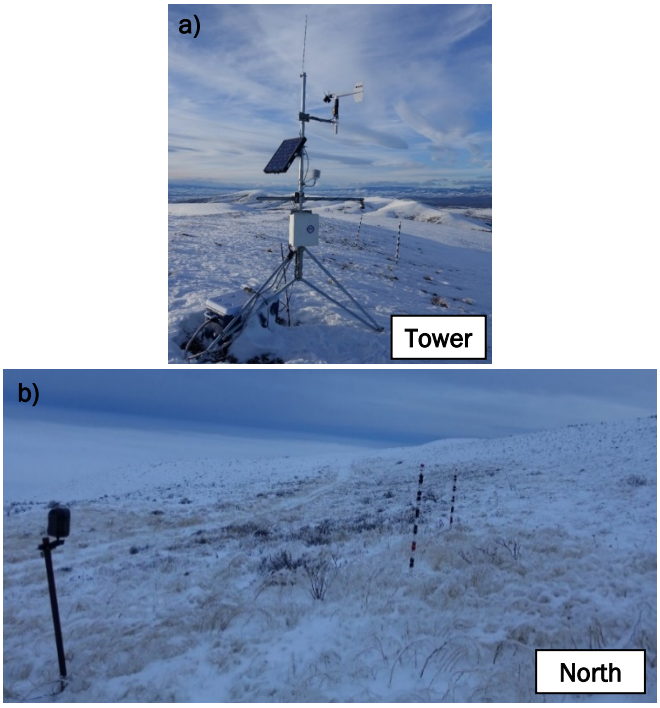

2.2.2 Fort Carson, Colorado

At Fort Carson, Colorado, we installed three cameras (Figure 2-4) on training ranges with relatively easy access. This included a site that had grassland and sparsely forested area (Gate 12). At Turkey Creek, two upland cameras were installed. One camera (Turkey Creek North) observed a ridgetop grassland, and the other (Turkey Creek South) observed grassland adjacent to a pinyon pine (*Pinus edulis*) forest.

Figure 2-4. Time-lapse cameras at Fort Carson, Colorado.

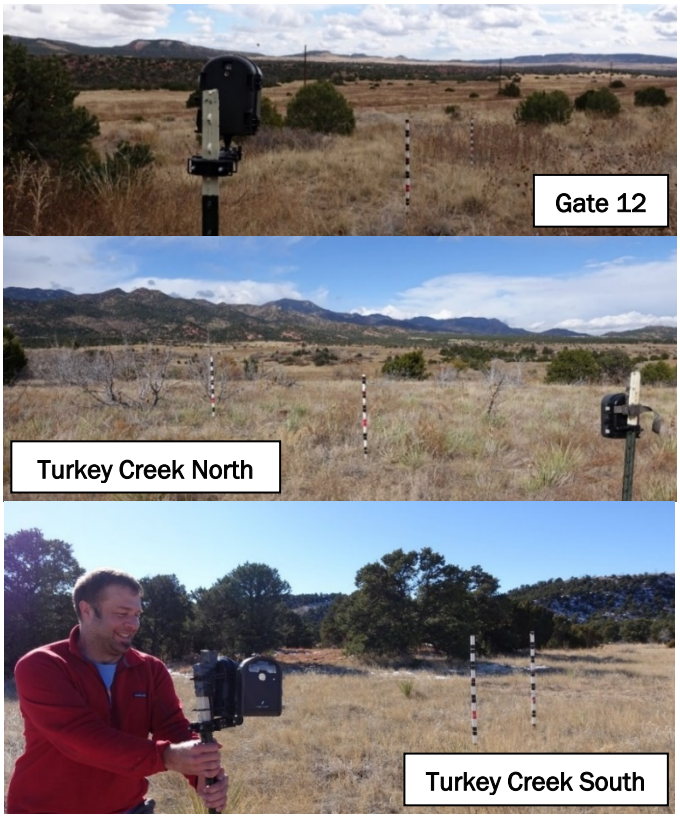

2.2.3 GFAFB, North Dakota

At GFAFB in North Dakota, we installed two cameras within the installation boundary (Figure 2-5). This included a site at a capped landfill (GFAFB Landfill) and a restored prairie site (GFAFB Prairie). The largest influence on snow from the landfill is mowing; the short vegetation stature in a windy environment tends to lose snow, and the area is among the shallowest snowpacks we measured. Because the installation land cover does not represent the larger site and GFAFB is relatively small, we also utilized nearby research lands owned by the University of North Dakota

(UND). The Mekinok site (UND Mekinok), located west of GFAFB, is dominated by tilled agricultural lands that represent the majority of the site's land cover type. For our manual snow-depth collection, we also included Oakville Prairie field station that is operated by UND. The Oakville Prairie site, located southeast of GFAFB, is preserved prairie that has never been tilled and is representative of a grassland environment.

Figure 2-5. Time-lapse cameras at GFAFB, North Dakota.

2.3 Snow-modeling simulations

For our snow-modeling effort, we used a spatially distributed model (SnowModel; Liston and Elder 2006; appendices listed in Liston et al. 2020). This model requires meteorological measurements in addition to topography and vegetation. For the local sites and the Western U.S., a historical time period of 1 September 1979 to 1 September 2015 for the SnowModel simulations was used. Topography data required for snow-model simulations were obtained from the National Elevation Database (accessed at https://www.usgs.gov/core-science-systems/national-geospatial-program/national-map). We obtained land cover data for the snow-model simulations from the National Land Cover Dataset (Homer et al. 2007) and converted to SnowModel classes for the simulations.

Meteorological data from the National Aeronautics and Space Administration's North American Land Data Assimilation System (NLDAS; accessed at https://disc.gsfc.nasa.gov/datasets?keywords=NLDAS) was used to drive the SnowModel simulations. We used a variety of atmospheric and precipitation measurements and surface meteorology reanalyses. NLDAS was available on a 1/8-degree grid, and retrospective NLDAS datasets extend back to January 1979. We aggregated 1 hr NLDAS atmospheric forcing data to 3-hourly data for the SnowModel simulations.

The local-scale simulations used a grid cell of 300 m, and the Western U.S. simulations used 1,000 m grid cells. Snow duration, ROS events, SWE, and snowmelt-runoff graphs were produced from these simulations. To validate the larger-scale snow model (300 m), a finer-scale snow model (30 m) was simulated for the Washington and North Dakota sites. The time step used in the simulations was 1 hr. Because of the limited snowpack in 2017–2018, only 2 years were simulated for the Washington site (2015–2016 and 2016–2017). At North Dakota, we simulated 3 years (2015–2016, 2016–2017, and 2017–2018). Because of the lack of snow at the installation level at Fort Carson, Colorado, we did not perform fine-scale simulations. These snow models were used in conjunction with the field measurements to validate the snow model at these sites. Snow-modeling verification occurred through field measurements where we resampled observations to snow-model-resolution scales (30 m), then reserved approximately 15% of our field measurements to form a verification dataset. The reserved snow measurements were compared directly against snow-modeling analyses to assess whether our snow-modeling approach was realistic and satisfactory for modeled processes.

The size of the Western U.S. site simulation encompassed all three local sites. The total area of this site was 3,459,356 km² (Figure 1-1). Figure 2-6 shows the topography and SnowModel land cover classes for this site.

Figure 2-6. (*a*) Topography where color indicates elevation in meters and (*b*) SnowModel land cover classes for the Western U.S. site.

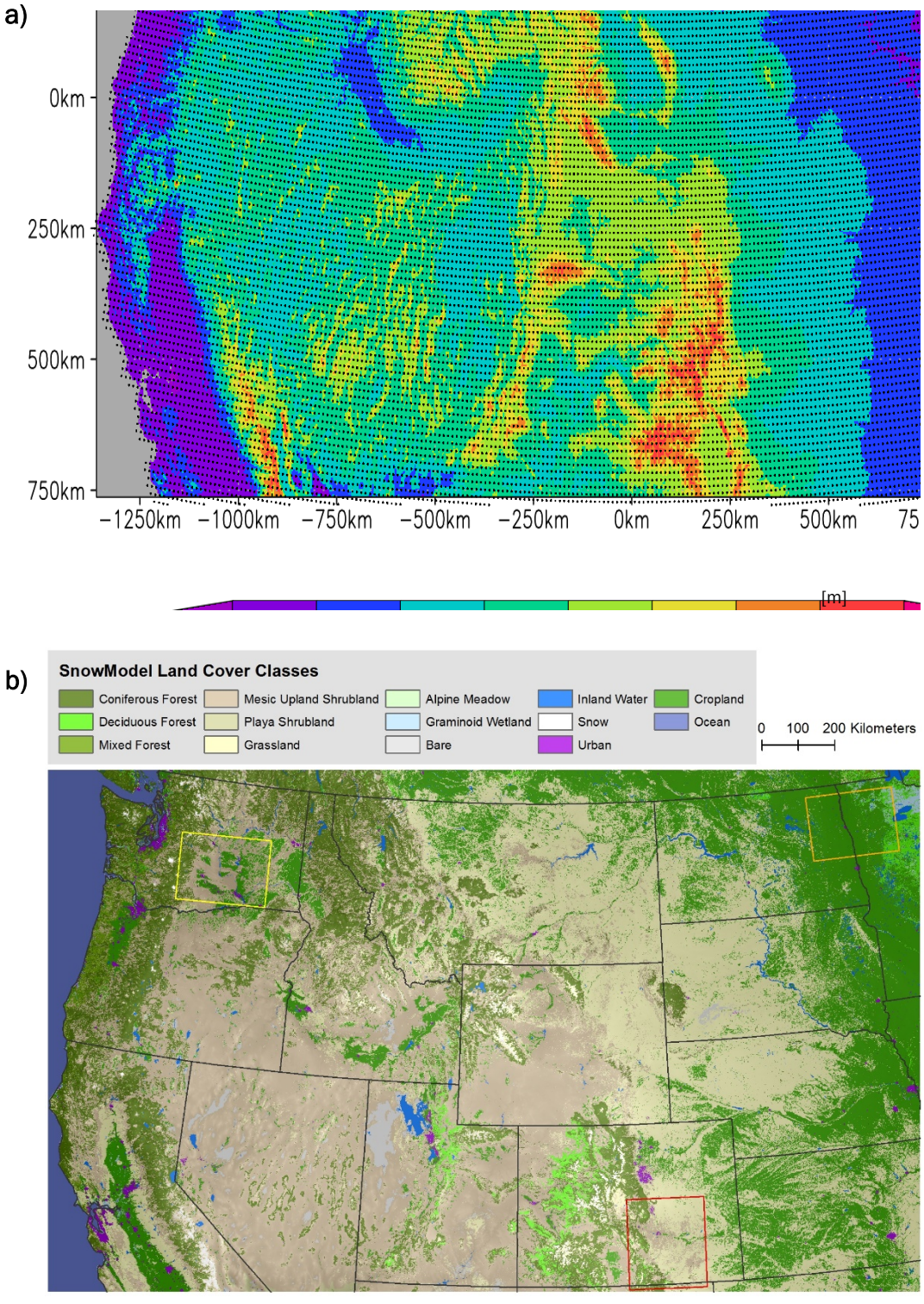

The SnowModel site that encompassed the YTC, Washington, training area was about 50,600 km², which, with a grid cell of 300 m, resulted in 561,750 grid cells (n_x = 875, and n_y = 642). The elevation of this site ranged from sea level to 3,000 m (Figure 2-7*a*). Coniferous forest (higher elevations), upland shrubs, and croplands (Figure 2-7*b*) dominated this area.

Figure 2-7. (*a*) Topography and (*b*) SnowModel land cover classes for the Washington site. The *black solid line* in (*a*) outlines the watershed boundary for the hydrological modeling and in (*b*) the fine-resolution snow-modeling boundary. The *closed triangle* indicates the U.S. Geological Survey (USGS) outlet (12500450). The location of the CRREL meteorological station is illustrated with the *black dot*.

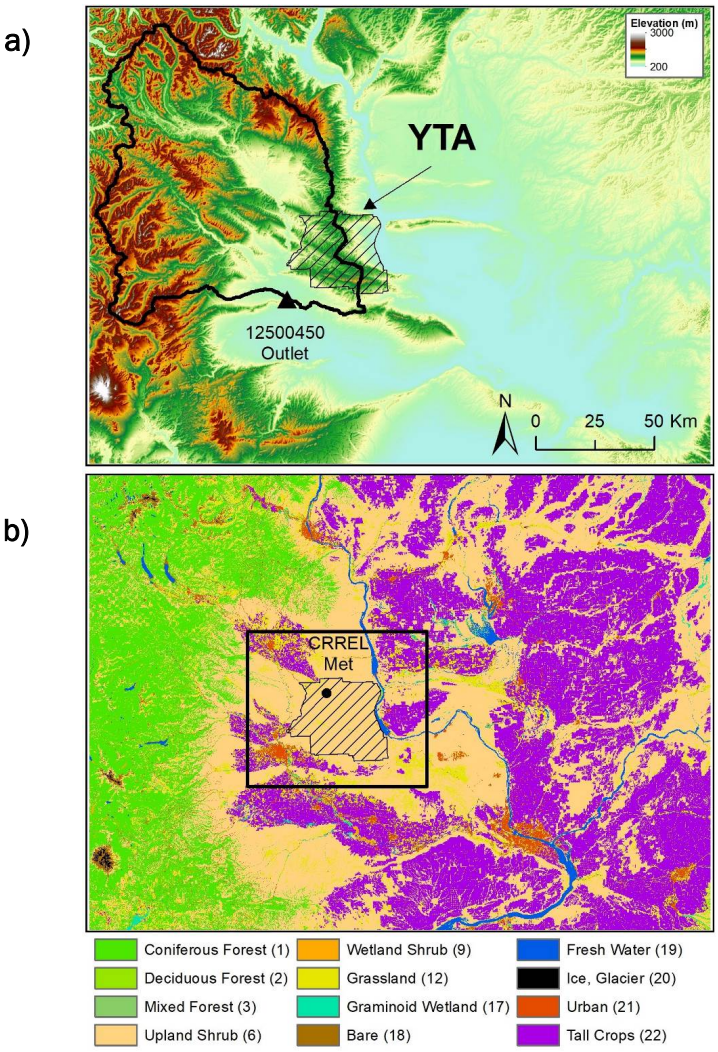

The snow-model area that encompassed Fort Carson, Colorado, was 53,200 km². With a grid cell of 300 m, this resulted in 591,552 grid cells for this site (n_x = 711, and n_y = 832). The elevation of this site spanned

from 1,200 to 4,300 m at Pikes Peak (Figure 2-8*a*). Grassland with some tall crops and upland shrublands at lower elevations (Figure 2-8*b*) dominated this area. Higher elevations consisted largely of coniferous forest upland shrubs and tall crops.

Figure 2-8. (*a*) Topography and (*b*) SnowModel land cover classes for the Colorado site. The *black solid line* outlines the watershed boundary used for the HydroFlow modeling, and the *blacked dashed line* outlines the Variable Infiltration Capacity (VIC) watershed boundary. *Closed triangles* indicate the USGS outlets.

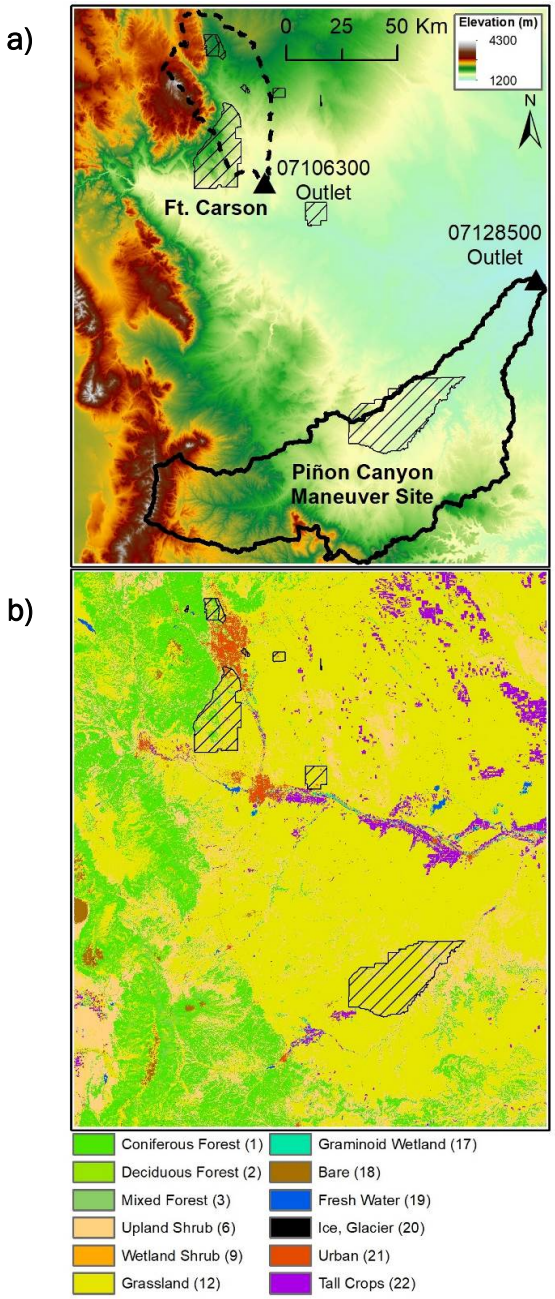

The North Dakota site that encompassed the GFAFB was the smallest, with an area of 43,500 km² (483,003 grid cells, n_x = 801, and n_y = 603). Out of the three snow-modeling sites, it also had the lowest topographic relief, with elevations of 250–550 m (Figure 2-9*a*). Mainly croplands dominated this site; but deciduous forest, wetland shrub, and some grasslands were also present (Figure 2-9*b*).

Figure 2-9. (*a*) Topography and (*b*) SnowModel land cover classes for the North Dakota site. The *black solid line* in (*a*) outlines the watershed boundary for the hydrological modeling and in (*b*) the fine-resolution snow-modeling boundary. The *closed triangle* indicates the USGS outlet of the modeled watershed.

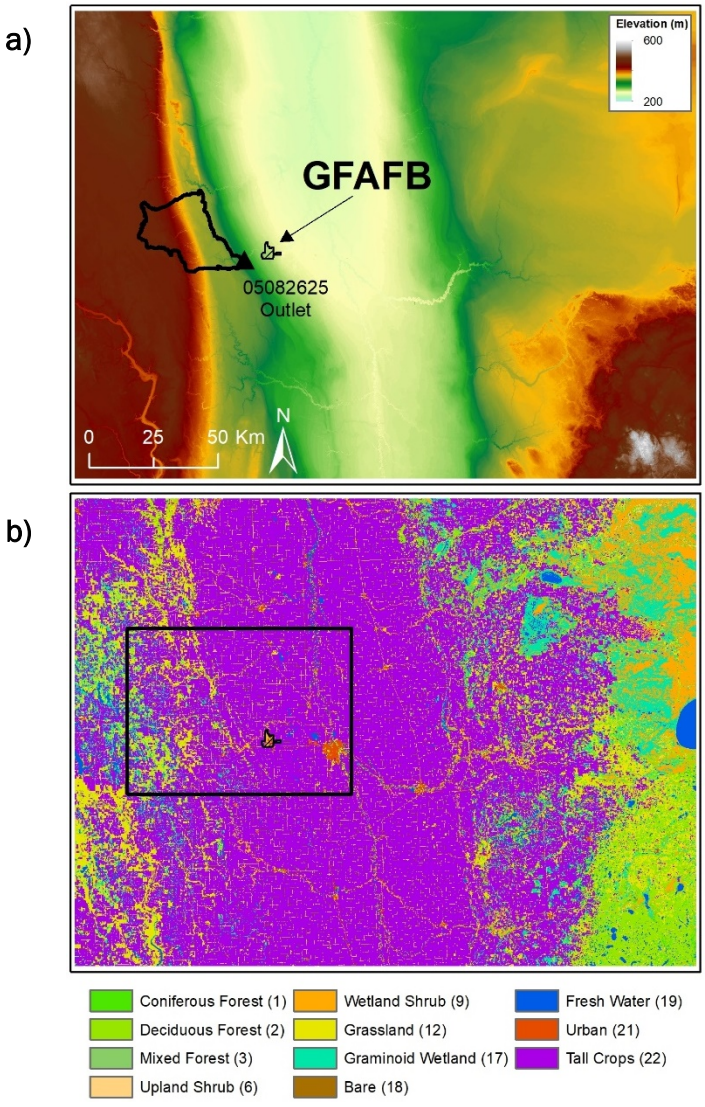

2.3.1 Snow-model validation using SNOTEL and metorological data

We compared the measured SWE at SNOTEL stations, snow depth (converted to SWE) at meteorological stations, and model SWE outputs (SnowModel and VIC) for snow-model validation. We identified fourteen SNOTEL stations within the Washington site (Figure 2-10 and also Table A-1 in Appendix A.1). Data for the Washington site was retrieved from the Natural Resources Conservation Service database. In the Colorado and North Dakota sites, one and zero SNOTEL stations existed, respectively. Therefore, snow-depth measurements at meteorological stations were used for snow-model validation. Snow depths were converted to SWE by using a mean assumed snow density of 300 kg/m^3. For the Colorado site, these measurements were downloaded from the Midwestern Regional Climate Center. Seventeen meteorological stations (including one SNOTEL station) were used for snow-model validation in the Colorado site (see Figure 2-11 and also Table A-2 in Appendix A.1). No SNOTEL stations were available in the North Dakota site, which resulted in 11 meteorological stations used for the SWE validation (see Figure 2-12 and also Table A-3 in Appendix A.1). Only one station reported SWE (GFAFB), and SWE was converted from snow depth (see description earlier in this paragraph) at the other meteorological stations.

Figure 2-10. Washington Hydrologic Unit Code (HUC) 8 watersheds and their gages were assessed for flood frequency and streamflow trends. SNOTEL stations and meteorological stations were used for SWE validation in the Washington site. Annual maximum daily precipitation depths were calculated for the meteorological stations. Appendix A.1 lists the station details. The different colors represent watershed for the USGS stations. Some subbasins are overlapped; and therefore, the entire basin may not be shown.

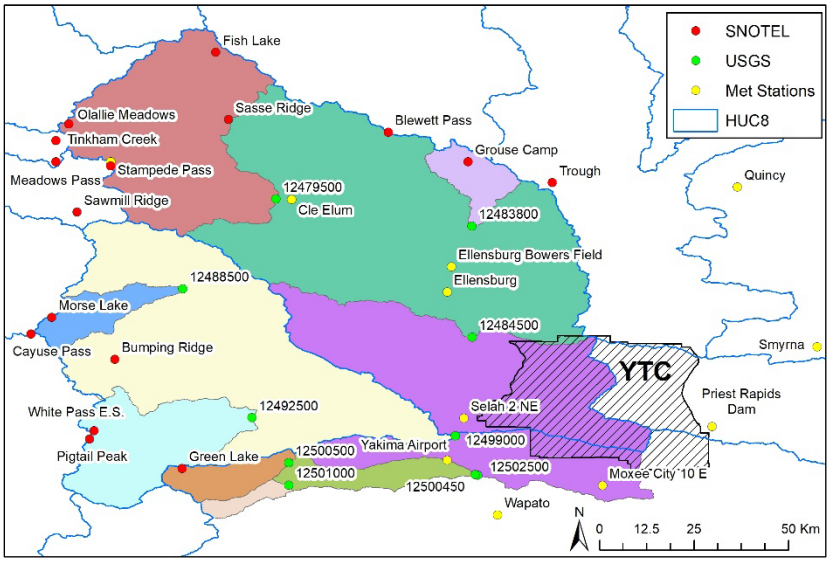

Figure 2-11. Colorado HUC 8 watersheds and their gages were assessed for flood frequency and streamflow trends. SNOTEL station and meteorological stations were used for SWE validation in the Colorado site. Annual maximum daily precipitation depths were calculated for the meteorological stations. Appendix A.1 lists the station details. The different colors represent watershed for the USGS stations. Some subbasins are overlapped; and therefore, the entire basin may not be shown.

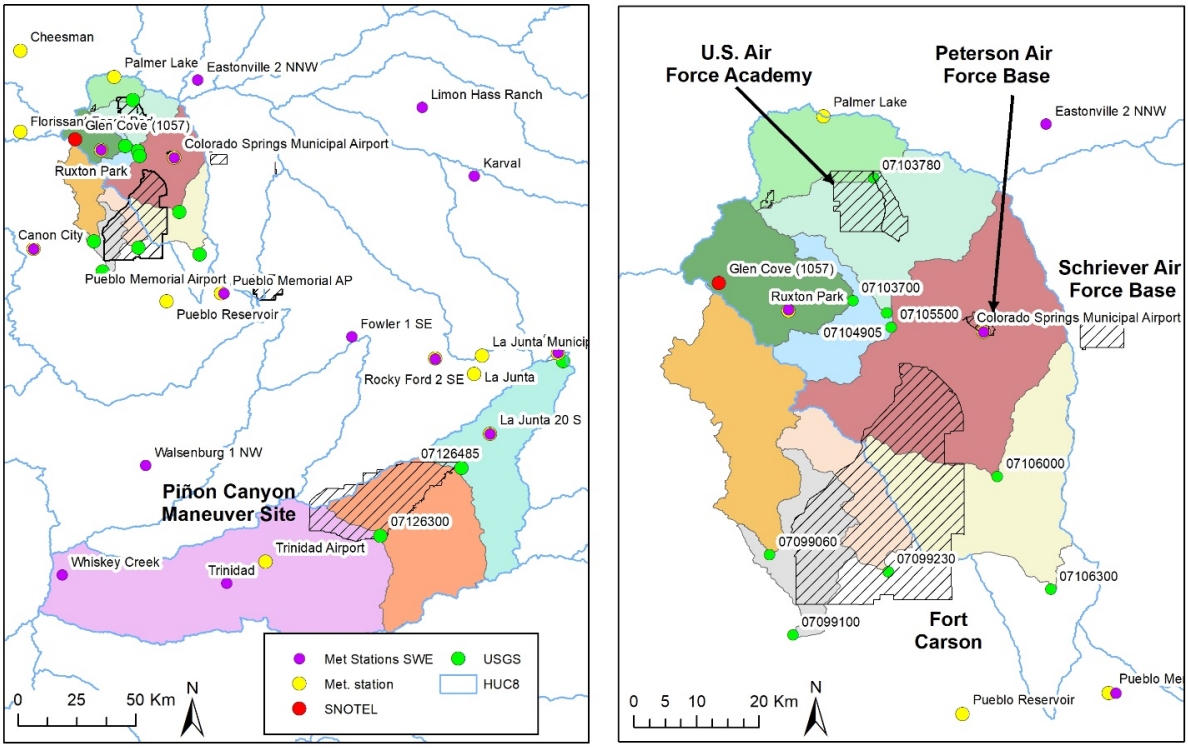

Figure 2-12. North Dakota HUC 8 watersheds and their gages were assessed for flood frequency and streamflow trends. Meteorological stations were used for SWE validation in the North Dakota site. Annual maximum daily precipitation depths were calculated for the meteorological stations. Appendix A.1 lists the station details. The different colors represent watershed for the USGS stations. Some subbasins are overlapped; and therefore, the entire basin may not be shown.

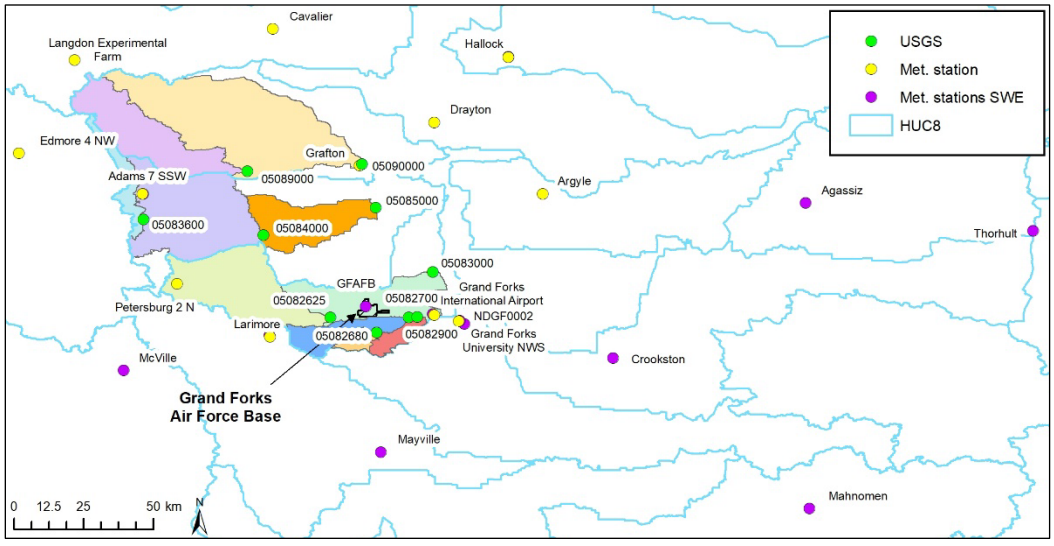

2.3.2 Future snow projections

For the future snow-model simulations, we forced our simulations with a high-resolution (4 km grid spacing) climate change dataset produced and available online by Rasmussen and Liu (2017). They used the Weather Research and Forecasting (WRF) model that permitted convection and resolved mesoscale orography, and they generated two 13-year simulation datasets: a historical control run (current-climate lateral [CTL]), and a pseudo-global-warming simulation (PGW). Several studies have evaluated precipitation output from the CTL model against observations (e.g., Dai et al. 2017; Liu et al. 2017; Prein, Liu, et al. 2017; Prein, Rasmussen, et al. 2017; Raghavendra et al. 2019). We produced one CTL (current) and one PGW (future) snow-model simulation. From these simulations, snow-duration maps of the three local sites were produced and subtracted to quantify the difference between the current and future climate.

2.4 Hydrological simulations

We used two models for the hydrological modeling effort. HydroFlow (Liston and Mernild 2012), a module of SnowModel (Liston and Elder 2006), is a gridded runoff routing model that uses the SWE and runoff output from SnowModel to calculate discharge. The second model, VIC, is a macroscale hydrologic model often used to simulate climate change impacts on coarse-scale basins (Liang et al. 1994; Liang, Wood, and Lettenmaier 1996). Our study forced this hydrologic model using the Livneh et al. (2013) soil and meteorological data from 1950 to 2010.

We compared modeled and observed daily streamflow on individual subbasins selected based on available flow data. Three HUC 8 watersheds (Upper Yakima, Naches, and parts of Lower Yakima) encompassed the simulated watershed in the Washington site (Figure 2-7). The total area was 9,465 km^2, and the simulated discharge for this site was compared to the USGS gage (12500450) at Yakima River above Ahtanum Creek at Union Gap (see Table A-4 in Appendix A.1).

The HUC 8 watershed (Purgatoire) that encompasses the Purgatoire River in the Colorado site was the largest watershed, with an area of 8,948 km^2 (Figure 2-8). This also includes most of the Piñon Canyon Maneuver Site. The simulated discharge using HydroFlow for this site was compared to the Purgatoire River near Las Animas (PTLA) USGS gage (07128500). The

VIC model was used to simulate the Fountain Creek discharge near Piñon (07106300), which was in the Fountain HUC 8 watershed.

The HUC 8 Turtle watershed was located in the North Dakota site, and the area of the modeled watershed was 672 km² (Figure 2-9). The simulated discharge for this site was compared to the Turtle River USGS station at the Turtle River at Turtle River State Park near Arvilla (05082625).

2.5 Flood and seasonal flow and trend analysis

We calculated flood frequency curves and streamflow trends using USGS maximum annual peak flows and discharge values. Flood frequency is a statistical technique to quantify the nature and magnitude of river discharge (Q). Statistical flood frequency curves were first introduced by Gumbel (1941) and are commonly referred to as extreme value distributions or Gumbel's equation. Design-flow values corresponding to specific return periods (T) can be used for hydrologic planning and design purposes. A return period is the inverse of the probability that an event will be exceeded in a given year (e.g., it provides an estimate of the likelihood of any event occurring in a year). For example, the 100-year return period flow value has a 1% chance that it will be exceeded in one year. This statistical tool is used to create flood frequency estimates that quantify intensities of flood events. The Gumbel's equation for annual extremes can be expressed as

$$Q_t = \mu + K_T \sigma, \tag{1}$$

where

Q_t = the exceedance value;
μ = mean;
σ = standard deviation;
T = return period in years; and
K_T = the Log Pearson frequency factor, which is

$$K_T = \frac{\sqrt{6}}{\pi}\left[0.5772 + ln\left[ln\left(\frac{T}{T-1}\right)\right]\right]. \tag{2}$$

Our flood discharge frequency estimates were performed on recorded peak flows at USGS gages in subbasins of our three sites (Figure 2-10 to Figure 2-12). Two areas in the Colorado study site were analyzed, with one area encompassing Fort Carson and the other area including Piñon Canyon Maneuver Site. Peak flows at the USGS gages were recorded as early as 1900

and through 2019 (see Table A-4 to Table A-6 in Appendix A.1), and basin sizes ranged from 60 to 9,000 km^2. We downloaded the USGS recorded peak values from the National Water Information System, and these values were retrieved through the USGS "dataRetrieval" R package.

A specialized version of the GEV theorem was applied to streamflow values to develop nonstationary curves. We used the R Project's Generalized Extreme Values conditional density estimation network package (Cannon 2010, 2011) to determine discharge stationarity (S), linear nonstationarity (LNS), or nonlinear nonstationarity. Nonstationary GEV analyses were generated for each quarter and averaged for the calendar year.

2.6 Probability of occurrence of annual maximum daily precipitation and intensity frequency curve analysis

We used the Gumbel's equation to derive the maximum precipitation for meteorological stations at the three sites (Figure 2-10 to Figure 2-12; see Table A-7 to Table A-9 in Appendix A.1). The earliest start year was 1894, and analysis was performed only for stations that included at least 20 years and where no full month was missing in the historical data. The analysis included precipitation if the air temperature was above freezing. For stations where air temperatures were not available, only values when the snow depth was zero were included. Data was downloaded from the National Centers for Environmental Information online repository (https://www.ncei.noaa.gov/). Additionally, for the meteorological stations in each site, we prepared rainfall IDF curves using a theoretical extreme value distribution (e.g., Gumbel Type I, which is based on the minimum or maximum distribution of a number of samples with various distributions) and calculated return periods of 2, 5, 10, 25, 50, and 100 years and durations of 1 hr to 24 hr.

Given the large uncertainty that exists in projected rainfall intensity from climate models, we used daily air temperature and precipitation outputs from 16 regional climate models (RCMs; Mearns et al. 2017) to calculate future annual maximum daily precipitation and to prepare future IDF curves. The selected models were RCP8.5 (Representative Concentration Pathway 8.5) models. The grid cell (0.22° native rotated-pole grid) closest to the center of each Installation (YTC in Washington, Fort Carson in Colorado, and GFAFB in North Dakota) was chosen for the output, and the time period included years 2006–2100. Only precipitation that occurred when air temperatures were above 0°C were included in the analysis.

3 Results and Discussion

3.1 Western U.S.

The Western U.S. 36-year average core snow season (Liston and Hiemstra 2011b) duration from our snow modeling results includes snow-free desert basins to high-elevation permanent snow (Figure 3-1*a–c*). The longest snow durations were in the mountainous areas of the Rocky Mountains, the Coast Range, the Cascades, and Sierra Nevada range. There was a decreasing trend of up to 20 days/decade in the Sierra Nevada range and the Cascades, but an increase of up to 20 days/decade was simulated in the Rocky Mountains. There was also an increase of snow duration up to 20 days/decade in the plains of Montana, North Dakota, and South Dakota. The yearly and area-averaged snow duration decreased by 10 days over the 36 years in the Western U.S. site.

The 36-year average number of ROS events was highest (40 days) in the Cascades, the Coast Range, and a small part of the northern Rocky Mountains (Figure 3-1*d–f*). The Sierra Nevada and Rocky Mountains also had a high number of ROS events. The trend of ROS events decreased by 4 days/decade in most of the Cascades, Sierra Nevada, the Coast Range, and parts of the southern Rocky Mountains. An increase of 4 days/decade can be seen in the northern part of the Rocky Mountains and in some of the Cascades. A general decrease of ROS events (1 day) was seen for the site over the 36-year period.

The 36-year average snowmelt-runoff maximum for the Western U.S. site was 300 cm (Figure 3-1*g–i*). The model showed the highest runoff in the mountain ranges. At the Cascades and the Coast Range, we simulated a decrease up to 20 cm/decade in snowmelt runoff. There was a 20 cm/decade increase in snowmelt runoff in the Rocky Mountains. A snowmelt-runoff decrease of 4 cm was seen for the Western U.S. site during the 36-year simulation.

Figure 3-1. (*a*) The 36-year average snow duration during the core snow season (days) for the Western U.S. site, (*b*) the trend in snow-cover duration (days/decade), and (*c*) yearly and area-averaged snow duration for the simulation in (*a*) and (*b*). (*d*) The 36-year average ROS events (days), (*e*) the trend in ROS events (days/decade), and (*f*) yearly and area-averaged ROS events (days) for the simulation site in (*d*) and (*e*). (*g*) The 36-year average total annual water equivalent snowmelt runoff (cm), (*h*) the trend in snowmelt runoff (cm/decade), and (*i*) yearly and area-averaged total annual snowmelt runoff for the simulation site in (*g*) and (*h*).

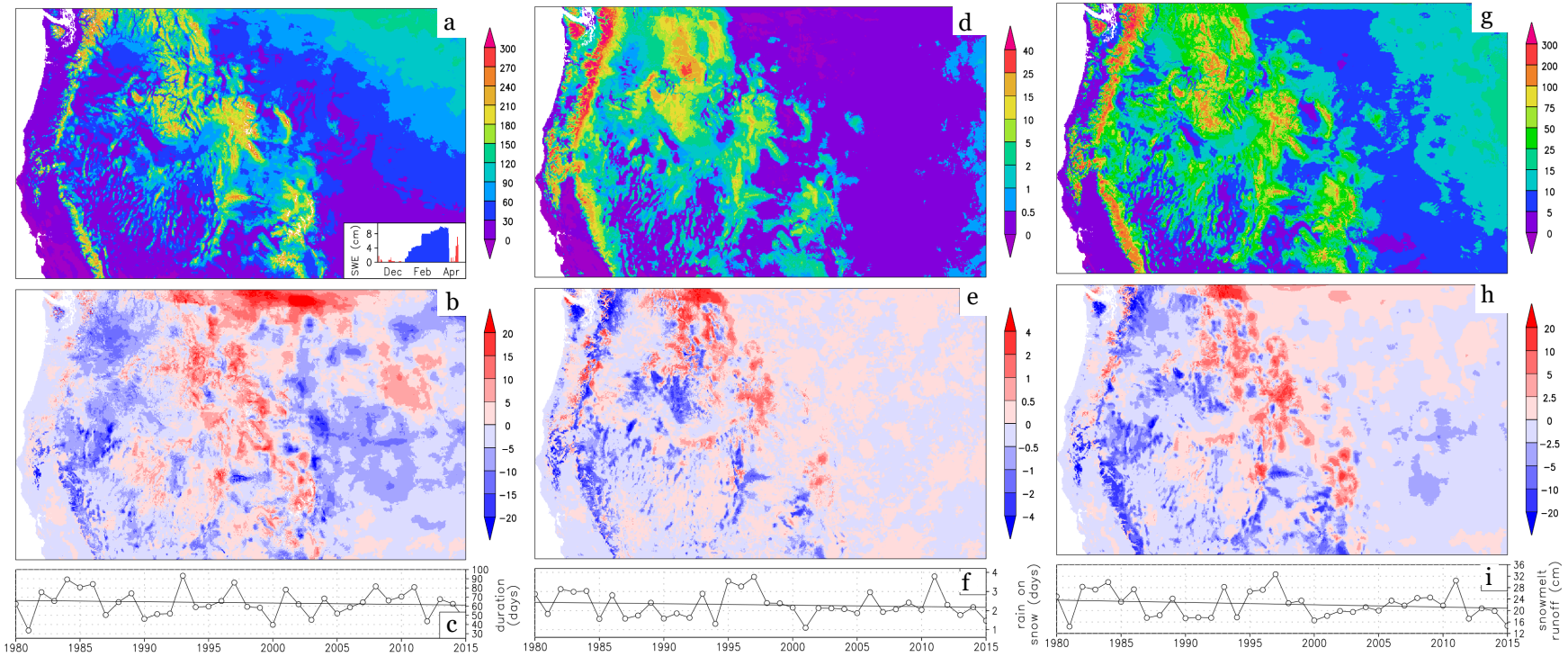

3.2 Washington

3.2.1 Field measurements, Washington

The average tower air temperature in 2016 and 2017 was 7.1°C. The lowest air temperature measured during this time was –17.7°C and occurred in early January 2016 (Figure 3-2). The prevalent wind direction was from the west. The highest recorded wind speeds were 32 m/s (19 October 2017), which is equivalent to 115 km/hr (whole gale). The wind sensor broke off of its mount in February 2017, resulting in missing wind velocity data for 6 months.

Figure 3-2. (*a*) Air temperature, (*b*) wind direction, and (*c*) wind velocity at the YTC meteorological tower.

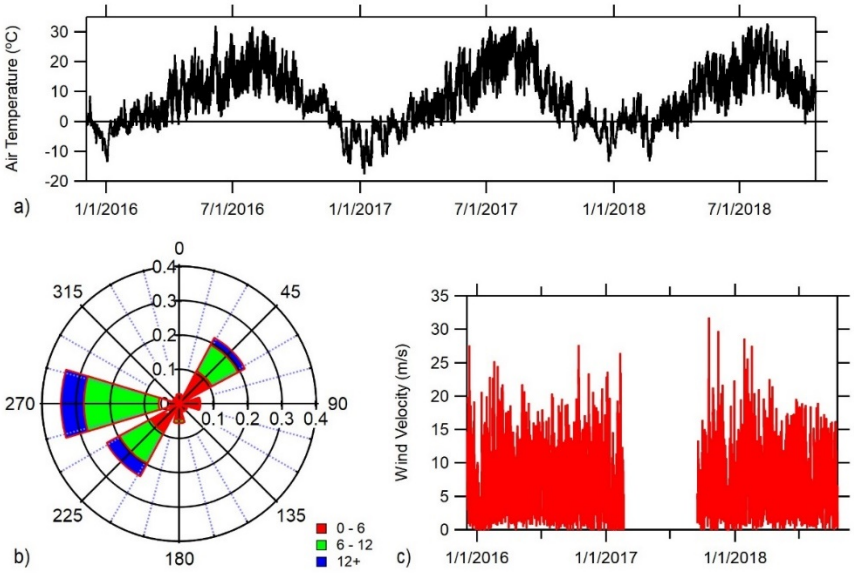

Figure 3-3 shows the daily snow depths during 2015–2018 from the Saddle Mountains' tower-mounted sonic sounder (Tower Sounder) and its time-lapse cameras (Tower). All years exhibited different snow accumulation and melt characteristics. Additionally, in this ridgetop environment, snow was scoured from ridgetops where the tower was located, accumulating into drifts on the north-facing slope (North). Tower and North peak snow depths do not occur at the same time in all years. In 2015–2016, Tower and North site snow depths were highest in late January at 25 and 68 cm, respectively. The following winter brought shallower snow at the Tower, peaking near 1 February 2017; however, the drift managed to accumulate snow (over 120 cm) until mid-March 2017. The sounder at the tower tracks snow depth similar to the Tower time-lapse camera. Comparing years, the 2015–2016 season peaked in midwinter; 2016–2017 had a

late accumulation into spring, and 2017–2018 had intermittent shallow snow all winter. The 2017–2018 winter had no snowpack or cover, with no snow observed 14–15 February 2018. Subsequently, snow-depth data are missing from the North site from 14 February onward.

Figure 3-3. Daily snow depths as measured at the windswept tower (both from the sounder and time-lapse camera) and at the time-lapse camera at the North drift site at YTC, Washington, in 2015–2018.

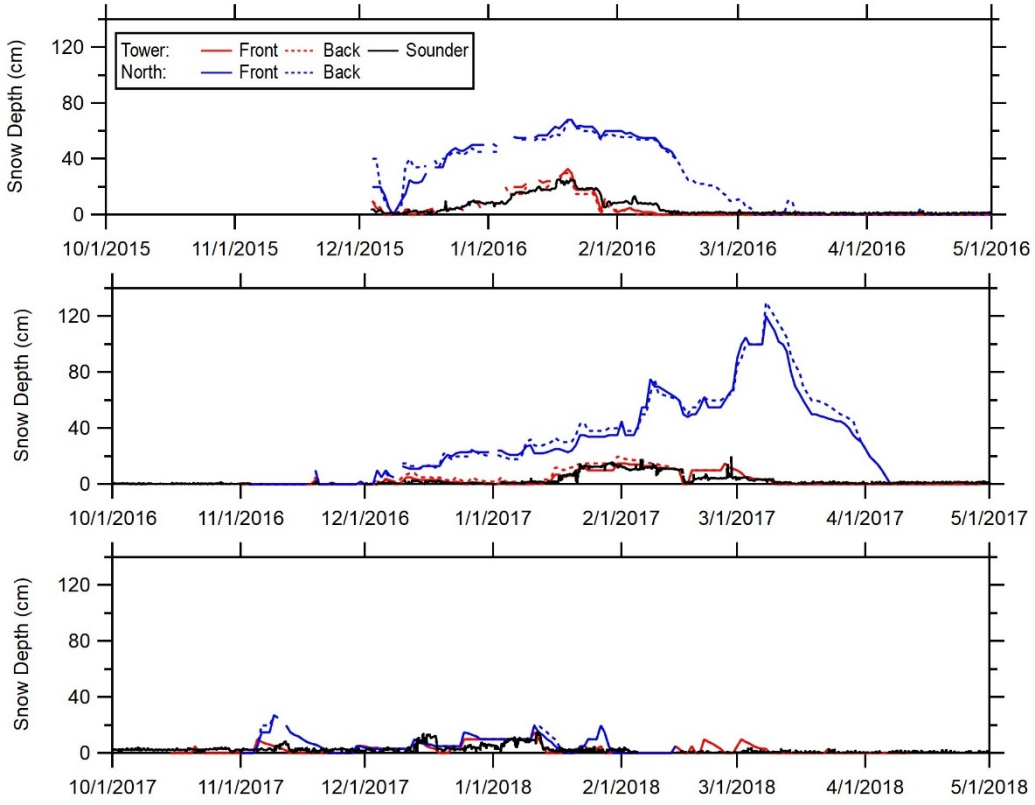

During the 2015–2016 field campaign, we visited eight locations for manual snow measurements 1–2 February 2016. This included a larger area located in the vicinity of the meteorological tower, and the other locations were opportunistically measured in the southern part of the installation along the higher elevations of Yakima Ridge (Figure 3-4) where training was not being conducted. The sample locations measured were primarily sagebrush dominated (*Artemisia tridentata*), but we also measured bare and grassland sites.

About 5,800 snow depths were measured at this location in winter 2015–2016 (Figure 3-4*a*). The average snow depth was 31.7 cm and ranged from 0 to 230 cm. Seventy-nine SWE samples were collected, and the mean SWE was 102.4 mm. The snow density ranged between 250 and 412 kg/m^3.

Figure 3-4. Snow depths and measurement locations during the (*a*) 2015–2016 and (*b*) 2016–2017 field campaigns. The *red solid line* outlines the YTC boundary.

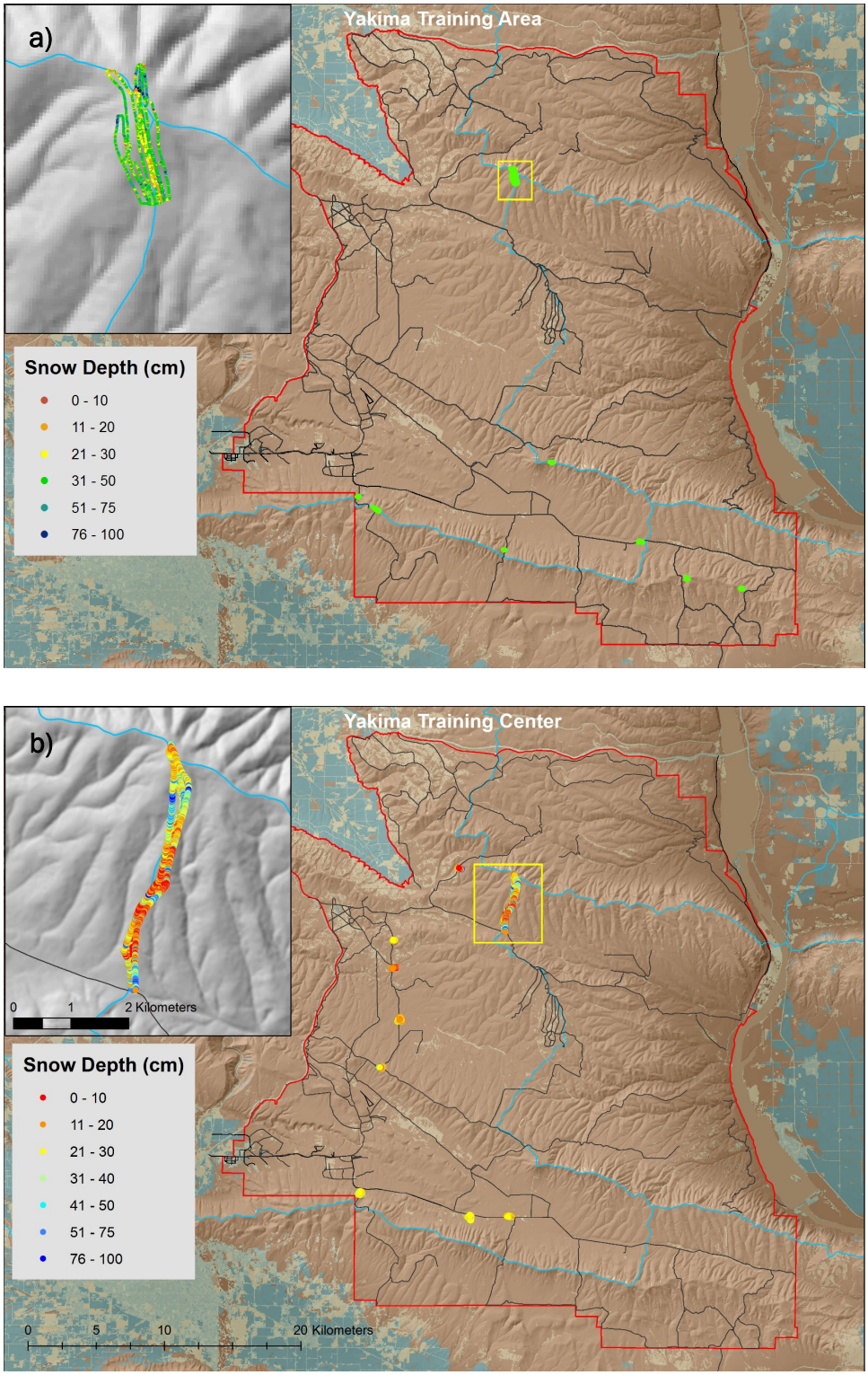

Nearly 10,250 snow depths were observed at YTC on 24–25 January 2017 (Figure 3-4*b*). Unlike the previous year, which was measured later in the

season, snow was more widespread, even at lower elevations; but snow depths were shallower overall. In addition, we made a more substantial effort to measure snow around the meteorological tower. The average snow depth was 23.1 cm and spanned 0 to 120 cm. We collected 102 SWE samples, and the mean SWE for the 16 pit locations was 61 mm. Snow density values were between 170 and 372 kg/m^3.

3.2.2 Snow model (VIC and SnowModel) validation, Washington

3.2.2.1 Snow-model validation to field measurements, Washington

An analysis of the SnowModel to field data shows that monthly snow depths were highly variable between years and dates (Figure 3-5). Snow was shallow overall in winter 2016 compared with 2017. Snow arrived later in 2017, after measurements in January 2017 (section 3.2.1), but lasted much longer. We withheld from assimilation a 15% subset of depth observations, converted the subset to SWE, and compared it with coincident SnowModel output for February 2016 and January 2017. Differences were smallest in the valleys and greater (although both positive and negative) where the ridges were dissected by ravines (Figure 3-6). Mean differences between observed and modeled SWE (modeled minus observed) were –4 mm in February 2016 and 4 mm SWE in January 2017.

Figure 3-5. Snow-modeling output for the 2015–2017 fine-scale simulations for the Washington site. The *white solid line* outlines the YTC boundary.

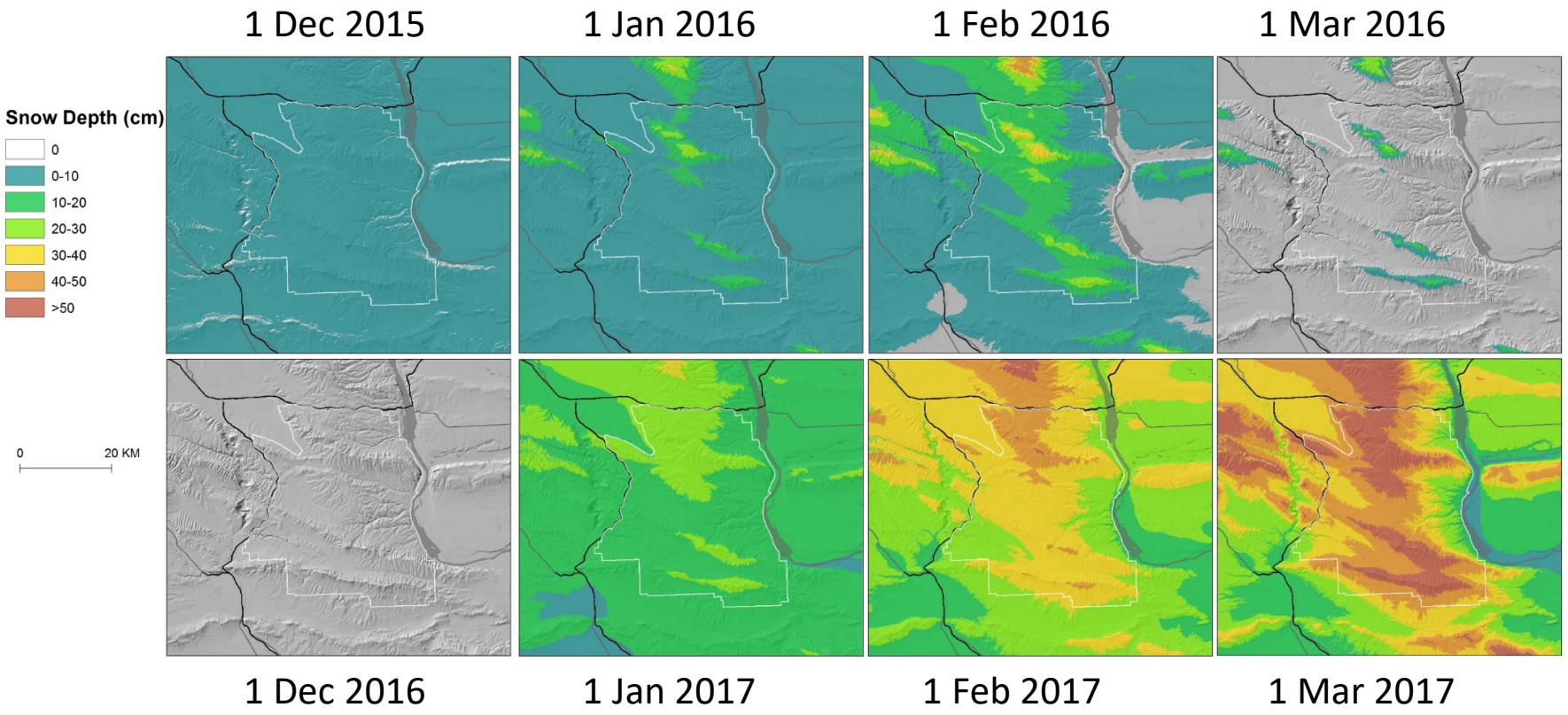

Figure 3-6. SWE comparison of observed (obs) snow depths and modeled snow depths for February 2016 and January 2017. The *white solid line* outlines the YTC boundary.

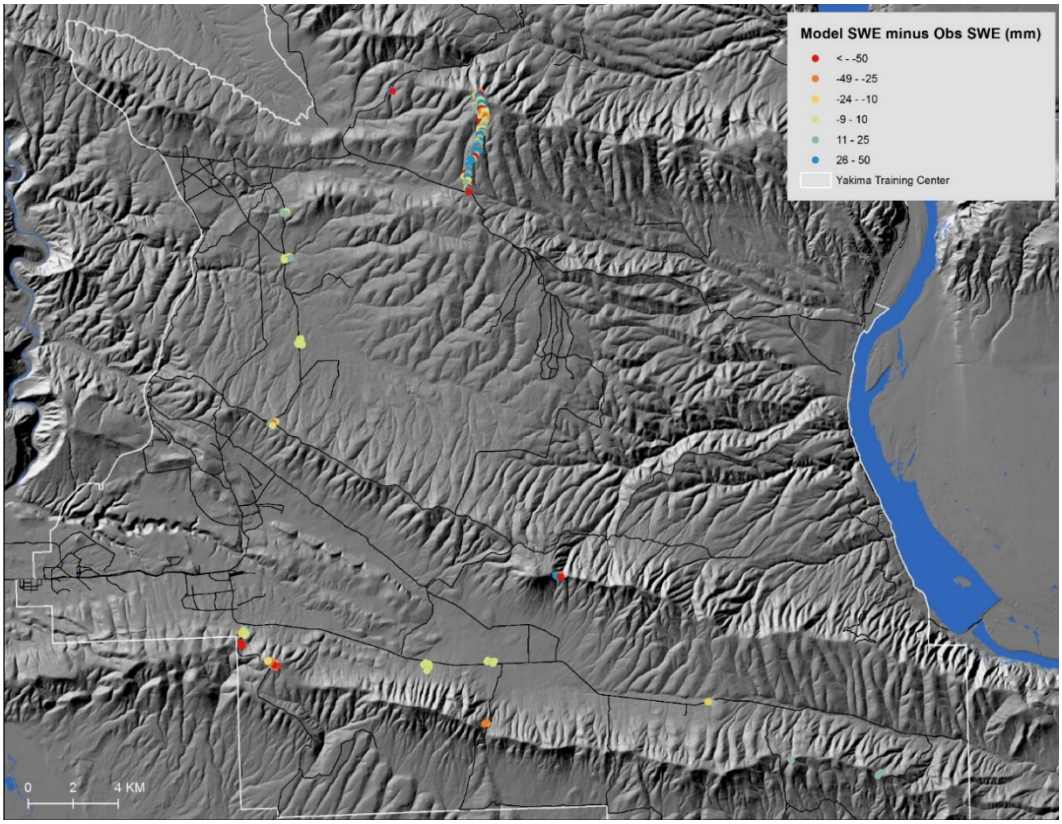

3.2.2.2 Snow-model validation to SWE, Washington

Fourteen SNOTEL sites were used for the VIC and SnowModel validation where elevations were from 900 to 1,800 m (see Table A-1 in Appendix A.1). Available SWE from the SNOTEL sites varies from 1978 to present, and all sites reported a wide range of SWE (see Figure A-1 in Appendix A.2). For example, at Olallie Meadows (1,228 m elev.), the lowest SWE was 280 mm in 2015, almost tenfold lower than its peak of 2,500 mm in 1999. At Morse Lake (1,649 m elev.), the lowest SWE was 540 mm, and the highest was 2,600 mm (1999). The lowest-ranked SWE values on average were tied to Trough and Blewett Pass, which were relatively high-elevation sites (1,670 and 1,292 m elev.).

To validate the snow modeling, we compared SWE from 14 SNOTEL stations, SnowModel, and VIC. Figure A-1 (Appendix A.2) shows the comparison for the 36-year SnowModel simulation time period (1979–2015). The end date of VIC SWE was 2010 because of the forcing dataset used during the modeling. For the 36-year time period, both models reproduced similar SWE accumulation and ablation curves when compared with measured

SWE at the SNOTEL sites. There was a wide variation of how well the SnowModel and VIC fit to the SNOTEL SWE. In some years, there was an underestimation or overestimation by one or both models. For example, at Olallie Meadows, the SnowModel SWE was lower than SNOTEL; but a fairly close fit was shown for VIC (Figure 3-7*a*). Conversely, SnowModel has a closer fit to SNOTEL at Fish Lake compared to VIC (Figure 3-7*b*). In general, the VIC simulations show a delay in snowmelt (see the example in Figure 3-7*c*).

Figure 3-7. Model (SnowModel and VIC) and SNOTEL SWE comparison at Washington for (*a*) Olallie Meadows (1983–2010), (*b*) Fish Lake (1983–2010) and (*c*) close-up (2000–2010) of Fish Lake. All SWE modeling results are reported in Appendix A.2.

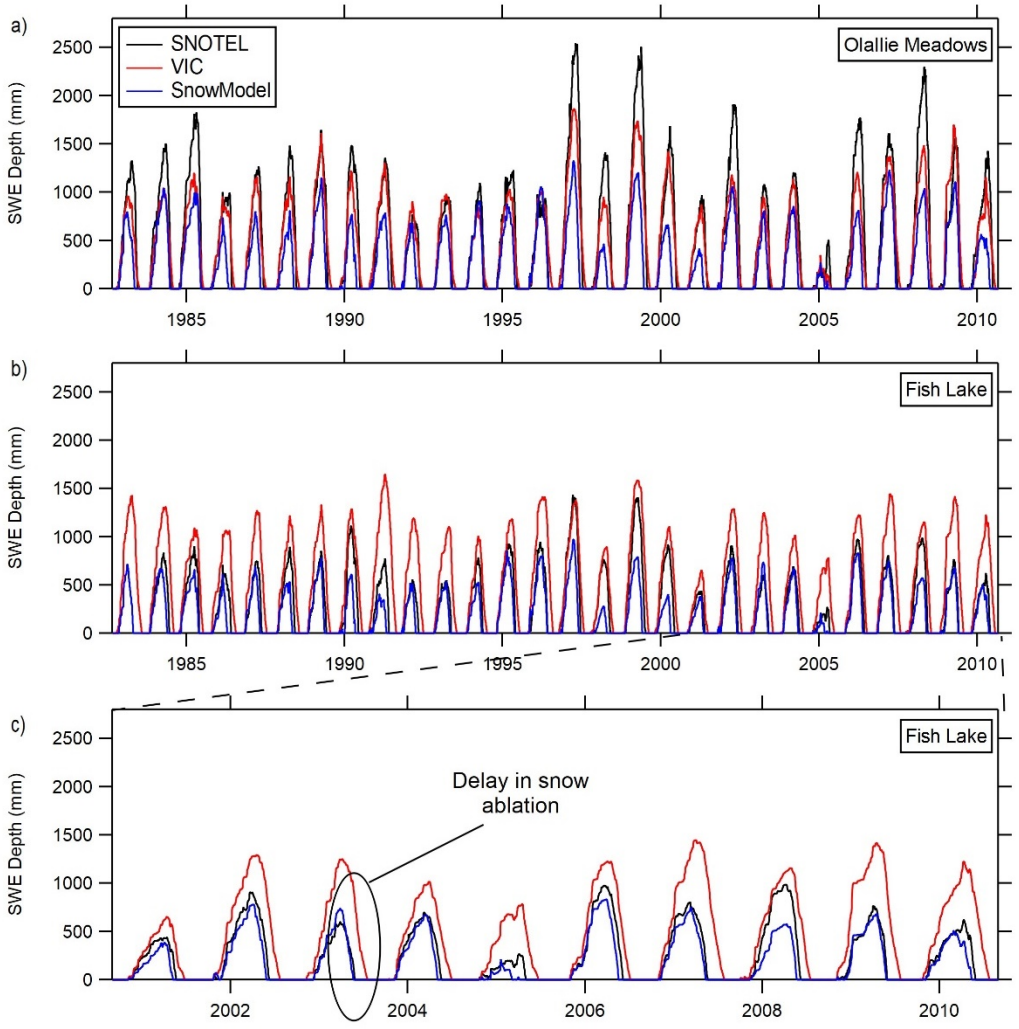

3.2.3 Snow trends and future projections, Washington

Longer-term SWE trends in the Washington site contrast based on elevation. To illustrate this, a high-elevation location (Stampede Pass) and a

low-elevation site (CRREL YTC meteorological station) comparison showed a wide range of yearly maximum SWE between these locations from water years 1980 to 2015 (Figure 3-8). Peak and lowest SWE values occurred at both sites in water year 1997 and 2015, respectively. In most years there was a general correlation between the sites, but this correlation did not occur every year. During this time period, a decreasing and significant trend of 2 mm/year occurred at the lower-elevation CRREL YTC meteorological station, while no trend was identified for Stampede Pass.

Figure 3-8. SWE evolution and trends at the CRREL meteorological station at YTC (Met. Station) and Stampede Pass.

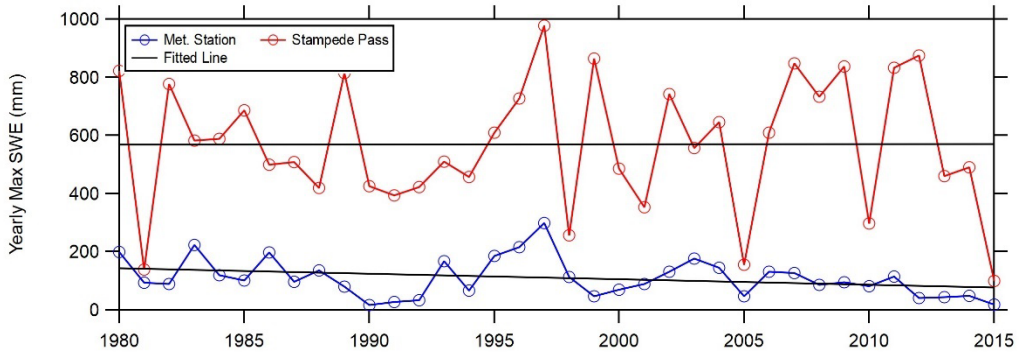

Figure 3-9 shows the snow modeling results from the Washington site, and Figure 3-9*a–c* shows the 36-year average of snow duration during the core snow season. The core season varies depending on site and was defined to be the longest yearly uninterrupted snow duration (e.g., the blue shading in the [*a*] inset; Liston and Hiemstra 2011b). At the highest elevations, the average snow duration was over 300 days during the 36-year period. In contrast, snow duration was only 30 to 90 days at lower elevations. Snow-cover-duration trends were also mixed. At intermediate and higher elevations, there was a widespread snow-cover duration decrease of 10–20 days/decade. Lower elevations (up to 350 m) showed an increase of 10–40 days/decade. Modeling results show a decrease of up to 40 days/decade at some areas with elevations that range from 350 to 1,000 m. The area-averaged snow-cover duration declined 20 days/decade (Figure 3-9*c*).

ROS event counts and trends were also tied to elevation. Higher-elevation locations had frequent ROS events (30–50 days) as those snowpacks were long-lived (Figure 3-9*d–f*) while low-elevation ROS events were rare. ROS trends illustrated that there was an increase or decrease of 1 day/decade over most of the site, with an exception at higher elevations where an increase of 4 days/decade occurred. However, not all high-elevation trends

were positive; in the northwestern part of the site, a decrease of 4 days/decade was apparent. Overall, the simulated yearly and area-averaged ROS events for the simulation site decreased 1 day over the entire 36 years.

Not surprisingly, higher snowmelt runoff corresponded to elevation (Figure 3-9*g–i*). With few exceptions, snowmelt runoff was predominantly negative for 1980–2015 with an average decline of 10 cm/decade. There was a high variation in the total snowmelt; the lowest value was in 2015 (15 cm), and the highest occurred in 1997 (60 cm). That was a difference of 45 cm, which can have a big influence in the overall snowmelt of the area.

The only future projection of snowpack was performed for the snow duration (Figure 3-10). The CTL simulation was similar to the 1979–2015 simulation at higher elevations (see Figure 3-9*a*). In the northeast, where lower elevations were encountered, the CTL simulation indicated a longer snow duration than the 1979–2015 simulation. When comparing the PGW simulation and the CTL, the majority of this site experienced a decrease in snow duration with an overall difference of up to 40 days (Figure 3-10).

Figure 3-9. (*a*) The 36-year average snow duration during the core snow season (days) for the Washington site, (*b*) the trend in snow-cover duration (days/decade), and (*c*) yearly and area-averaged snow duration for the simulation in (*a*) and (*b*). (*d*) The 36-year average ROS events (days), (*e*) the trend in ROS events (days/decade), and (*f*) yearly and area-averaged ROS events (days) for the simulation site in (*d*) and (*e*). (*g*) The 36-year average total annual water equivalent snowmelt runoff (cm), (*h*) the trend in snowmelt (cm/decade), and (*i*) yearly and area-averaged total annual snowmelt runoff for the simulation site in (*g*) and (*h*). North is *up*.

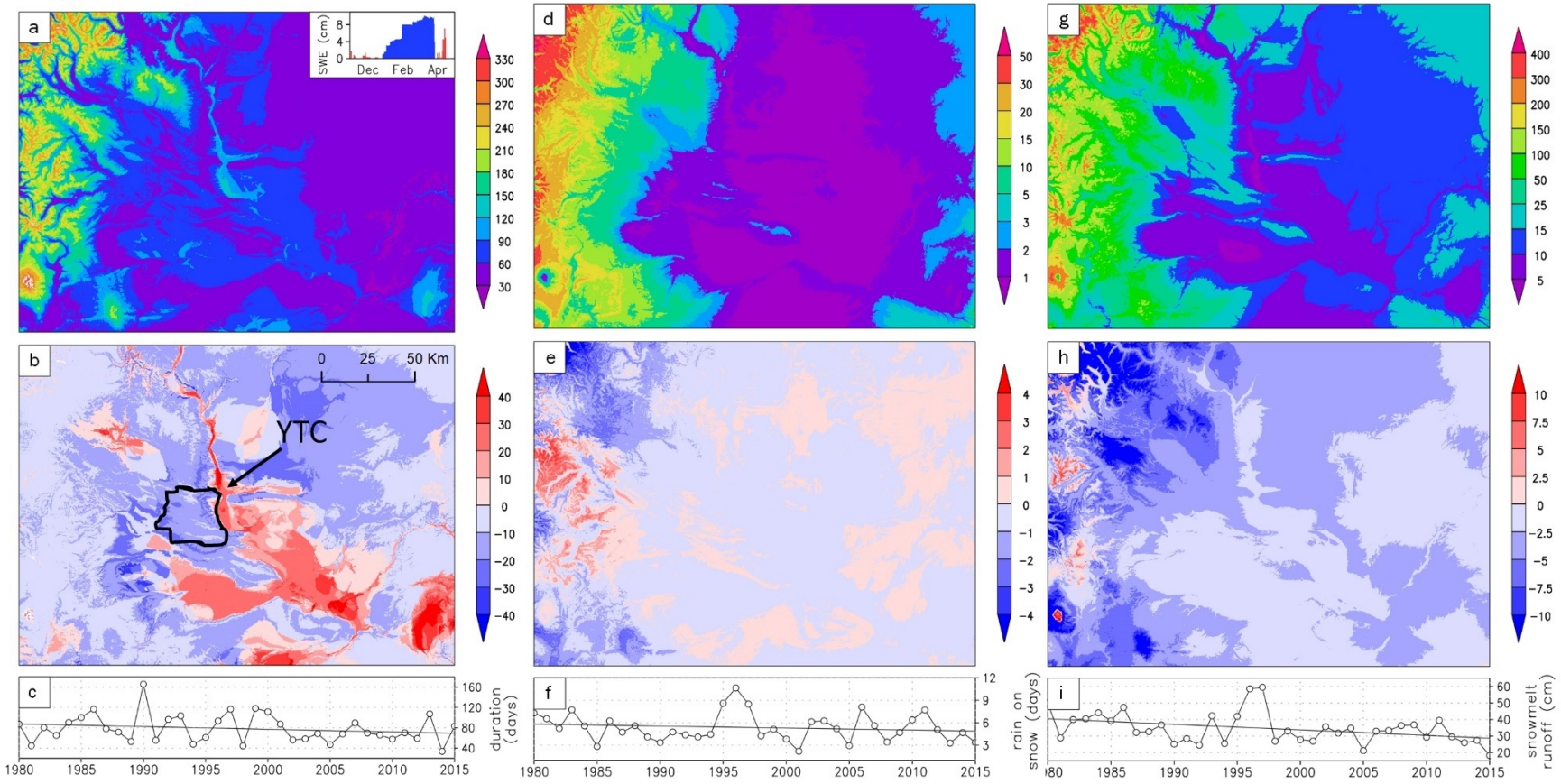

Figure 3-10. Snow duration for historical (CTL) and future (PGW) climate models (*left*) and the difference and trend in snow-cover duration (days) between the future and control (*right*) for the Washington site. North is *up*.

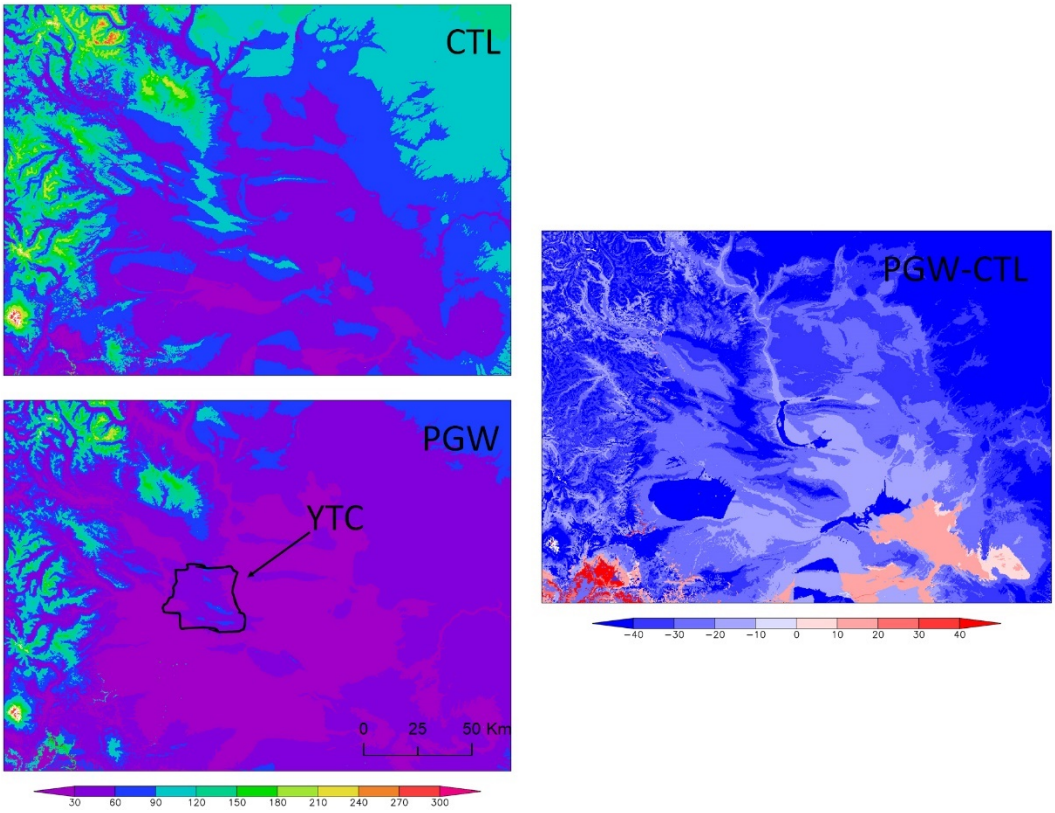

3.2.4 Flood and streamflow analysis, Washington

3.2.4.1 Historical flood frequency curve analysis, Washington

We calculated flood frequency curves at 10 USGS stations for basin sizes ranging from about 70 to 9,000 km² (see Figure 2-10 and also Table A-4 in Appendix A.1). The longest peak flow record was 97 years for the Yakima River at Umtanum (12484500). The maximum peak flow (95% confidence level) at the watershed that encompasses parts of YTC was 1,600 m³/s (Figure 3-11).

Appendix A.2 (see Figure A-2) shows the return period of annual maximum peak flows for the 10 USGS stations. The lowest 100-year return period (30 m³/s) was at Naneum Creek near Ellensburg (12483800), which was also the smallest subwatershed (178 km²) analyzed within the HUC 8 Upper Yakima watershed. The Yakima River gage above Ahtanum Creek at Union Gap (12500450), located in the HUC 8 Lower Yakima watershed, yielded the highest value of 1,500 m³/s for the 100-year return period.

Figure 3-11. Return period of annual peak flow and upper- and lower-boundary 95% confidence level (CL) for the Yakima River gage above Ahtanum Creek at Union Gap (12500450) in the Washington site (all annual peak flow results are reported in Appendix A.2).

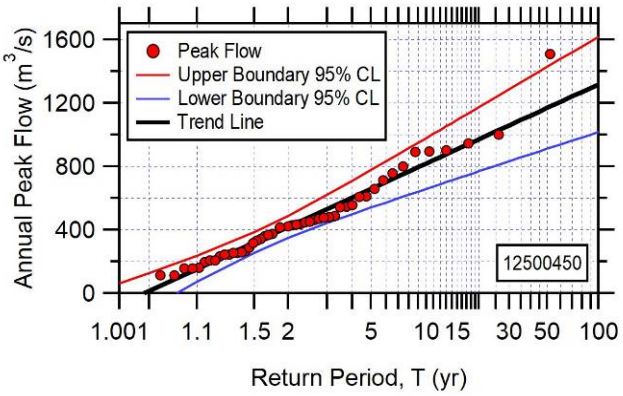

3.2.4.2 Historical streamflow analysis, Washington

To capture the most recent streamflow record, we selected for the seasonal streamflow analysis of the Washington site only those USGS gages monitored through 2019 (see Table A-4 in Appendix A.1). Because of our selection criteria, we analyzed discharge for four USGS gages within this site for the mean, maximum, and minimum streamflow and peak flows (Figure 3-12). These gages were located in the Naches (12488500, basin size 205 km^2), Upper Yakima (12484500, basin size 4,128 km^2), and parts of Lower Yakima (12500450 and 12502500, basin size 9011 and 446 km^2, respectively) HUC 8 watersheds. The streamflow was lowest in August–September and increased gradually until peak flow in late spring or early summer. In all but one watershed, the peak flow occurred close to mid-May. A later peak flow of a few weeks was identified at the American River near the Nile gage (12488500), located in the upper Naches HUC 8 watershed, indicating a later snowmelt occurred in this watershed. The Morse Lake SNOTEL site, located at the higher elevations of this HUC 8 watershed, measured one of the highest SWE (see Figure A-2 in Appendix A.2), which likely explained the later peak flow. Another indication for this is that the watershed about twice its size (12502500) that experienced a lower snowpack produced only about 25% of the maximum peak flow (~7 m^3/s) when compared to the drainage basin measured at the American River gage near Nile (28 m^3/s). The highest peak measured at these four gages (~250 m^3/s) was at the Yakima River USGS station above Ahtanum Creek at Union Gap (12500450), which was also the furthest downstream gage and thus also encompassed the largest drainage basin.

Figure 3-12. Mean (*dashed*), maximum, and minimum streamflow hydrographs for 12-day composites for the USGS gages (*upper left* and *right corners*) in the Washington site. The *vertical line* indicates peak streamflow. *Gray* shaded fields show January–March (JFM) and July–September (JAS), and *white* fields indicate April–June (AMJ) and October–December (OND). Midmonth dates are shown on the x-axis. Sites are ordered by basin size.

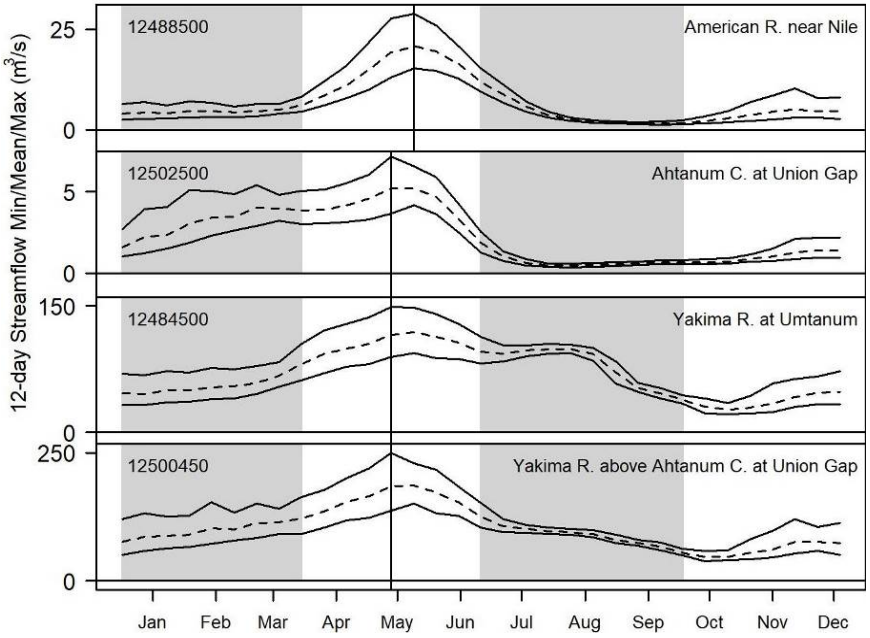

We analyzed the streamflow trends for the four USGS gages (12484500, 12488500, 12500450, and 12502500; see Table A-10 in Appendix A.2). No statistically significant increase for the maximum annual trend in streamflow was found (Figure 3-13). Only at the Yakima River stations is an increasing trend in minimum annual streamflow evident. There was a statistically significant increase in seasonal maximum streamflow for the Yakima River at Umtanum station (12484500; JFM and JAS) and American River near Nile (12488500; JFM). A statistically significant increase in minimum streamflow trends for almost the full year at the Yakima River at Umtanum (12484500) was found. At a Yakima River downstream station (above Ahtanum Creek at Union Gap, 12500450) an increase was found in OND. For the one other station (12488500), only one season (JFM) indicated a statistically significant increase in streamflow.

The S model was the best fit for the annually averaged maximum flow of the rivers analyzed at this site (Figure 3-14). This was also the best GEV model for the early spring (AMJ) and late fall (OND) (see Figure A-3 in Appendix A.2). These stationary results are indicative of no significant trend. The LNS model was the best fit for the American River near Nile

(12488500) for JFM, where only a small increase in the trend was modeled. That GEV model was also the best fit for the Yakima River at Umtanum (12484500) for JAS. In fact, GEV results indicated that this was the largest increasing trend for this site.

Figure 3-13. (*a*) Maximum and (*b*) minimum streamflow (*Q*) trends (%) for the USGS stations in Washington. *Circles* indicate the trends for 12 days, *rectangles* indicate seasonal results, and the annual trend is given in the *lower left box*. Statistical significance is shown: the 99th percentile (*dark gray*), the 95th percentile (*light gray*), and nonsignificant results (*white*). Midmonth dates are shown on the x-axis. Sites are ordered by basin size.

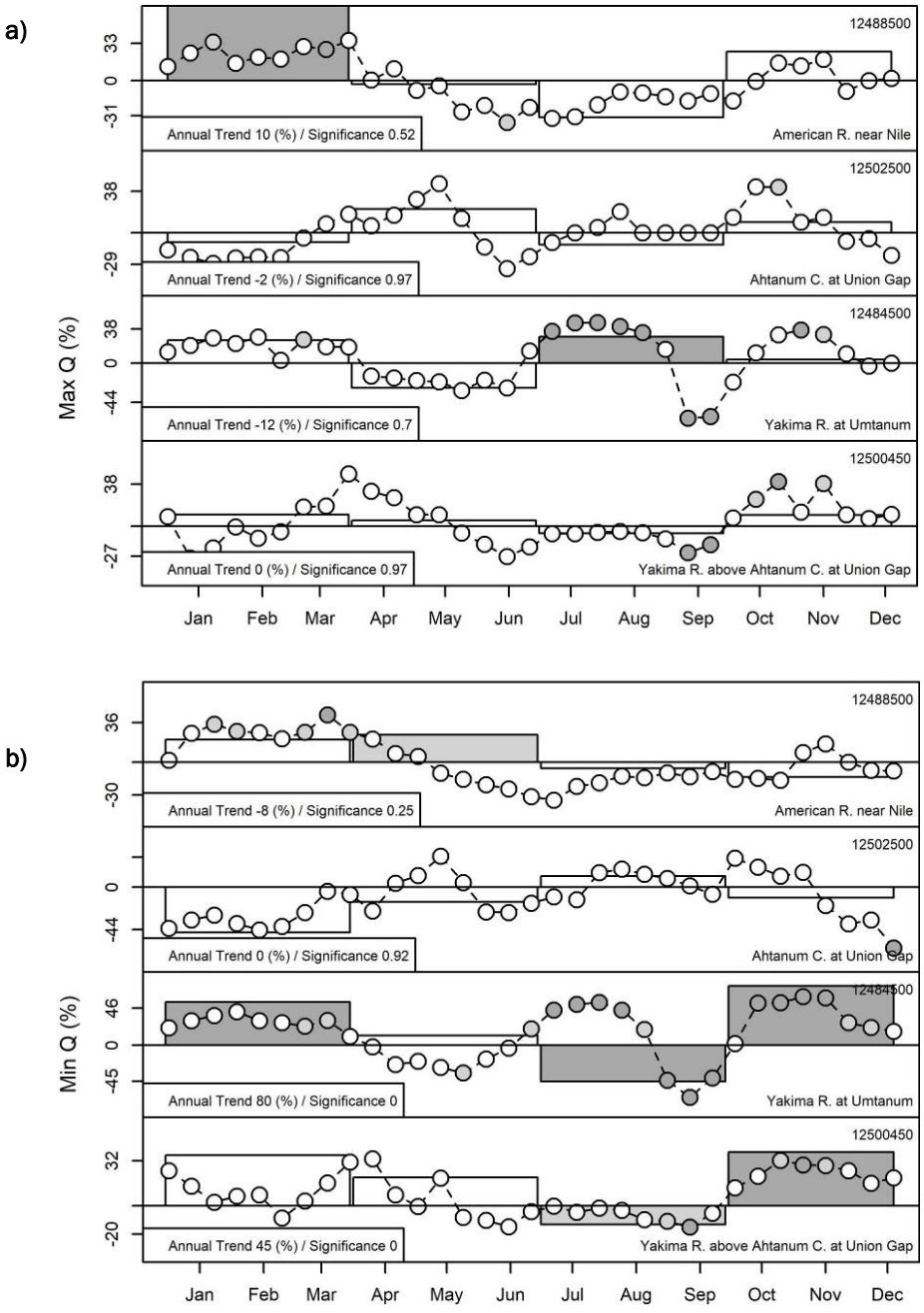

Figure 3-14. Annual maximum streamflow GEV results and streamflow seasonal maximums (*blue circles*) for the Yakima River at Umtanum (YAKUM), American River near Nile (AME), Yakima River above Ahtanum Creek at Union Gap (YAKUN), and Ahtanum Creek at Union Gap (AHTUN) basins at Washington. Return intervals (T = 2, 5, 10, 20, 50, and 100 years) from the GEV fits are shown in *dashed lines*. All GEV results are reported in Appendix A.2.

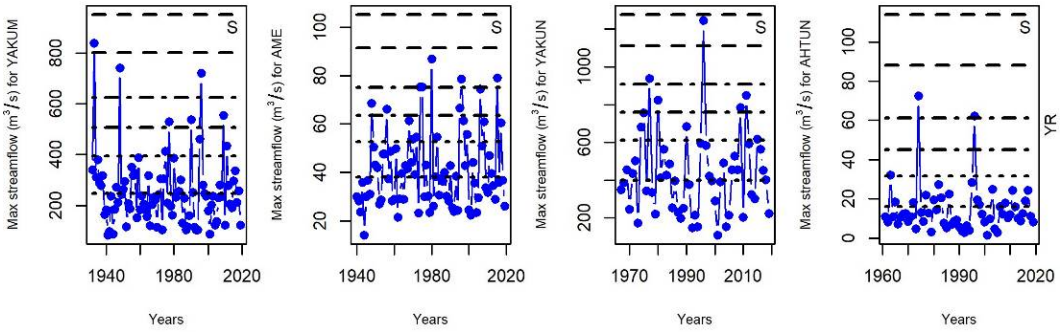

3.2.4.3 Projection of future streamflow, Washington

We compared the historical streamflow for VIC (1970–2010) and Hydro-Flow (1979–2015) to the adjusted streamflow at USGS gage 12505001 (Figure 3-15). HydroFlow generated a closer seasonal streamflow with the gage than VIC did. The simulated peak flow is somewhat higher than observed, but HydroFlow duplicated the timing of the peak flow and the also the late-fall increase in streamflow. The projected pseudo-global-warming streamflow for HydroFlow (Hydro PGW) indicated a higher and later peak flow of 2 weeks (from mid-May to early June) compared to the current climate (Hydro). Although the maximum peak value was not quite duplicated for the current climate, the higher peak values are still an indication that projected streamflow is increasing in this watershed. The projected streamflow showed a more even end-of-season streamflow where streamflow is higher from July through October and almost no flow is occurring in early winter.

Figure 3-15. Mean (*dashed*), maximum, and minimum streamflow hydrographs for 12-day composites for the adjusted streamflow at USGS gage 12505001 (Yakima River adjusted). Historical VIC and HydroFlow (Hydro) simulations and future HydroFlow (Hydro PGW) are also shown. The name of model is shown in *upper right corners*. The *vertical line* indicates peak streamflow. *Gray* shaded fields show JFM and JAS, and *white* fields indicate AMJ and OND. Midmonth dates are shown on the x-axis.

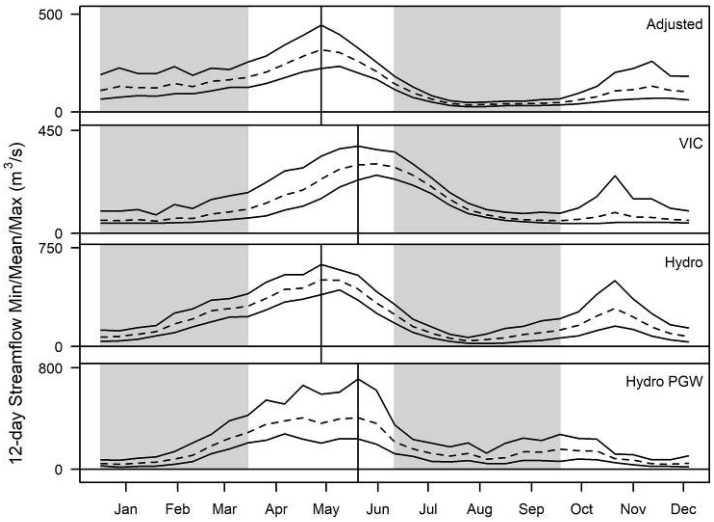

3.2.5 Probability of occurrence of annual maximum daily rainfall depths, Washington

We calculated the probability of the annual maximum daily precipitation for 11 meteorological stations in the Washington site (see Figure 2-3 and also Table A-7 in Appendix A.2). The shortest record for the analysis was 21 years (Selah 2), and the longest record was 102 years (Cle Elum). The maximum annual precipitation of these stations started at a low of 35 to a high of 200 mm, as shown in Appendix A.2 (see Figure A-4). Most stations had a maximum annual precipitation at this return period of less than 50 mm. Two of the highest annual maximum daily precipitation stations were the Stampede Pass (1,207 m elev.) and Cle Elum (579 m elev.). Both stations were located within the Upper Yakima HUC 8 watershed and upstream of YTC. In fact, the highest annual maximum daily precipitation at the Stampede Pass station (comparable to the high degree of variability also seen for the SWE, Figure 3-8) was five times higher than at the Yakima Airport station (Figure 3-16). The Stampede Pass station also had the widest range of the 95% confidence level of 80 mm at a return period of 100 years.

Projected annual maximum daily precipitation curves for the center of the YTC installation were derived from selected global climate models ([GCMs]

see section 2.6). In general, the projected annual maximum daily precipitation curves for the global models were higher than the historical curves at Yakima Airport (Figure 3-17). At a return period of 100 years, the highest projected precipitation was 90 mm higher than at the historical precipitation measured at the Yakima Airport. The range between the lowest and highest 95% confidence level was 65 mm at a return level of 100 years. In comparison, at Yakima Airport, this range was only 14 mm for the current climate. The highest confidence value doubled at this return period.

Figure 3-16. Annual maximum daily precipitation depths for the Stampede Pass and Yakima Airport meteorological stations in the Washington site. All annual maximum daily precipitation results are reported in Appendix A.2.

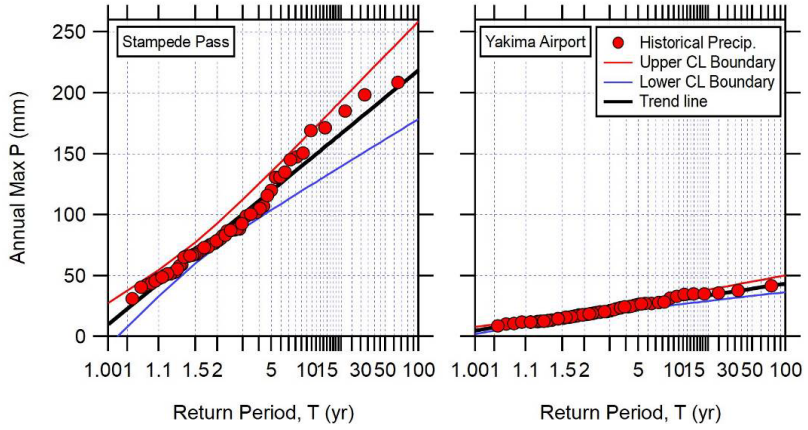

Figure 3-17. Projected annual maximum daily precipitation depths at YTC, Washington, from global climate models (*circles*) as compared to the historical annual maximum daily precipitation curve at Yakima Airport (*solid red circles*), including the upper (*red line*) and lower (*blue line*) 95% confidence levels. *Dashed lines* indicate the upper- and lower-boundary confidence levels for Yakima Airport 1946–2019.

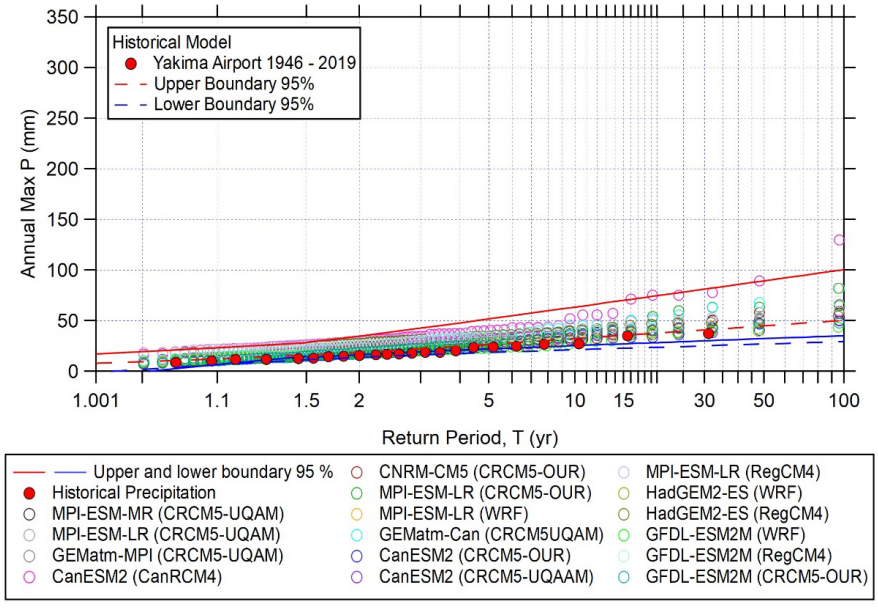

3.2.6 IDF curves, Washington

IDF curves were produced from three meteorological stations (a location with low, medium, and high precipitation). These were selected from the annual maximum precipitation analysis (section 3.2.5). Many stations had similar maximum annual precipitation as measured at Yakima Airport; and therefore, that station was chosen as an example of a low-intensity station (see Figure A-9 in Appendix A.2). The station selected for the analysis with a slightly higher annual maximum daily precipitation was Cle Elum. The highest annual maximum daily precipitation was also the station located at the highest elevation (Stampede Pass, 1,207 m elev.). For all three locations, IDF curves with six return periods (2, 5, 10, 25, 50, and 100 year) were derived for durations of 1 to 24 hr (Figure 3-18). Yakima Airport, the lowest annual precipitation, has a rainfall intensity range of 25 mm (from 18 to 43 mm/hr) at a 1 hr duration. In comparison, the rainfall intensity at Stampede Pass ranges from 80 to 220 mm/hr, a total width of 140 mm, almost six times more than at the Yakima Airport.

Figure 3-18. IDF curves for three meteorological stations (Cle Elum, Stampede Pass, and Yakima Airport) in the Washington site.

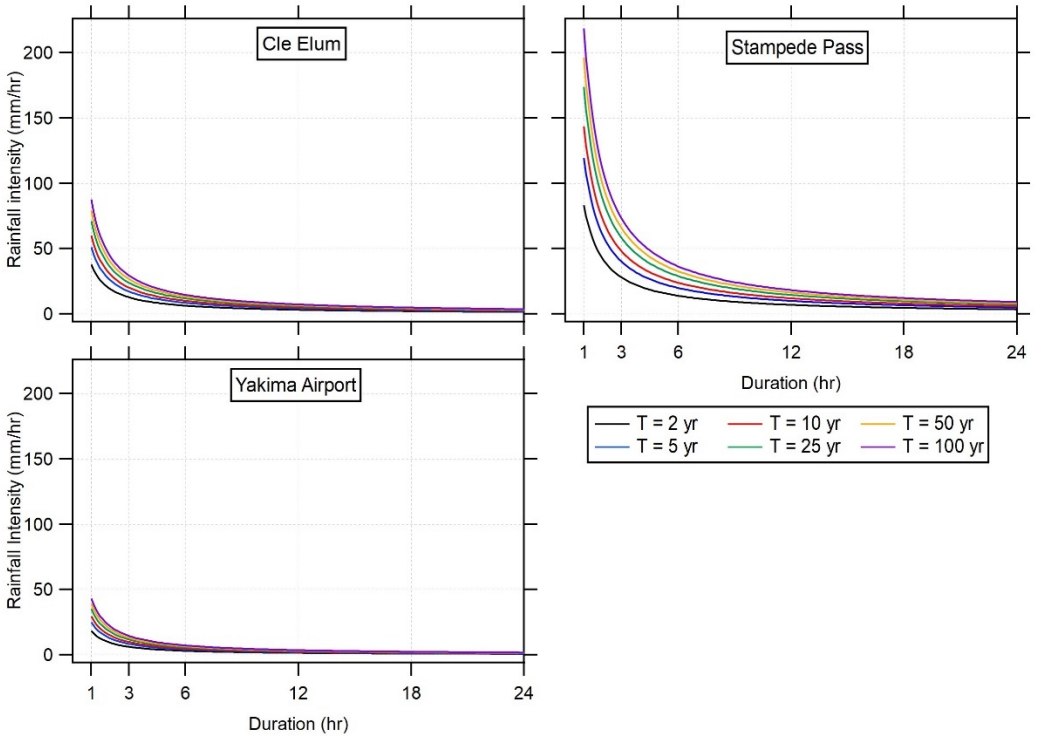

For the future IDF curves, we used the climate models that had the lowest and highest confidence level for the annual maximum daily rainfall (Figure

3-17) to define the range of rainfall intensity at the YTC installation. The climate models indicated higher IDF curves compared to historical IDF curves (Figure 3-19). The lowest-confidence-level climate model (lowest maximum annual precipitation) was the Geophysical Fluid Dynamics Laboratory's Earth System Weather Research Forecasting Model (GFDL-ESM2M [WRF]), which resulted in a rainfall intensity ranging from 19 to 41 mm/hr at a 1 hr duration. The second-generation Canadian Earth System Regional Climate Model (CanESM2 [CanRCM4]), the highest maximum annual precipitation model, indicated a rainfall intensity range of 55 mm (32 to 87 mm/hr) at a 1 hr duration. At a 1 hr duration and a return period of 100 years, the rainfall intensity is about twofold higher (from 43 to 87 mm/hr) than the current climate at the Yakima Airport.

Figure 3-19. Estimated future IDF curves for a location at the center of the YTC installation, Washington. For comparison, the *black dashed lines* illustrate historical IDF curves from the Yakima Airport.

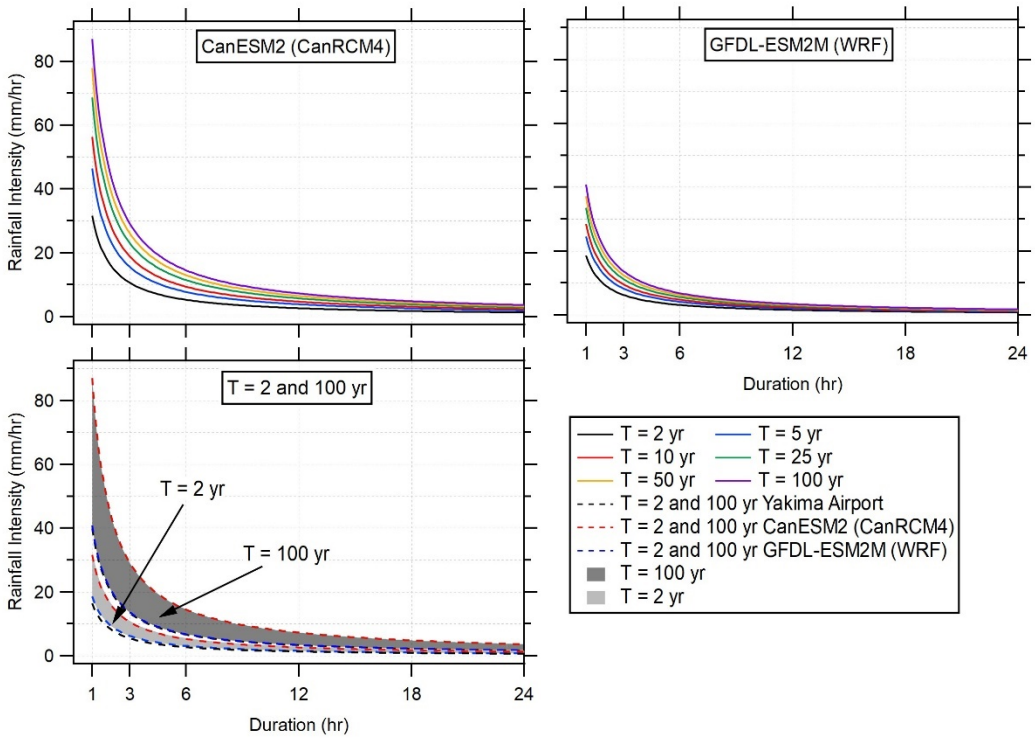

3.3 Colorado

3.3.1 Field measurements, Colorado

Snow arrival and departure during all seasons were intermittent (Figure 3-20), with snowstorms depositing up to 30 cm of snow before it melted. There were 10 to 13 distinct snow deposition events each year. Almost

every time, snowmelt occurred in between snowstorms. At times, there was no snow for almost a month. Earliest snow arrival in the fall occurred in November 2017. The latest snow deposition occurred in May 2016 (~20 cm), which was comparable to other higher snow dispositions.

Figure 3-20. Daily snow depths at Fort Carson, Colorado, in 2015–2018.

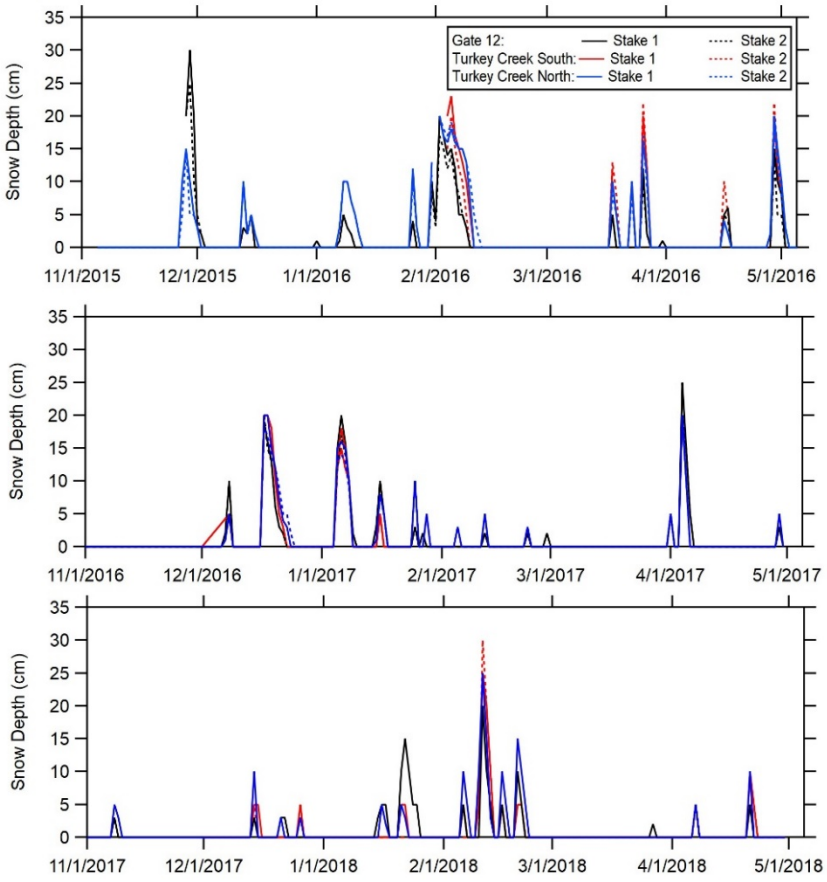

During 4–5 February 2016, we measured 3,571 snow depths at six locations (Figure 3-21*a*). The average snow depth was 20.5 cm and the overall snow depth ranged from 0 to 92 cm. We collected 67 SWE samples, and the mean was 41 mm. The snow density ranged between 56 and 368 kg/m^3. Snow arrival and departure during winter 2015–2016 was intermittent (Figure 3-20), with storms depositing up to 30 cm of snow before it melted. There were 10 distinct snow deposition events during this season.

The following year, 19 January 2017 experienced a lower snowpack at Fort Carson, with a few tree-shaded thin patches (<3 cm) of snow remaining (estimated and not measured with a Magnaprobe). However, higher up in

the basin (3,000 m) toward Pikes Peak, we measured 207 snow depths, and we dug two snow pits (Figure 3-21*b*). The average snow depth was 27 cm and ranged from 10 to 68 cm. We collected 10 SWE samples two snow pits, and the mean total SWE was 10 mm. Snow density sample values were from 134 to 328 kg/m^3.

Figure 3-21. Snow-depth measurements and locations at the Colorado site during the (*a*) 2015–2016 and (*b*) 2016–2017 field campaigns. The *black solid line* outlines the Fort Carson boundary.

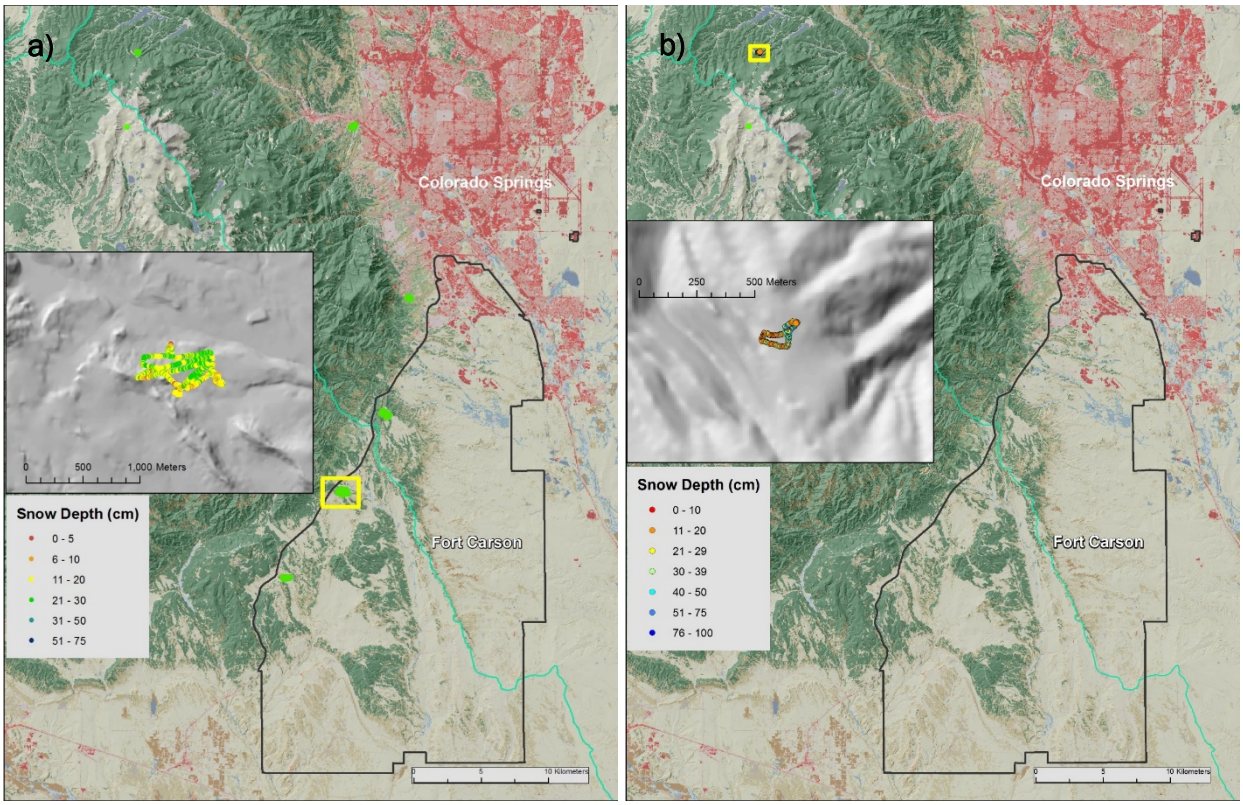

3.3.2 Snow-model (VIC and SnowModel) validation, Colorado

At this site, we used 16 meteorological stations and one SNOTEL station for the snow-model validation (see Table A-2 in Appendix A.1). The elevations at the stations studied were from 1,200 to 3,500 m. SWE varied substantially between years and stations during 1979–2015 (see Figure A-5 in Appendix A.3). One example of a station that had a lower SWE was the Colorado Spring Airport (1,884 m elev.), the meteorological station closest to Fort Carson. In 1997, the maximum SWE was 153 mm (Figure 3-22). In comparison, at a higher-elevation station (Glen Cove SNOTEL station, 3,493 m elev.), the maximum SWE was 381 mm (2007); the minimum was 43 mm in 2011 (Figure 3-22). At Whiskey Creek, also a higher-elevation

station (3,115 m elev.), the annual maximum SWE was 500 mm. Most stations this far south in the Rocky Mountains have a shallow snowpack with a maximum SWE of less than 200 mm. A slightly higher SWE of 300 mm was recorded at Eastonville 2 NNW and Ruxton Park (above 2,000 m elev.).

Figure 3-22. SWE comparison between VIC and SnowModel for Colorado Springs Airport (AP), Glen Cove (SNOTEL station), and Whiskey Creek, Colorado. No VIC results for the Whiskey Creek are shown because they were outside the model boundary. All SWE results are reported in Appendix A.3.

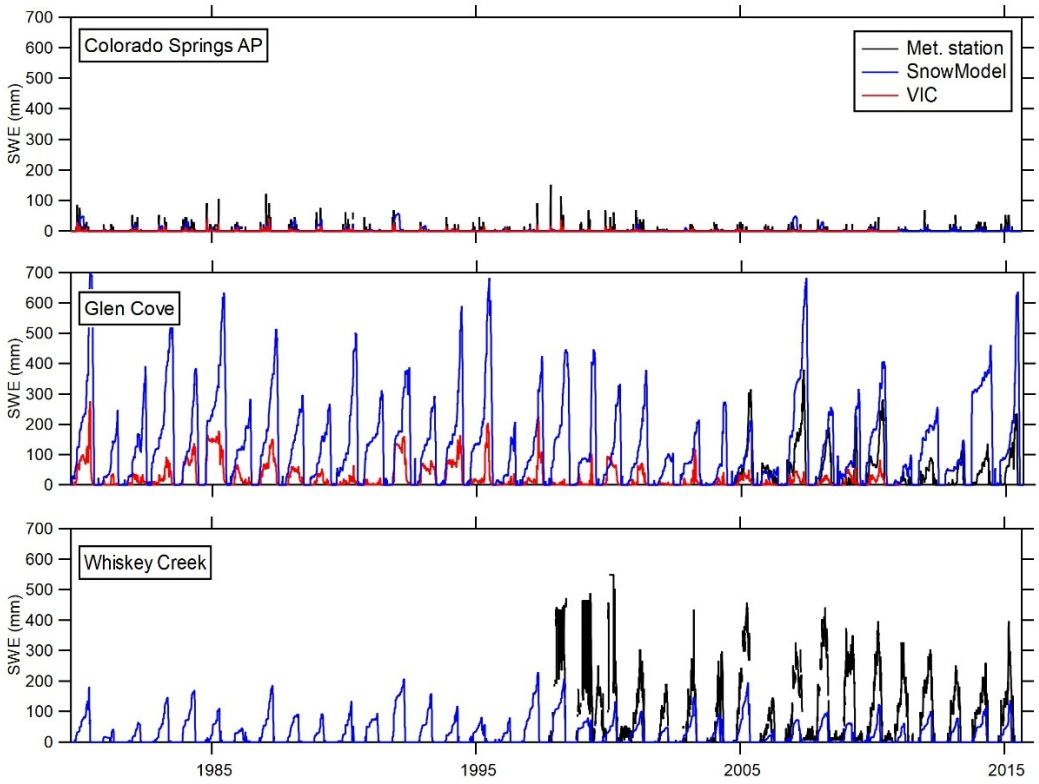

SnowModel performed better than VIC, but there was a tendency for the models to both underestimate and overestimate SWE (see Figure A-5 in Appendix A.3). For example, at the Glen Cove SNOTEL site, simulated SWE from VIC was substantially lower than SnowModel's (Figure 3-22) and the observed SWE. SnowModel compared well with the measured SWE at this station during some years; and other years, SWE was much higher than measured. For timing, VIC captured snow-up and snowmelt periods closely, despite a mismatch in SWE. SnowModel delayed snowmelt in some years.

3.3.3 Snow trends and future projections, Colorado

The simulated yearly maximum SWE evolution for a high-elevation site in the HUC 8 Fountain watershed (Glen Cove, 3,493 m elev.) and at the center of the Fort Carson installation indicated a downward trend in 1979–2015 SWE (Figure 3-23). For the 36-year period, there was a 115 mm decrease in Glen Cove maximum SWE, and Fort Carson experienced little snow overall. Similar downward trends were shown in the Purgatoire watershed at its high-elevation Whiskey Creek site (3,115 m elev.), where a 30 mm decrease in maximum SWE was simulated. The Piñon Canyon Maneuver Site declined as well, but by approximately only 5 mm overall.

Figure 3-23. SWE evolution and trends at (*a*) Glen Cove SNOTEL site and Fort Carson and (*b*) Whiskey Creek and the Piñon Canyon Maneuver Site.

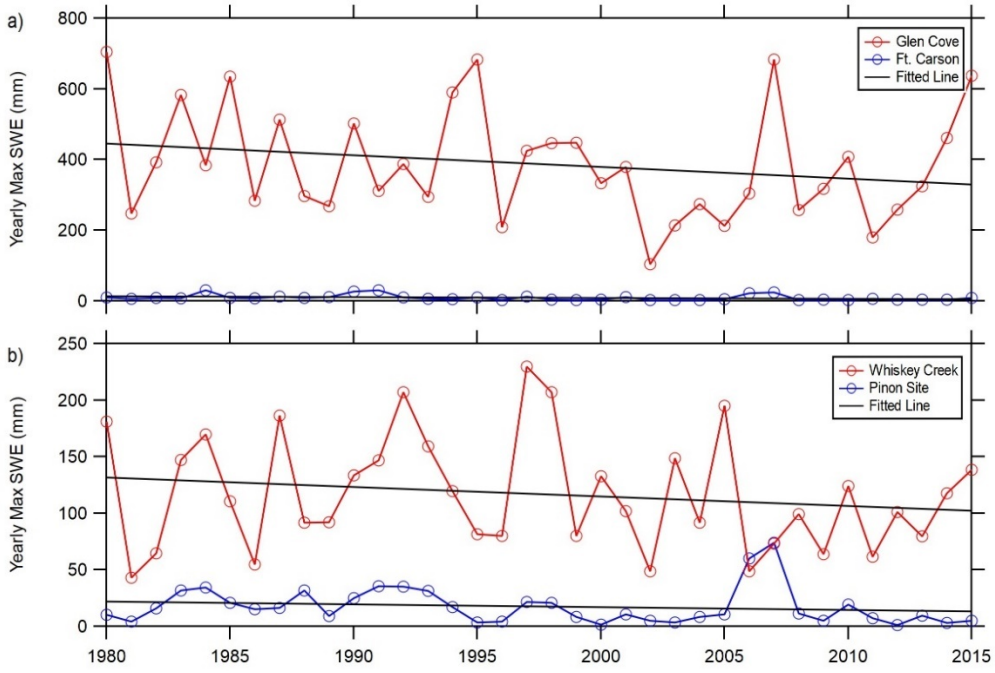

The 36-year core snow-season duration varied with elevation (Figure 3-24*a*–*c*). At higher elevations with deeper snowpacks, snow duration was 300 days; mid- to low-elevation snow duration was only 30 days. Snow-cover duration increased at lower elevations by up to 40 days/decade. A decreasing trend of up to 40 days/decade can be seen in some parts up north of the site, and a slightly smaller decrease was simulated in the site's southwestern area. The yearly and area-averaged snow duration for the 36-year time period increased 10 days overall. Snow trends indicated a

longer-lasting snowpack, up to 40 days in some lower-elevation areas (Figure 3-25). Higher-elevation areas had decreased snow duration by up to 4 days/decade.

Thanks to Colorado's continental climate, the historic 36-year average ROS event maximum was only 10 days, and these events occurred in higher-elevation locations (Figure 3-24*d–f*). At lower elevations, the simulations showed no changes for ROS events; less than plus or minus 1 day/decade of ROS events was seen throughout the simulated area. The greatest decrease in ROS occurred in high-elevation areas. The simulated yearly and area-averaged ROS events for the simulation site had a negligible decreasing trend (only about half a day) over the entire 36-year-simulation period.

During the 36 years, the simulations showed a snowmelt runoff up to 100 cm within the site (Figure 3-24*h–i*). The greatest amount of snowmelt runoff was tied to higher elevations. Throughout the site, a downward trend occurred up to 4 cm/decade. In the mountainous southwest part of the site, snowmelt runoff increased 4 cm/decade. Overall, the yearly and site-averaged total annual snowmelt runoff decreased a few centimeters in 36 years.

As previously mentioned, a future projection of snow duration was the only climate change simulation performed. In the west, at higher elevations, the snow duration was longer for both the CTL (current climate) simulation (Figure 3-25) and the 1979–2015 simulation (see Figure 3-24*a*). In the northeast, where lower elevations were encountered, the CTL simulation indicates a shorter snow duration than the 1979–2015 simulation. The comparison between the PGW and the CTL simulations indicated an increase in snow duration for lower elevations (maximum of 40 days); but the majority of this site experience a decrease in snow duration (maximum of 40 days).

Figure 3-24. (*a*) The 36-year average snow duration during the core snow season (days) for the Colorado site, (*b*) the trend in snow-cover duration (days/decade), and (*c*) yearly and area-averaged snow duration for the simulation in (*a*) and (*b*). (*d*) The 36-year average ROS events (days), (e) the trend in ROS events (days/decade), and (*f*) yearly and area-averaged ROS events (days) for the simulation site in (*d*) and I. (*g*) The 36-year average total annual water equivalent snowmelt runoff (cm), (*h*) the trend in snowmelt (cm/decade), and (*i*) yearly and area-averaged total annual snowmelt runoff for the simulation site in (*g*) and (*h*). North is *up*.

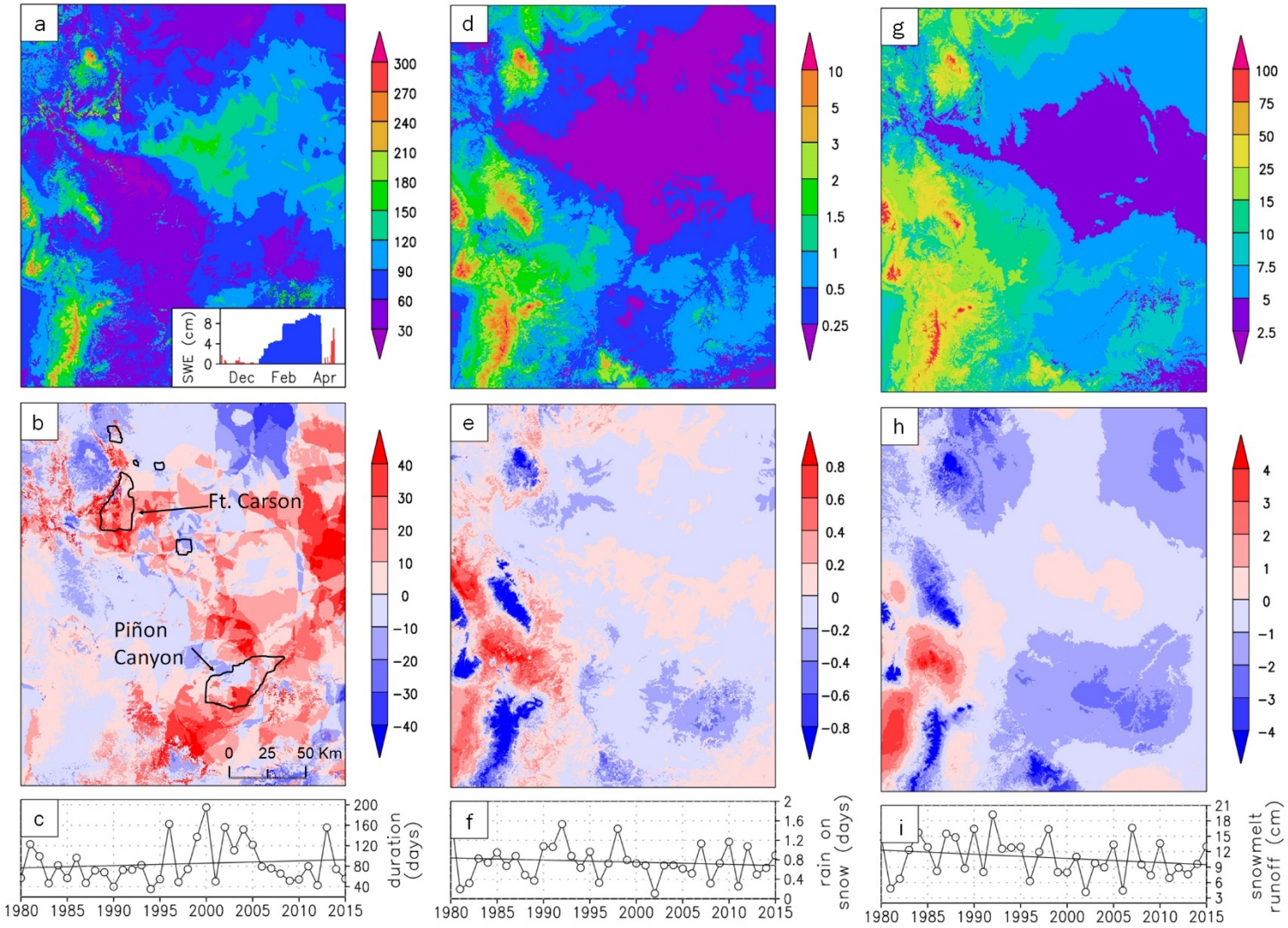

Figure 3-25. Snow duration for historical (CTL) and future (PGW) climate models, (*left*) and the difference trend in snow-cover duration (days) between the future and control (*right*) for the Colorado site. North is *up*.

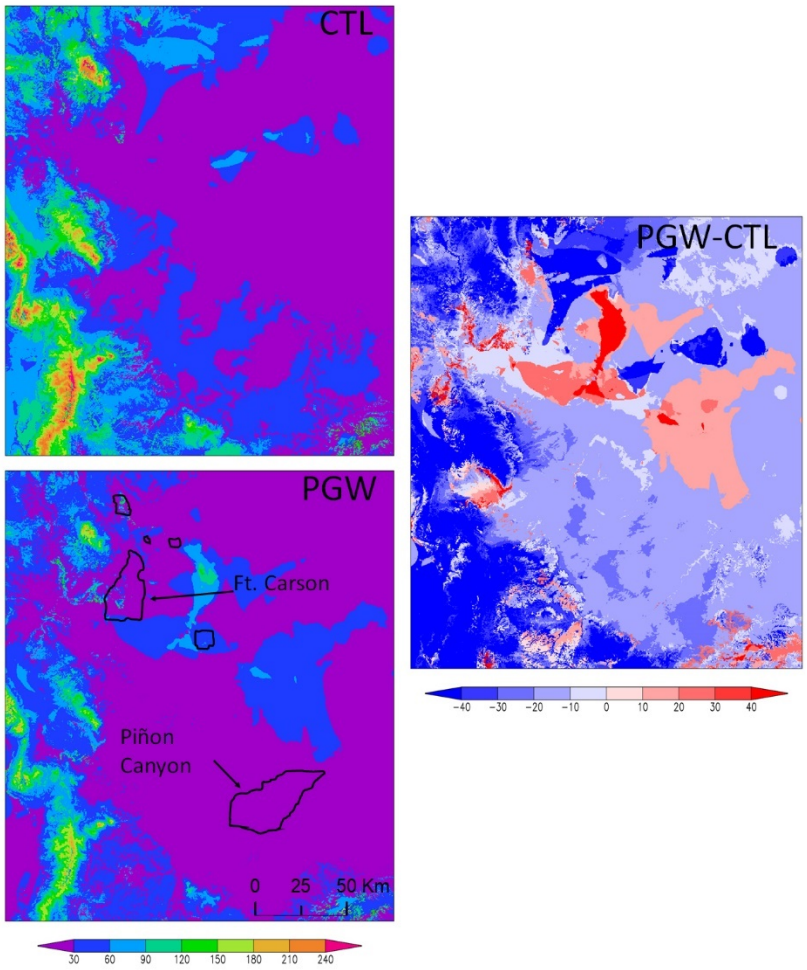

3.3.4 Flood and streamflow analysis, Colorado

3.3.4.1 Historical flood frequency curves, Colorado

We calculated flood frequency curves of 12 USGS stations, where the smallest basin was 160 km², measured at the Turkey Creek above Teller Reservoir near Stone City (07099230), to a basin size of 9073 km², measured at Purgatoire River near Las Animas (see 07128500 in Figure 2-11 and also Table A-5 in Appendix A.1). The length of available peak flow values was up to 71 years with the longest record for the Purgatoire River near Las Animas (07128500). Figure 3-26 shows a subset of the return period for the annual maximum peak flow of these stations with the full record from the analyzed stations shown in Figure A-6 (Appendix A.3). The Fountain Creek near Piñon (07106300, basin size 2,240 km²), located to the east of the Fort Carson site and in the Fountain HUC 8 watershed, had a

maximum annual peak flow of 560 m³/s. At the Purgatoire River near Las Animas (07128600, basin size 9,073 km²), downstream of the Piñon Canyon Maneuver Site and in the Purgatoire HUC 8 watershed, an annual peak flow of 1,960 m³/s was observed. The range of the 95% confidence level at a return period of 100 years at the Fountain Creek near Piñon was 300 m³/s. At the Purgatoire River near Las Animas, with a basin size four times larger, this spanned 650 m³/s. The minimum peak flow of the 12 selected USGS stations was 50 m³/s, measured at the Monument Creek above North Gate Blvd. at the U.S. Air Force (USAF) Academy (07103780, basin size 212 km²) as shown in Appendix A.3.

Figure 3-26. Return period of annual peak flow and upper- and lower-boundary 95% CL for the Fountain Creek near Piñon (07106300) and Purgatoire River near Las Animas (07128500) stations in the Colorado site. Note the different scales. All annual peak flow results are reported in Appendix A.3.

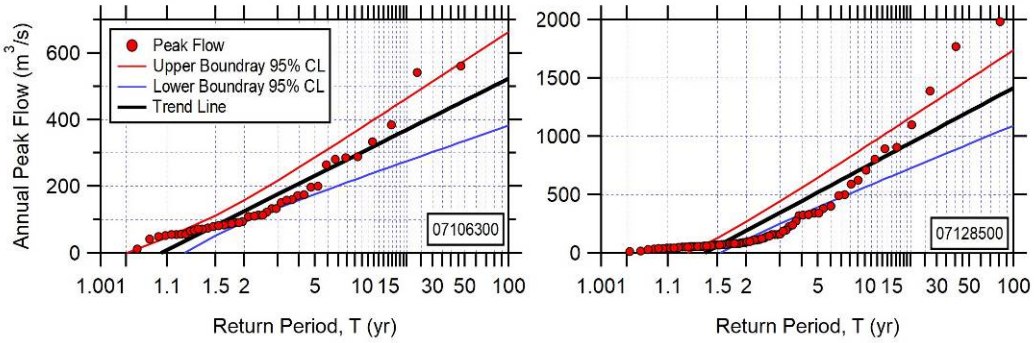

3.3.4.2 Historical streamflow analysis, Colorado

We performed historical streamflow analysis for the USGS gages within our site that met our site-selection criteria, a station with more than 20 years and active in 2019. The selected stations for the Colorado site were located in the Fountain, Upper Arkansas, and Purgatoire HUC 8 watersheds (see Figure 2-11 and also Table A-5 in Appendix A.1). We analyzed a total of 10 USGS gages for the mean, maximum, and minimum streamflow and peak flows (Figure 3-27). At these sites, the peak streamflow date varies widely. One of the earliest dates (mid-April) for peak flow was at the Monument Creek above North Gate Blvd. at the USAF Academy (07103780), and the latest peak (early September) occurred also at Monument Creek but farther downstream (Bijou St. at Colorado Springs, 07104905), both in the Fountain HUC 8 watershed. In fact, more than half the stations had a peak flow later in the summer (end of July or later). At most gages, the flow increased gradually, peaked, then decreased starting at the end of September. Many sites experienced multiple peaks where snowmelt likely drove the first peak

flows. Out of the analyzed gages, Fountain Creek near Fountain and Piñon and Purgatoire River near Las Animas had the largest streamflow.

We analyzed streamflow trends for 10 USGS gages (Figure 2-11 and also Table A-5 in Appendix A.1). Figure 3-28 shows a subset of the analysis for the two largest basins, the Fountain Creek near Piñon (07106300, basin size 2,240 km^2), which encompassed the east of Fort Carson, and the Purgatoire River near Las Animas (07128500, basin size 9,073 km^2), which included the Piñon Canyon Maneuver Site. The remaining streamflow trend analysis results are in Appendix A.3 (see Figure A-7*a*). A yearly statistically significant increase (>90th percentile) in annual maximum and minimum streamflow trends for three stations (all within the Fountain Creek HUC 8 watershed: 07105500, 07106000, and 07106300) was found (see Table A-11 in Appendix A.3). Two other stations showed a statistically significant increase (>90th percentile) in minimum annual streamflow (Fountain Creek near Colorado Springs and Monument Creek above North Gate Blvd. at USAF Academy: 07103700 and 07103780). Only one station experienced a statistically significant yearly decrease in annual trends (>95th percentile) for the maximum and minimum streamflow (Turkey Creek at Teller Reservoir near Stone City: 0799230), which also was one of the smaller basins analyzed. No increase (or decrease) in yearly streamflow is seen in the Purgatoire HUC 8 watershed.

A statistically significant increase of monthly maximum streamflow occurred in several stations in the Fountain Creek HUC 8 watershed in winter (JFM) and later in the season (JAS). This watershed included the eastern parts of Fort Carson. In fact, a statistically significant increase in monthly minimum streamflow is also evident at several stations (see Figure A-7*b* in Appendix A.3).

Figure 3-27. Mean (*dashed*), maximum, and minimum streamflow hydrographs for 12-day composites for the USGS gages (*upper left* and *right corners*) in the Colorado site. The *vertical line* indicates peak streamflow. *Gray* shaded fields show JFM and JAS, and *white* fields indicate AMJ and OND. Midmonth dates are shown on the x-axis. USGS gages in the HUC 8 Fountain and Arkansas watersheds are shown in (*a*), and the HUC 8 Purgatoire watersheds are shown in (*b*). Sites are ordered by basin size.

a)

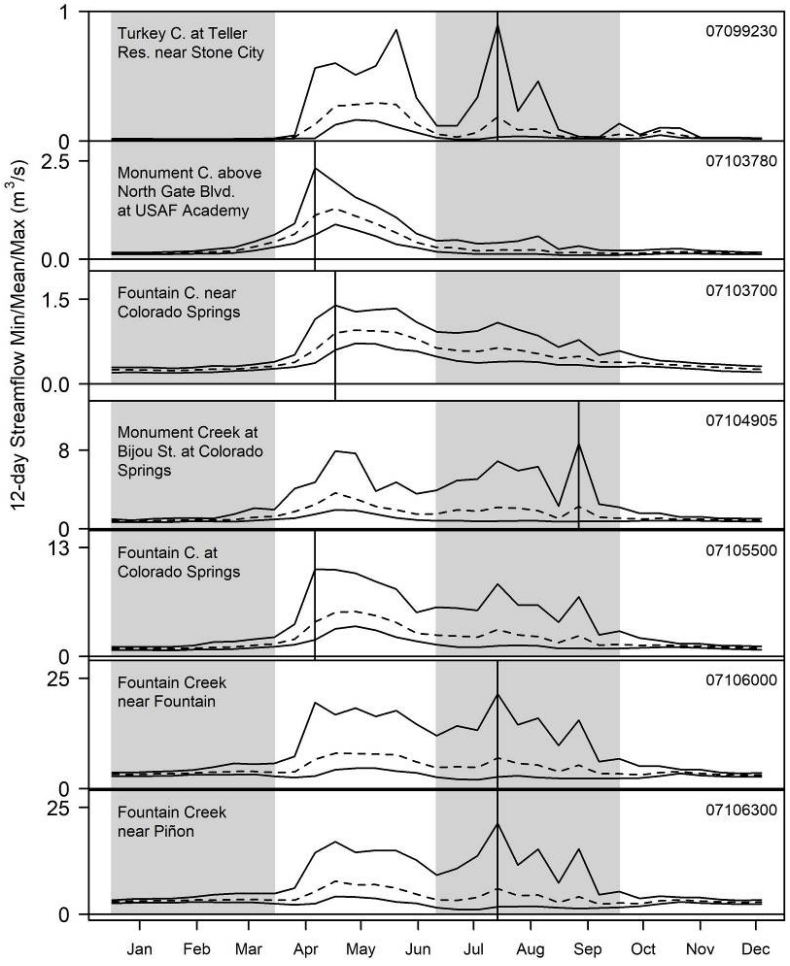

b)

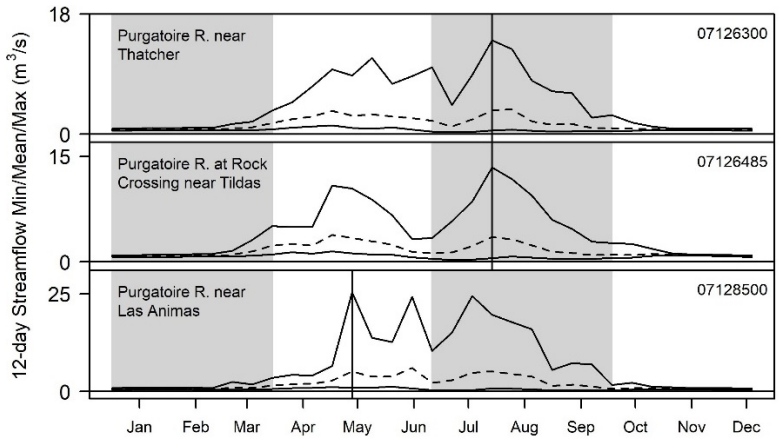

Figure 3-28. (*a*) Maximum and (*b*) minimum streamflow (*Q*) trends (%) for the USGS stations in Colorado. *Circles* indicate the trends for 12 days, *rectangles* indicate seasonal results, and the annual trend is given in the *lower left box*. Statistical significance is shown: the 99th percentile (*dark gray*), the 95th percentile (*light gray*), and nonsignificant results (*white*). Midmonth dates are shown on the x-axis. Sites are ordered by basin size. All trend results are reported in Appendix A.3.

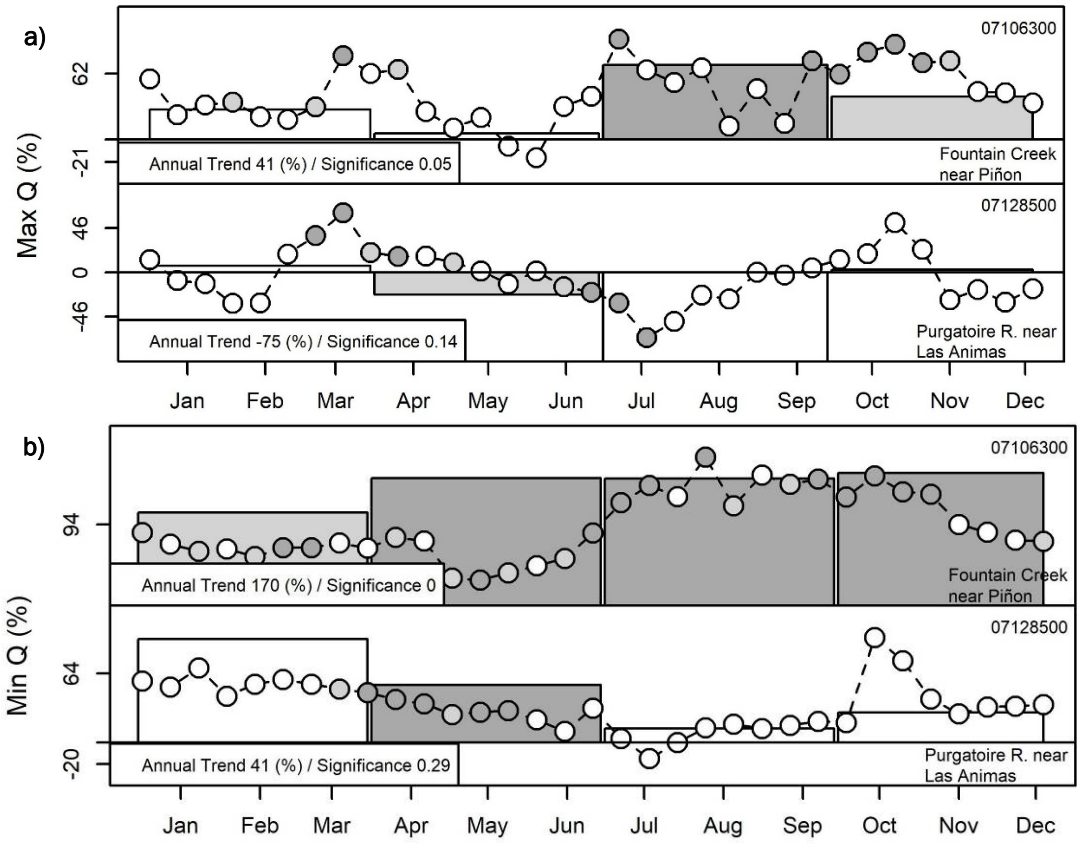

All stations in the river systems were best modeled with either an S or LNS for the yearly maximum streamflow (Figure 3-29). This was also true when looking at the GEV results for the seasonal analysis (see Figure A-8 in Appendix A.3). Monument Creek at Bijou Street at the Colorado Spring (07104905) station is the only station that did not result in an LNS model during any season. The only station that experienced a large increase in maximum streamflow was at the Fountain Creek near the Colorado Springs gaging station (07103700) during spring (JFM). The best fit GEV model overall during spring was an LNS model.

Figure 3-29. Annual maximum streamflow GEV results and streamflow seasonal maximums (*blue circles*) for the Colorado stations Turkey Creek at Teller Res near Stone City (TURK), Fountain Creek near Colorado Springs (FNCS), Monument Creek above North Gate Blvd. at USAF Academy (MCUSAF), Monument Creek at Bijou Street at Colorado Springs (MCCS), Fountain Creek at Colorado Springs (FCCS), Fountain Creek near Piñon (FCF), Purgatoire River near Thatcher (PURT), Purgatoire River at Rock Crossing near Timpas (PRRCT), and Purgatoire River near Las Animas (PTLA). Return intervals (T = 2, 5, 10, 20, 50, and 100 years) from the GEV fits are shown in *dashed lines*. All GEV results are reported in Appendix A.3.

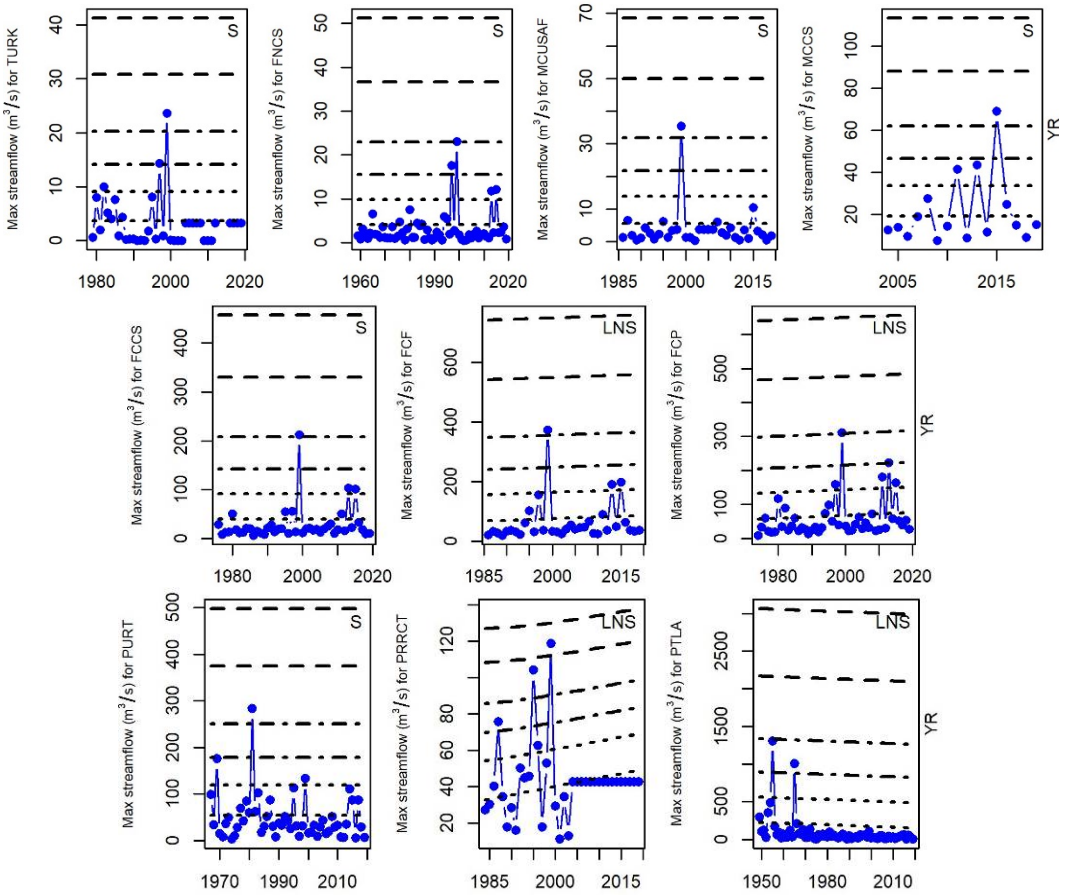

3.3.4.3 Projection of future streamflow, Colorado

In addition to the SWE comparison validation for the snow modeling presented in section 3.3.2, we compared measured and simulated streamflow for the Fountain Creek near Piñon (07106300) USGS station in the Fountain HUC 8 watershed. There was a shift in peak streamflow from early August to mid-May for the modeled (VIC) streamflow output when compared with the observed (Figure 3-30). The observed multiple higher flows in late summer were not duplicated with VIC. Because these streamflow modeling results did not reflect measured streamflow, we did not model future projections for this site.

Figure 3-30. Streamflow comparison between measured and modeled (VIC) for the Fountain Creek near Piñon USGS station. The *vertical line* indicates peak streamflow. *Gray* shaded fields show JFM and JAS, and *white* fields indicate AMJ and OND. Midmonth dates are shown on the x-axis.

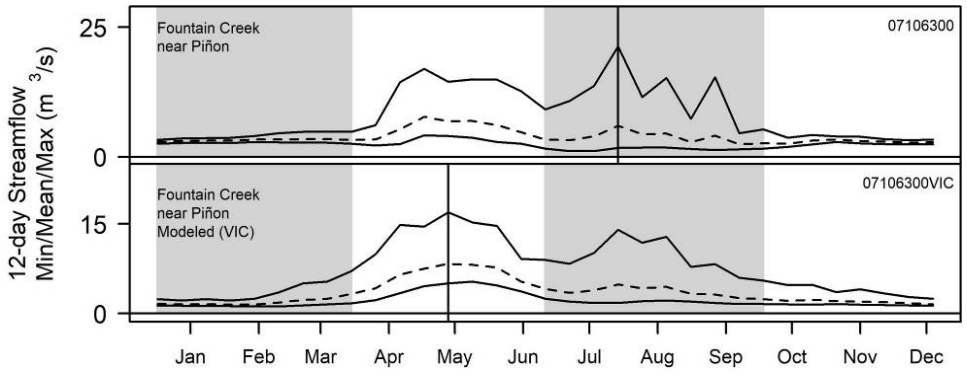

3.3.5 Probability of occurance of annual maximum precipitation depths, Colorado

We analyzed the maximum annual precipitation in the Colorado site for 15 meteorological stations, many located at lower elevations (~1,200 m); and the highest elevation station was at Ruxton Park at 2,800 m (see Table A-8 in Appendix A.1). Figure 3-31 shows the stations with the highest annual maximum precipitation; the analysis results of the other stations are in Appendix A.3 (see Figure A-9). The highest annual maximum daily precipitation of 160 mm was at the Rocky Ford 2 SE (southeast) station, one of the lowest-altitude stations (1,271 m). Other stations with annual maximum daily precipitation higher than 100 mm included Colorado Springs Municipal Airport, the meteorological station closest to Fort Carson, and the Trinidad Airport. The upper and lower boundary of the 95% confidence level at the 100-year return period of the annual maximum daily precipitation varies greatly between each site where the range was about 20 mm at the Las Animas station and 40 mm at the Colorado Springs Airport station.

We used selected global climate models to derive projected annual maximum daily precipitation curves for the center of the Fort Carson installation (see section 2.6). These curves were compared to the historical annual maximum daily precipitation at Colorado Springs Municipal Airport (Figure 3-32). The comparison indicated that the historical annual maximum daily precipitation was, on average, in the midrange of the global models. The highest annual maximum daily precipitation at a return period of 100 years of selected climate models was 320 mm. At a return period of 100

years, the upper range of the 95% confidence level for the projected precipitation was 227 mm, which is about a 70% increase when compared to the current climate at the Colorado Springs Municipal Airport. The range between the lower and upper boundary 95% confidence level between climate models at this return period was 160 mm.

Figure 3-31. Probability of annual maximum daily precipitation depths for meteorological stations at the Colorado site (Colorado Springs Municipal Airport, Rocky Ford 2 SE, and Trinidad Airport). All annual maximum daily precipitation results are reported in Appendix A.3.

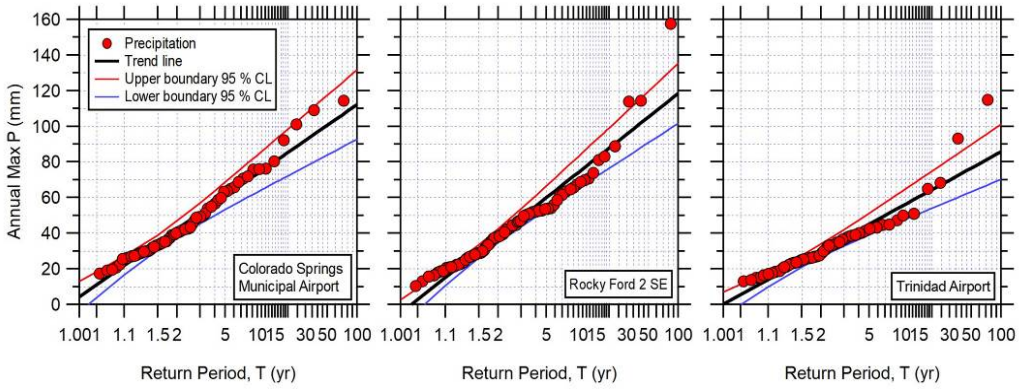

Figure 3-32. Projected annual maximum daily precipitation depths at Fort Carson, Colorado, from global climate models (*circles*) as compared to the historical annual maximum daily precipitation curve at Colorado Springs Municipal Airport (*solid red circles*), including the upper (*red line*) and lower (*blue line*) 95% confidence levels. *Dashed lines* indicate the upper- and lower-boundary confidence levels for Colorado Springs Airport 1948–2019.

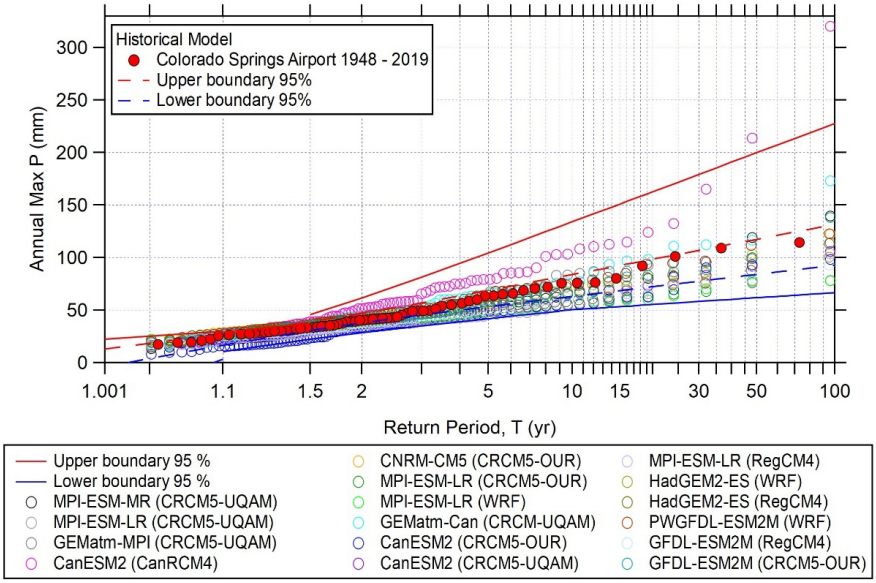

3.3.6 IDF curves, Colorado

We used three meteorological sites that each showed a trend of low, medium, and high annual maximum daily precipitation from section 3.3.5 to produce IDF curves. Many stations showed similar maximum annual precipitation; but we selected Colorado Springs Municipal station (high), Pueblo Memorial Airport (medium), and Rocky Ford 2 SE (low) as example datasets (see full set of stations in Figure A-9, Appendix A.3) for the analysis of IDF curves (Figure 3-33). Between these locations, the rainfall intensity for the 100-year return period at a 1 hr duration was about a twofold difference; the lowest intensity (63 mm/hr) was at Rocky Ford 2 SE, and the highest intensity (112 mm/hr) was at Colorado Springs Municipal Airport.

Figure 3-33. IDF curves for three meteorological stations in the Colorado site.

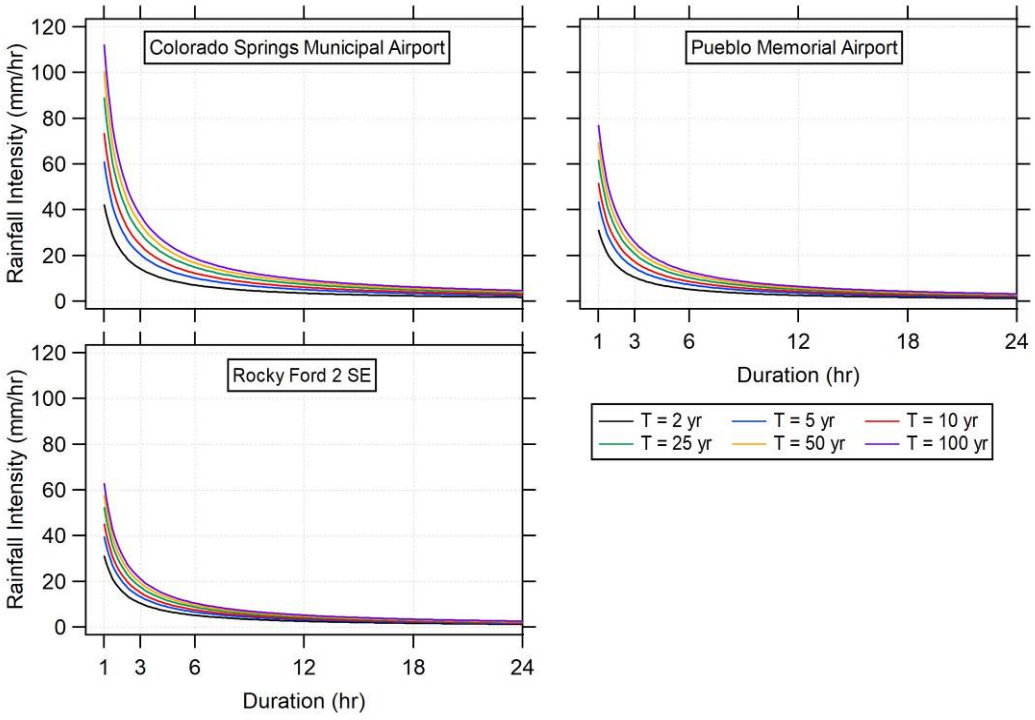

To define the future IDF curves, we selected the annual maximum daily rainfall from the climate model that produced the lowest confidence level (Max Planck Institute for Meteorology's Earth System WRF Model, MPI-ESM-LR [WRF]) and highest confidence level (CanESM2 [CanRCM4]) at Fort Carson (see confidence levels in Figure 3-32). Higher rainfall intensity was predicted at the Fort Carson installation when compared to Colorado Springs Municipal Airport (Figure 3-34). The MPI-ESM-LR (WRF) model produced the lowest rainfall intensity at a return period of 100

years and a duration of 1 hr, 76 mm/hr. In comparison, the CanESM2 (CanRCM4) model resulted in about a 2.5 times higher rainfall intensity (194 mm/hr) for the same return period and duration.

Figure 3-34. Estimated future IDF curves for a location at the center of the Fort Carson installation, Colorado. For comparison, *black dashed lines* illustrate historical IDF curves from the Colorado Springs Municipal Airport.

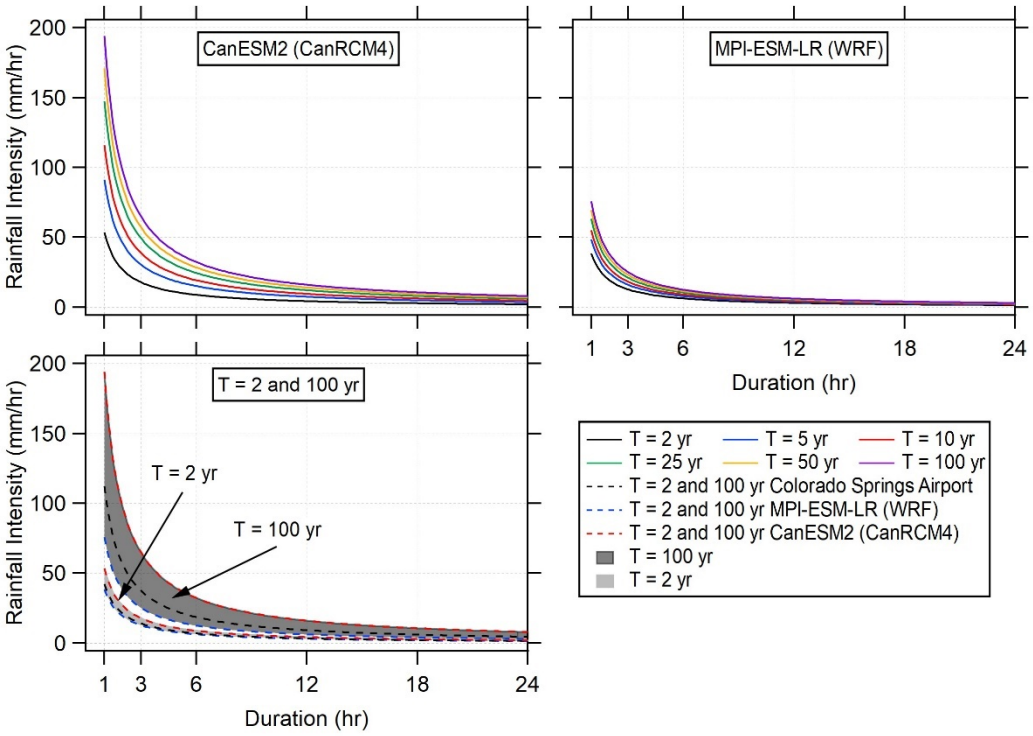

3.4 North Dakota

3.4.1 Field measurements, North Dakota

Figure 3-35 shows the daily measurements from the time-lapse cameras for 2015–2018 from our three sites (Landfill, Prairie, and Mekinok). One of the Landfill site's stakes is in a low-lying ditch where blowing snow accumulates, and the other stake is located in a mowed grass field; the other sites are grassland (Prairie) and tilled land (Mekinok). Winter 2015–2016 was unusually warm, and snow melted in late winter. At the Prairie and Mekinok sites, snowmelt occurred mid-February. The snow cover at the Landfill site's drift lingered for another month. In the following two seasons, the snowmelt season occurred later. In fact, in 2017–2018, the snowmelt at the Prairie and Mekinok sites occurred about two months later than in 2015–2016. A maximum snow depth of 100 cm was measured in early January 2016 at the Landfill site. In comparison, the maximum snow

depth at this site was 60 cm in late January 2015, indicating that the snow cover varied greatly between years and that wind played an outsized role in snow distributions. At the other sites, a maximum snow depth was closer to 40 cm.

Figure 3-35. Daily snow depths at the time-lapse cameras at or close to GFAFB, North Dakota, from 2015 to 2018. In 2017–2018, the Landfill time-lapse camera failed after deployment.

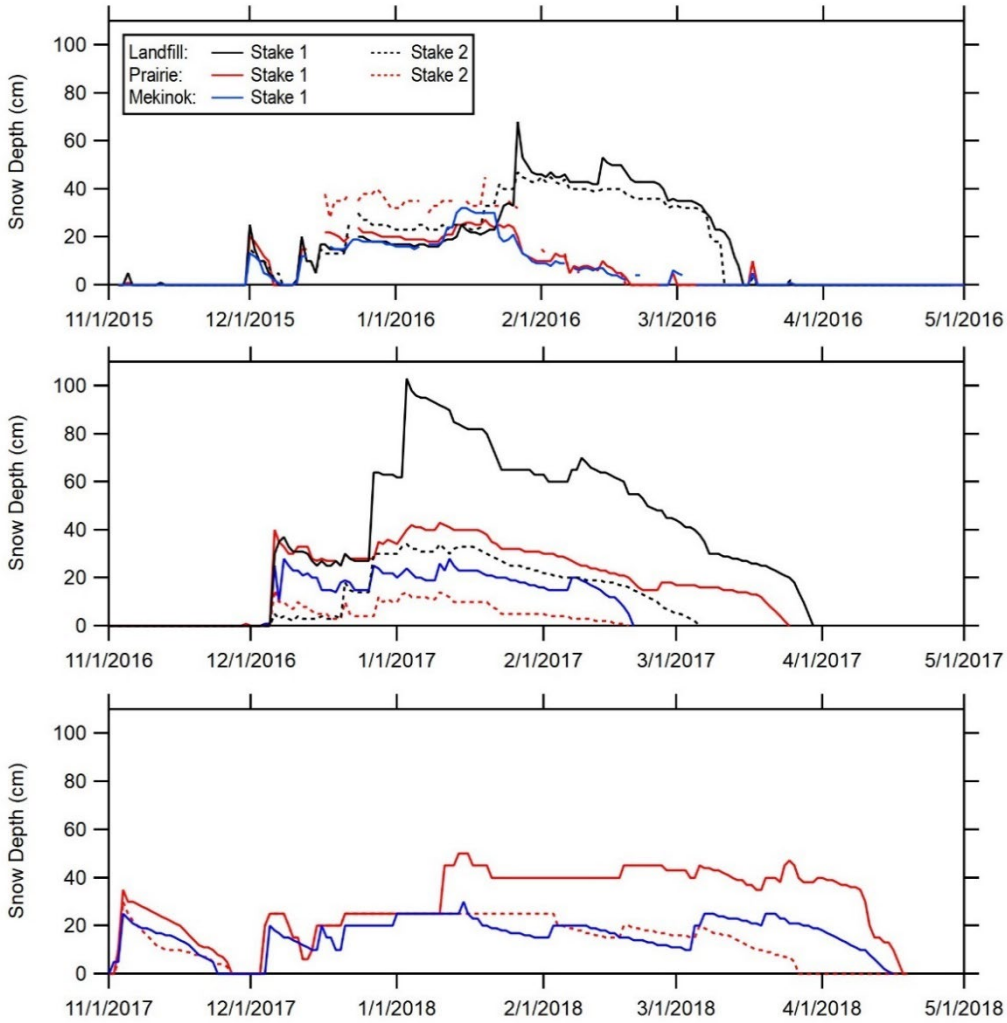

In 2016 (17 February) and 2017 (17 January), we measured nearly 3,400 snow depths each year at four locations (Figure 3-36). On 12 February 2018, close to 5,000 snow depths were measured. In 2015–2016, the average snow depth was 12.4 cm and the measured snow depths ranged from 0 to 108 cm. We collected 45 SWE samples, and the mean was 37 mm. The snow densities were between 244 and 452 kg/m^3. The maximum measured snow depth was more than 1.5 times deeper compared to the previous year (175 cm), and the mean snow depth was almost three times deeper

(33.7 cm). During the following year (2017–2018) the measured snow depth was similar to 2015–2016, with a maximum snow depth of 92 cm and a mean snow depth of 17.7 cm. There were 21 snow samples collected across 10 sites. On average, total SWE was from 2 to 12.5 mm; density values were from 200 to 319 kg/m^3.

Figure 3-36. (*a*) Snow-depth statistics and locations of observed (obs) measurements and modeled (mod) and (*b*) a close up of snow-depth measurement locations at GFAFB, North Dakota, during the 2015–2018 field seasons.

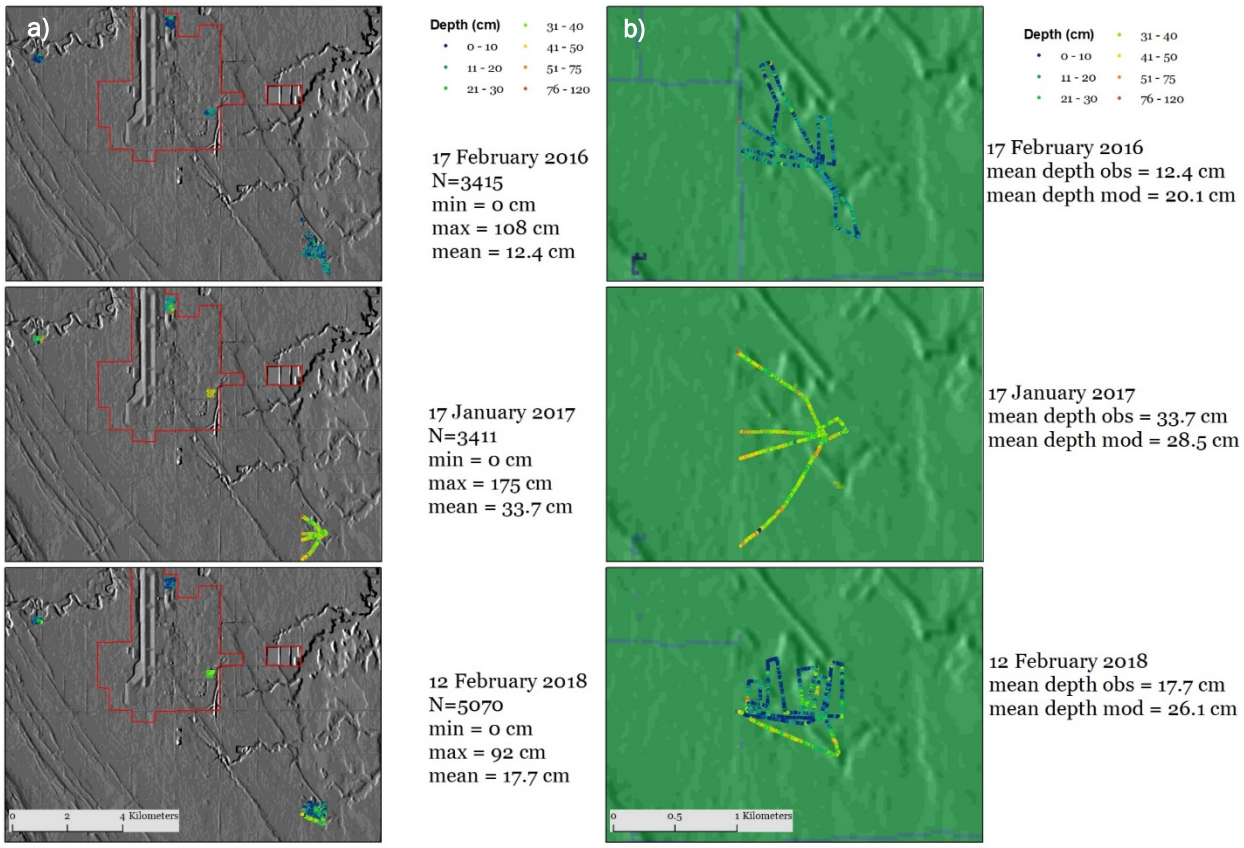

3.4.2 Snow-model (VIC and SnowModel) validation, North Dakota

3.4.2.1 Snow-model validation to field measurements, North Dakota

We performed with SnowModel fine-resolution snow-depth simulations for the North Dakota site for three winter seasons to validate the snow model (Figure 3-37). The observed snow depth was 8 cm higher than the modeled snow depths for 2 years (2015–2016 and 2017–2018) and slightly lower (5 cm) for the 2016–2017 season (Figure 3-36). These results were an indication that the snow model performs well for this site.

Figure 3-37. Fine resolution snow-depth simulation for the North Dakota site.

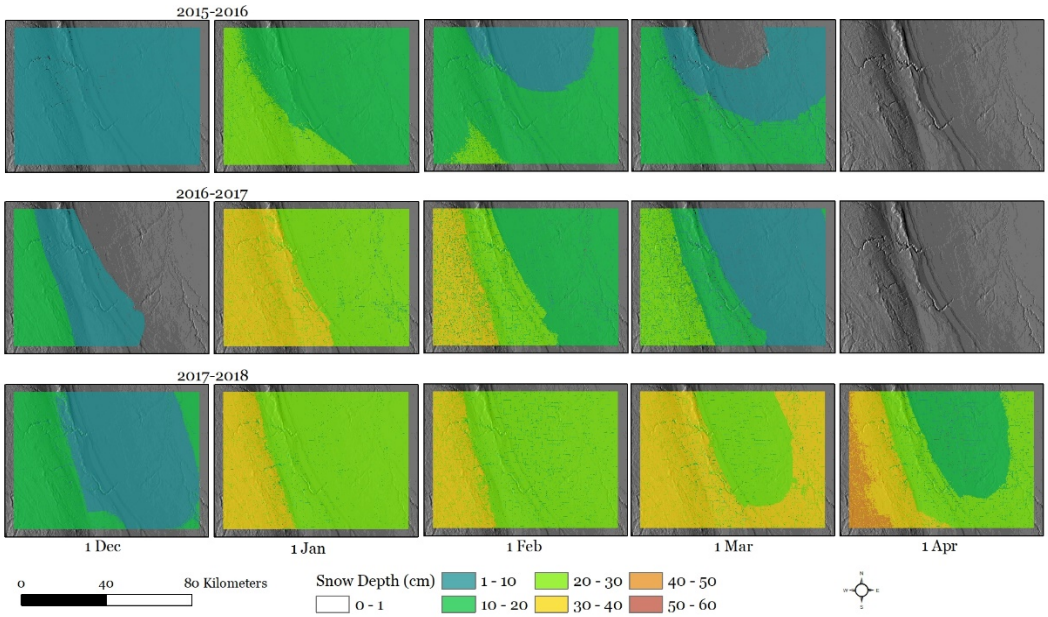

3.4.2.2 Snow-model validation to SWE, North Dakota

In addition to the fine-resolution snow-model validation, we also compared the snow-model snow-depth outputs with measurements from 11 meteorological stations where elevations varied from 260 to 480 m (see Table A-3 in Appendix A.1). Not surprisingly, there was a clear variation of SWE between years and stations. At Grand Forks International Airport, the lowest measured SWE between 1979 and 2015 was 23 mm (1999), and the maximum SWE was more than tenfold higher 10 years earlier (275 mm in 1989; Figure 3-38). Most stations had a maximum SWE of 200 mm or less, and only three stations (Thorhult, Grand Forks International Airport, and Mahnomen) measured maximum SWE over 300 mm (see Figure A-10 in Appendix A.4).

Only one meteorological station, Grand Forks Air Force Base (AFB), was located within the watershed where the VIC hydrological model was performed. At this station, the SnowModel slightly underestimated SWE and VIC even more so (see Figure 3-38). In general, the SnowModel produced slightly lower SWE than observed values (Figure A-10 in Appendix A.4).

Figure 3-38. SWE comparison between VIC, SnowModel, and measured for Grand Forks AFB and Grand Forks International Airport, North Dakota. All SWE results are reported in Appendix A.4.

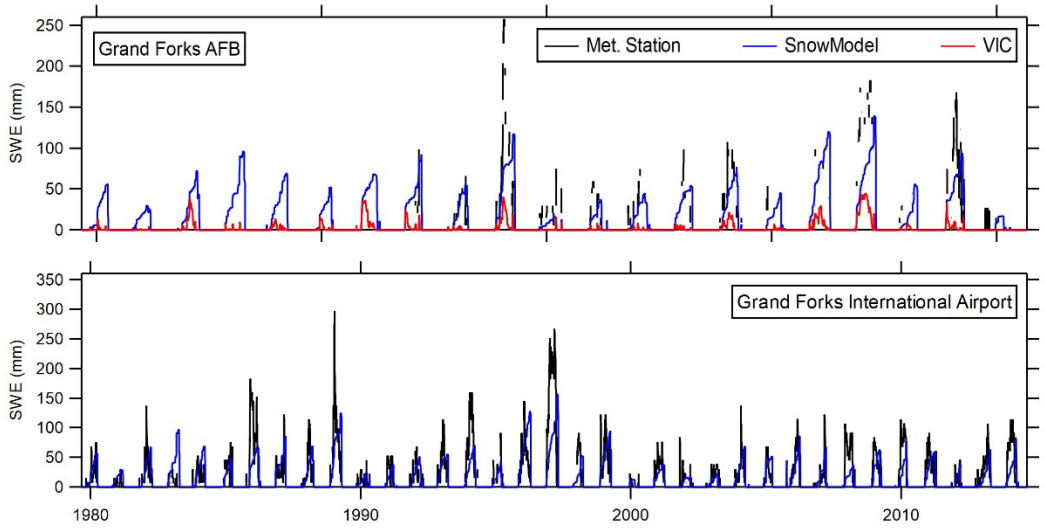

3.4.3 Snow trends and future projections, North Dakota

We compared the simulated SWE evolution for a higher-elevation location in the Turtle River watershed and at the Grand Forks AFB meteorological station for the simulations from 1979 to 2015 (Figure 3-39). Both locations indicate a slight downward trend with a decrease of less than 4 mm/decade.

Figure 3-39. SWE evolution and trends at two stations in the North Dakota site.

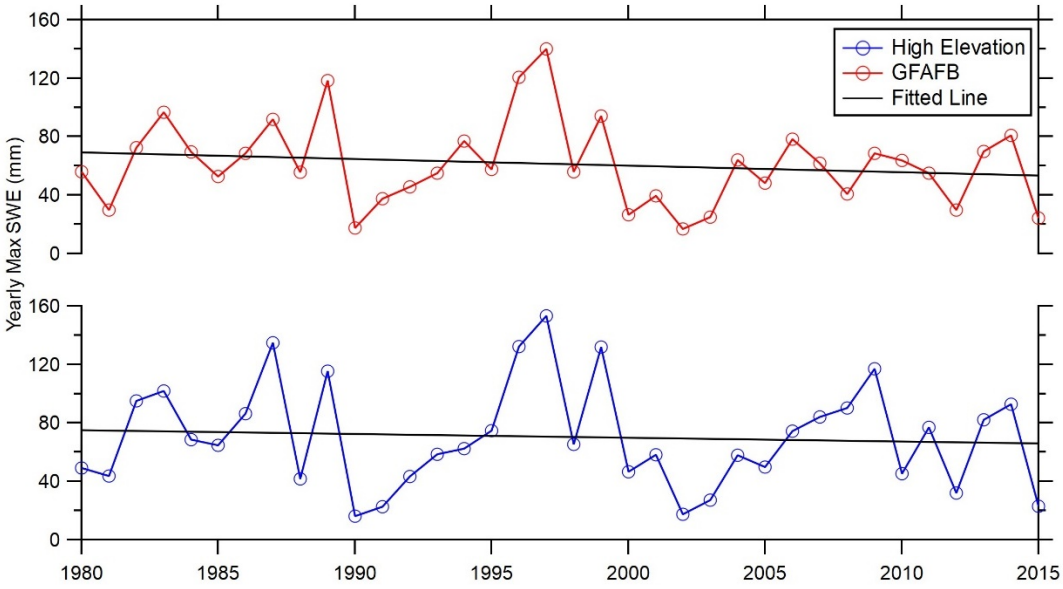

The SnowModel simulations indicate that the 36-year average (1979–2015) of snow duration during the core snow season varies between 90 and 140 days (Figure 3-40*a*–*c*), with a longer duration in the north compared to the south. The trend in snow-cover duration during the 36-year simulations indicated that most of the site experience a decreasing number of snow-covered days with areas of up to 16 days/decade. Only some localized areas in the southeast increased the number of snow-covered days up to 16 days/decade. The yearly and area-averaged snow duration for the 36-year period shows a decreasing trend of about 30 days.

There were almost no ROS events in the simulation site (Figure 3-40*d*–*f*). An increasing trend in the northwest compared to the southeast for ROS was simulated, but the increase and decrease were negligible (between −0.4 to 0.4 days/decade). The maximum number of ROS events (2 days) occurred only twice (Figure 3-40*f*) during the 36-year simulation (the yearly and area-averaged ROS events for the site).

During the 36-year period, simulations resulted in an average yearly snowmelt runoff between 9 and 17 cm within the site (Figure 3-40*g*–*i*). An increasing trend of snowmelt runoff is evident in the northwest and southern area while the remaining area of this site experienced a decreasing trend. Conversely, the remaining area of the site experienced a decreasing trend. Overall, these trends were very small (±2 cm/decade). The yearly and area-averaged snowmelt runoff for the 36-year period decreased by 4 cm.

We performed a future projection of snow duration and compared it with the current climate (CTL). The current snow duration (Figure 3-41) was the same length of season as the 1979–2015 simulation (Figure 3-40*a*), but the pattern was slightly different. When comparing the PGW with the CTL simulations, there was an overall decreasing trend in snow duration down to 60 days with the greatest decrease in the northeast.

Figure 3-40. (*a*) The 36-year average snow duration during the core snow season (days) for the North Dakota site, (*b*) the trend in snow-cover duration (days/decade), and (*c*) yearly and area-averaged snow duration for the simulation in (*a*) and (*b*). (*d*) The 36-year average rain ROS events (days), I the trend in ROS events (days/decade), and (*f*) yearly and area-averaged ROS events (days) for the simulation site in (*d*) and I. (*g*) The 36-year average total annual water equivalent snowmelt runoff (cm), (*h*) the trend in snowmelt (cm/decade), and (*i*) yearly and area-averaged total annual snowmelt runoff for the simulation site in (*g*) and (*h*). North is *up*.

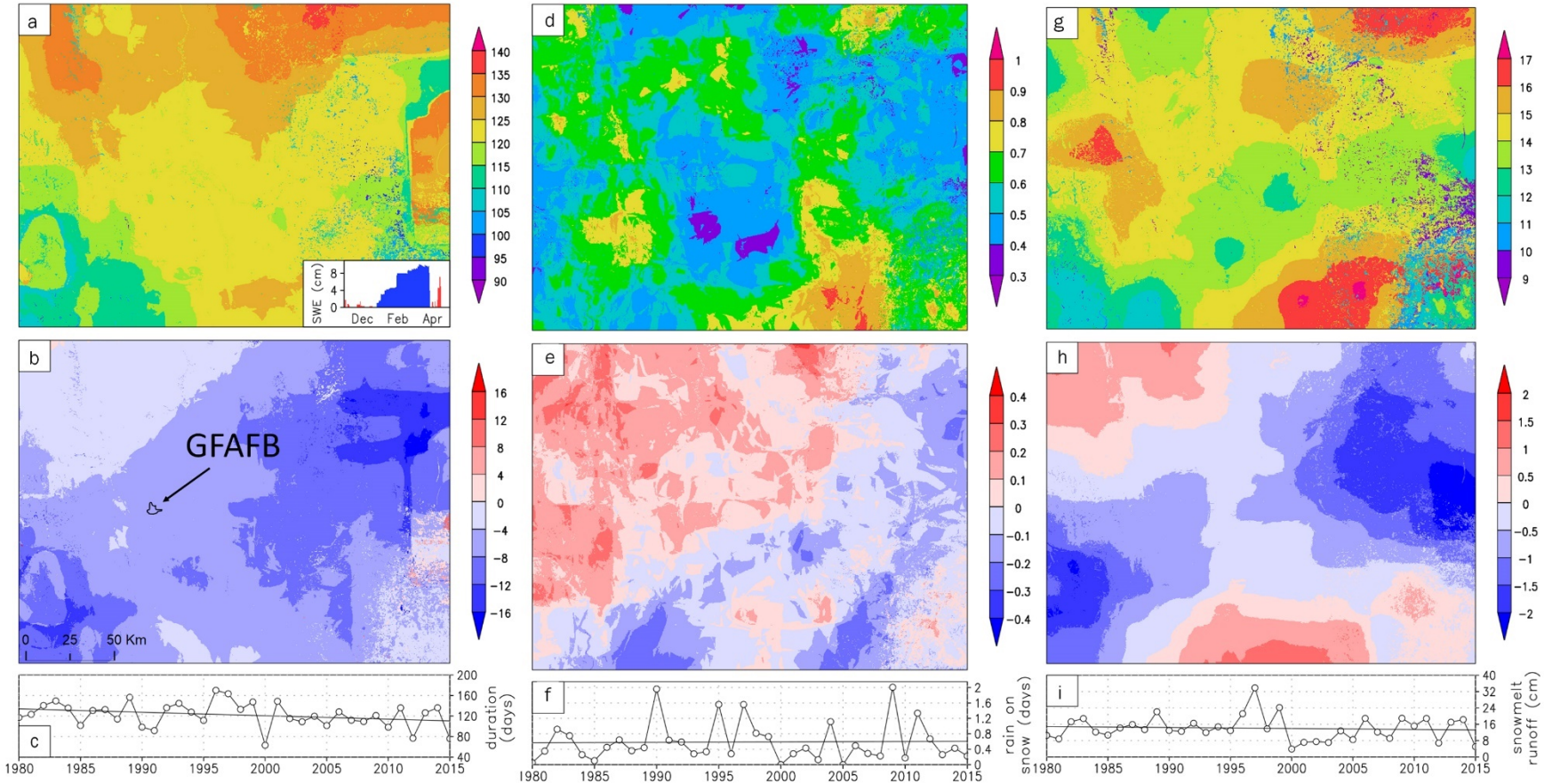

Figure 3-41. Snow duration for historical (CTL) and future (PGW) climate models (*left*) and the difference trend in snow-cover duration (days) between the future and control (*right*) for the North Dakota site. North is *up*.

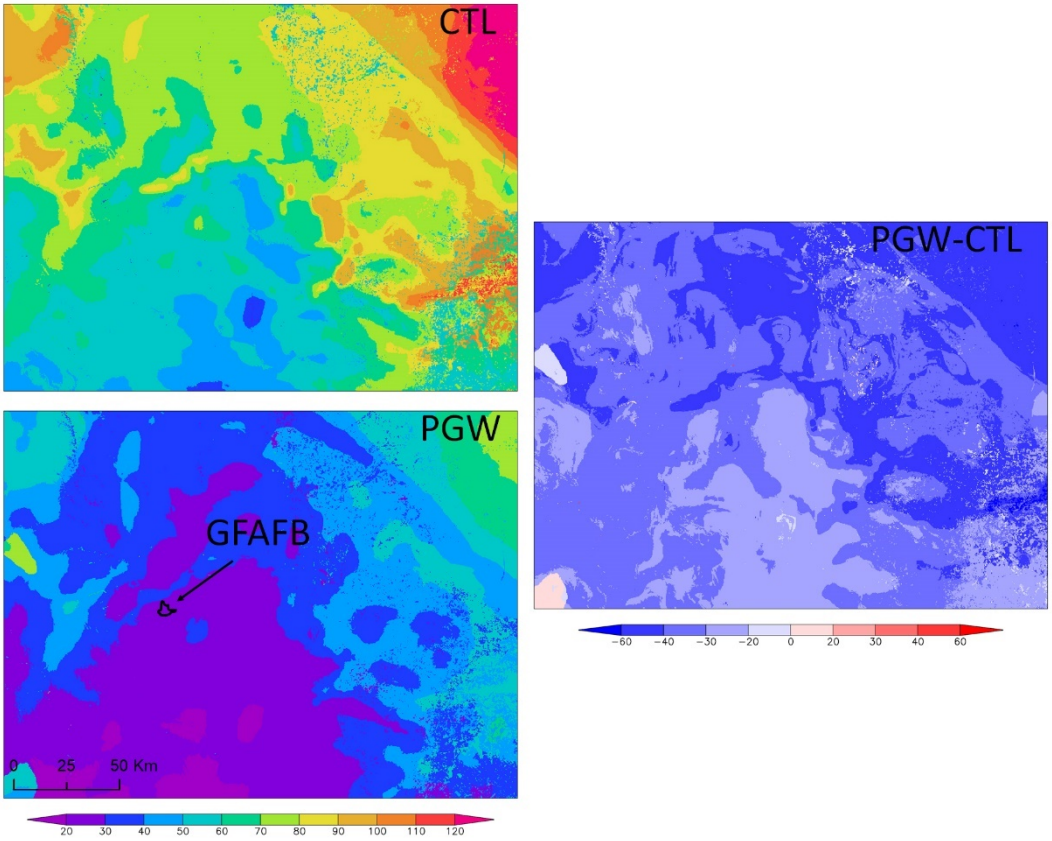

3.4.4 Flood and streamflow analysis, North Dakota

3.4.4.1 Historical flood frequency curves, North Dakota

We used discharge from 10 USGS gaging stations within the study site to calculate the return period of annual peak flows for basin sizes ranging from 60 to 1,900 km^2 (see Figure 2-12 and also Table A-6 in Appendix A.1). The annual maximum peak flow at the USGS station within the watershed upstream of GFAFB, North Dakota, was 350 m^3/s (Turtle River at Turtle River State Park near Arvilla, USGS station 05082625; Figure 3-42). Appendix A provides the return periods for the other stations (see Figure A-11 in Appendix A.4). The highest annual maximum peak flow recorded of the 10 stations was 800 m^3/s, and it was measured downstream of GFAFB at Turtle River at Manvel (05083000). The longest available peak flow record, 90 years, was at the Park River at Grafton gage (05090000).

Figure 3-42. Return period of maximum annual peak flow at the Turtle River at Turtle River State Park near Arvilla in the North Dakota site. All annual peak flow results are reported in Appendix A.4.

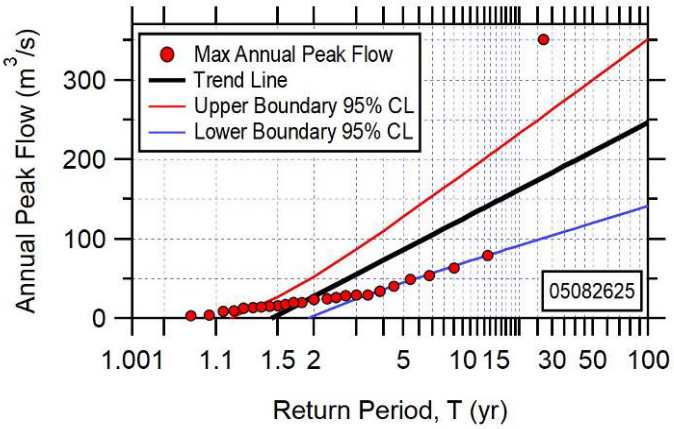

3.4.4.2 Historical streamflow analysis, North Dakota

Out of the 10 USGS stations, we selected for the seasonal streamflow analysis only those where discharge was monitored by USGS through 2019 (see Figure 2-12 and also Table A-6 in Appendix A.1). This included four USGS gages in the Park, Forest, and Turtle HUC 8 watersheds: Turtle River at Turtle River State Park near Arvilla (050862625), Forest River near Fordville (05084000), Forest River at Minto (05085000), and Park River at Grafton (05090000). Figure 3-43 shows the mean, maximum, and minimum streamflow and peak flows. The peak 12-day streamflow at the four stations occurred between late March to mid-April, where the largest watersheds, with areas of 1,917 (05085000) and 1,801 km^2 (05090000), had maximum peak flow of 30 m^3/s and 35 m^3/s, respectively. The streamflow at the Turtle River at Turtle River State Park near Arvilla station (05082625), the only station upstream of GFAFB that was analyzed, indicated a second peak occurring in early June that was not measured at any of the other three gages.

We analyzed the same four USGS gages used for seasonal streamflow trends. Only the Park River at Grafton station (05090000) indicated a statistically significant increase in annual streamflow (>90th percentile; see Table A-12 in Appendix A.4). Turtle River at Turtle River State Park near Arvilla (50862625) was the only station that did not experience a statistically increasing trend (>90th percentile) for annual minimum streamflow. There was a statistically significant increase of maximum streamflow both early and later in the season (January–February and May–December) for

three of the four stations (Figure 3-44). In fact, April was the only month not showing any increasing streamflow trends. The upstream station of GFAFB (the Turtle River at Turtle River State Park near Arvilla, 05082625) had a statistically significant increase in minimum flow for 4 months and no statistically significant difference for the monthly maximum streamflow.

The annual maximum streamflow at all stations was best modeled with the stationary GEV model (Figure 3-45). This model was also the best fit for early spring (AMJ) (see Table A-12 in Appendix A.4). For the other seasons, the stations were best modeled with either an S or an LNS model. For the late season (JAS and OND), an LNS model was the best fit for all stations except one (Turtle River at Turtle River State Park near Arvilla, 050862625).

Figure 3-43. Mean (*dashed*), maximum, and minimum streamflow hydrographs for 12-day composites for the USGS gages (*upper left* and *right corners*) in the North Dakota site. The *vertical line* indicates peak streamflow. *Gray* shaded fields show JFM and JAS, and *white* indicate AMJ and OND. Midmonth dates are shown on the x-axis. Sites are ordered by basin size.

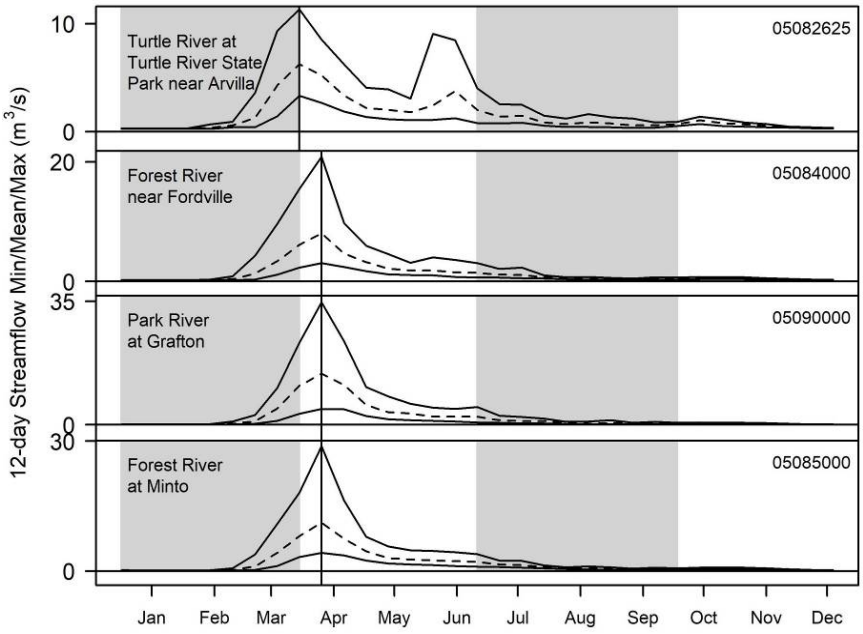

Figure 3-44. (*a*) Maximum and (*b*) minimum streamflow (*Q*) trends (%) for the USGS stations in North Dakota. *Circles* indicate the trends for 12 days, *rectangles* indicate seasonal results, and the annual trend is given in the *lower left box*. Statistical significance is shown: the 99th percentile (*dark gray*), the 95th percentile (*light gray*), and nonsignificant results (*white*). Midmonth dates are shown on the x-axis. Sites are ordered by basin size.

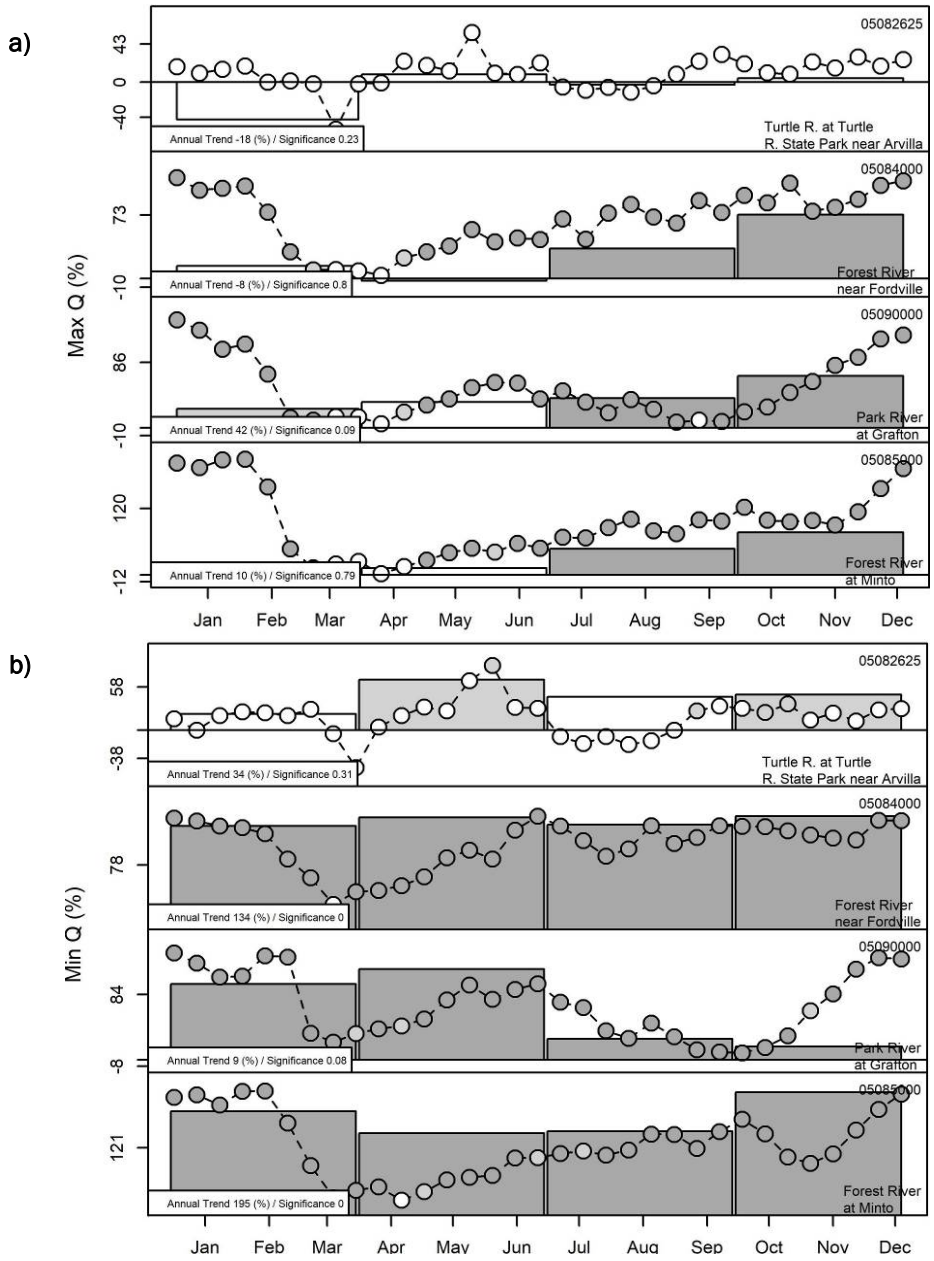

Figure 3-45. Annual maximum streamflow GEV results and streamflow seasonal maximums (*blue circles*) for the North Dakota stations Turtle River at Turtle River State Park near Arvilla (TUR), Forest River near Fordville (FOR), Forest River at Minto (MIN), and Park River at Grafton (PAR) Return intervals (T = 2, 5, 10, 20, 50, and 100 years) from the GEV fits are shown in *dashed lines*. All GEV results are reported in Appendix A.4.

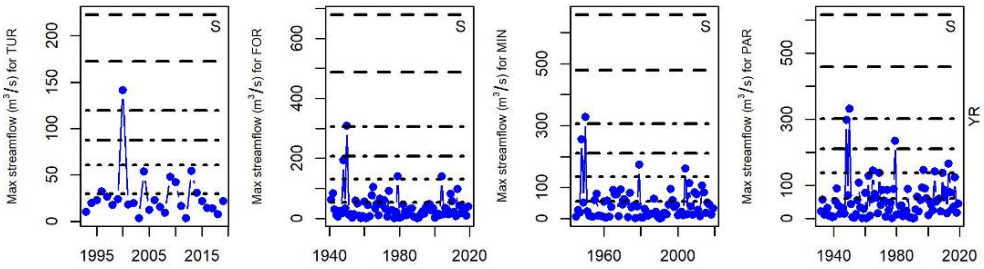

3.4.4.3 Projection of future streamflow, North Dakota

We compared the 12-day average streamflow at the Turtle River at Turtle River State Park near Arvilla (05082625) and the hydrological models to determine if the hydrological models could be used to generate a projected streamflow (Figure 3-46). The VIC model output for the USGS station 05062625 (05062625VIC) resulted in a later peak flow than observed at the USGS gage, and the peak flow generated at the same station from the HydroFlow model (05082625Hydro) coincides with the peak flow at the USGS gage; but the modeled magnitude was smaller than observed. The secondary peak measured in June was also duplicated with HydroFlow, but the model also produced a streamflow from June through November that was higher than the observed. Because of these results, we did not pursue future projections of streamflow for this site.

Figure 3-46. Mean (*dashed*), maximum, and minimum streamflow hydrographs for 12-day composites for the Turtle River at Turtle River State Park near Arvilla (05082625) (*top panel*) in the North Dakota site. The *vertical line* indicates peak streamflow. *Gray* shaded fields show JFM and JAS, and *white* fields indicate AMJ and OND. Midmonth dates are shown on the x-axis. Historical VIC (05082625VIC) and future HydroFlow (05082625Hydro) are also shown.

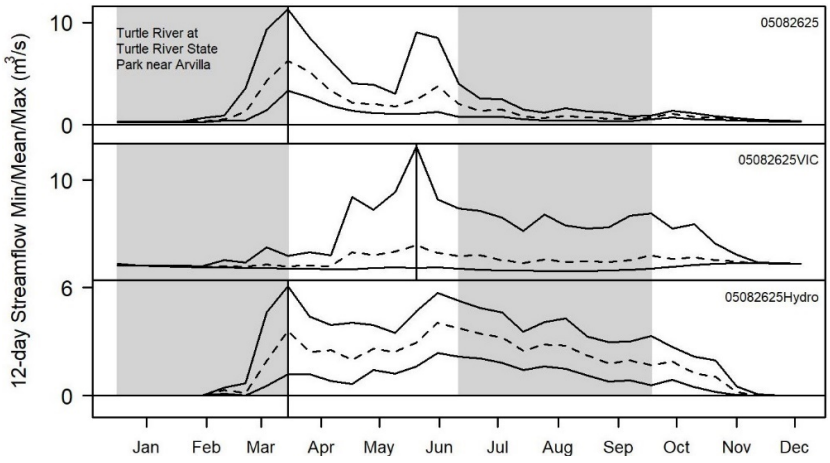

3.4.5 Probability of occurance of annual maximum daily precipitation depth, North Dakota

We analyzed 12 meteorological stations for maximum annual precipitation (see Table A-9 in Appendix A.1). The topographic relief at this site was only 240 m (from 250 m to 490 m). The annual maximum daily precipitation for the 100-year return period at the Grand Forks International Airport, the station closest to GFAFB, was 110 mm (Figure 3-47); and the range of the 95% confidence level at a return period of 100 years was 40 mm. The lowest and highest annual maximum precipitation for the 100-year return period (100 mm and 200 mm) was at the Petersburg and Larimore station, respectively (see Figure A-13 in Appendix A.4). The widest range of the 95% confidence level at the 100-year return period of the annual maximum daily precipitation was at the Drayton station (75 mm).

A projection of annual maximum daily precipitation curves for the center of the GFAFB was performed using a selection of climate models (see section 2.6). The closest station to GFAFB, Grand Forks International Airport, was used in the comparison to the global models. Results indicated that projected annual maximum daily precipitation at this location produced similar return periods as observed in the current climate (Figure 3-48). The maximum annual precipitation of the global models was close to 190 mm at a return period of 100 years. The range of the 95% confidence level of the annual maximum daily precipitation between the global climate models was 100 mm at a return level of 100 years.

Figure 3-47. Annual maximum daily precipitation depth for the Grand Forks International Airport meteorological station at the North Dakota site. All annual maximum daily precipitation results are reported in Appendix A.4.

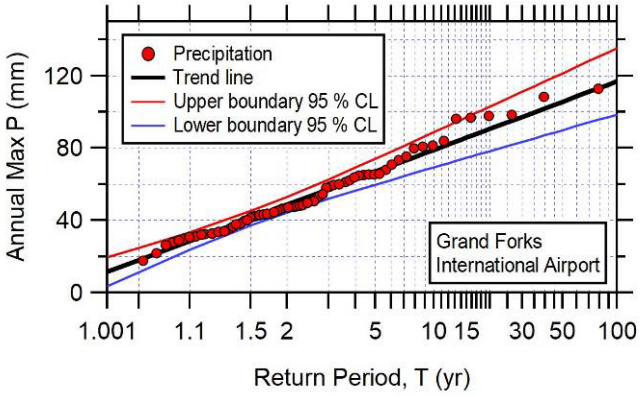

Figure 3-48. Projected annual maximum daily precipitation depth at GFAFB, North Dakota, from global climate models (*circles*) as compared to the historical annual maximum daily precipitation curve at Grand Forks International Airport (*solid red circles*), including the upper (*red line*) and lower (*blue line*) 95% confidence levels. *Dashed lines* indicate the upper- and lower-boundary confidence levels for Grand Forks International Airport 1942–2019.

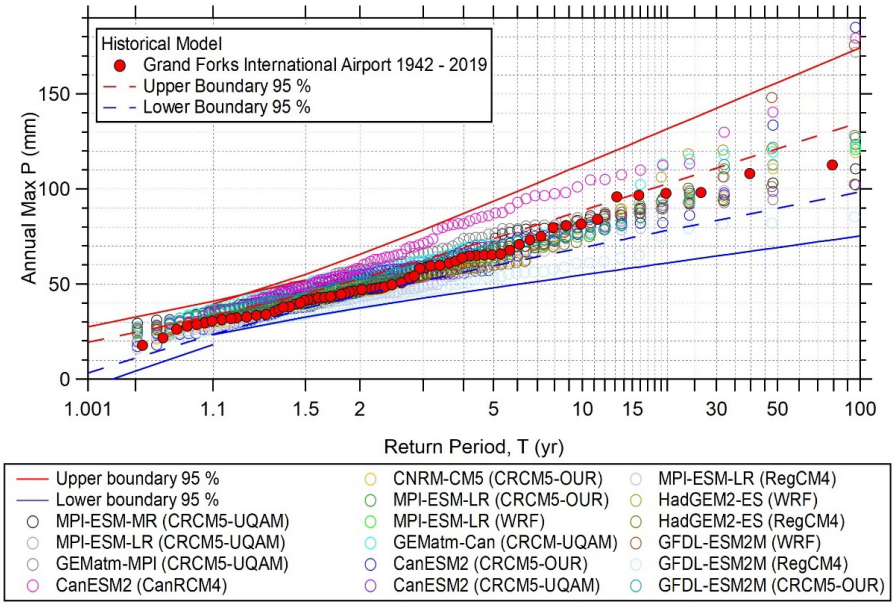

3.4.6 IDF curves, North Dakota

IDF curves were produced from three meteorological stations (a location with low, medium, and high precipitation) from section 3.4.5 in the North Dakota site. The station with the lowest and highest maximum annual precipitation was Petersburg (467 m elev.) and Larimore (351 m elev.), respectively (see Figure A-13 in Appendix A.4). The Grand Forks International Airport (257 m elev.) was chosen as a representative station for the medium annual precipitation, and this station was also located closest to GFAFB. Six return periods (2, 5, 10, 25, 50, and 100 years) were calculated for durations of 1 to 24 hr and are presented in Figure 3-49. IDF curves of these stations showed a wide variation of rainfall intensity. For example, at Larimore, which experienced the highest annual precipitation, the rainfall intensity for a 100-year return period at a 1 hr duration was 156 mm/hr. At Petersburg, the 1 hr duration at the same return period was about half that at the Larimore station.

A range of projected IDF curves was produced for the lowest (GFDL's Earth System Regional Climate Model, GFDL-ESM2M [RegCM4]) and highest (CanESM2 [CanRCM4]) confidence level climate models for the annual maximum daily rainfall (see Figure 3-48). Figure 3-50 shows the

IDF curves and range of rainfall intensity for different return periods of these climate models. The GFDL-ESM2M (RegCM4) (low) and CanESM2 (CanRCM4) (high) models showed a difference in rainfall intensity of 63 mm/hr (89 to 152 mm/hr) for the 1 hr duration at a return period of 100 years (shaded dark gray in Figure 3-50*c*).

Figure 3-49. IDF curves for three meteorological stations, Grand Forks International Airport, Larimore, and Petersburg, at the North Dakota site.

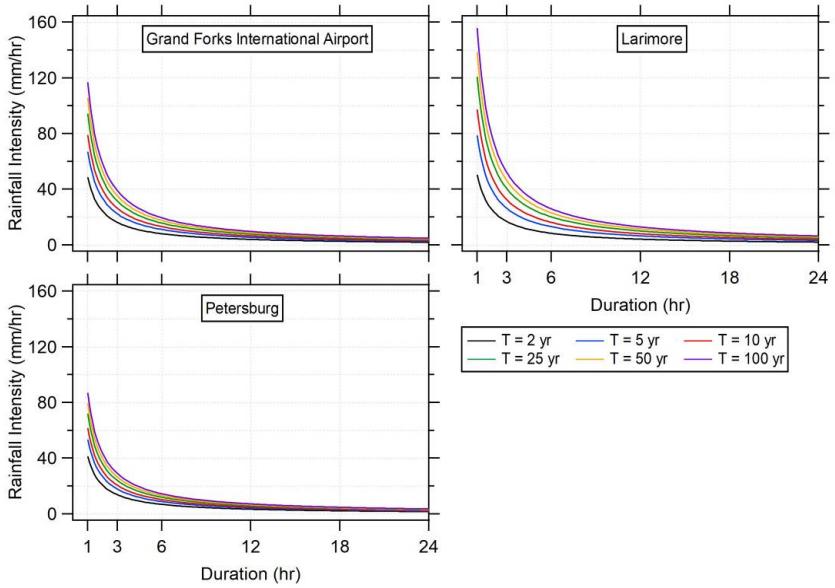

Figure 3-50. Estimated future IDF curves for a location closest to the center of GFAFB, North Dakota, as generated from (*a*) CanESM2 (CanRCM4) and (*b*) GFDL-ESM2M (RegCM4) climate models. (*c*) For comparison, this shows results from both climate models; and *black dashed lines* illustrate the historical IDF curves from Grand Forks International Airport.

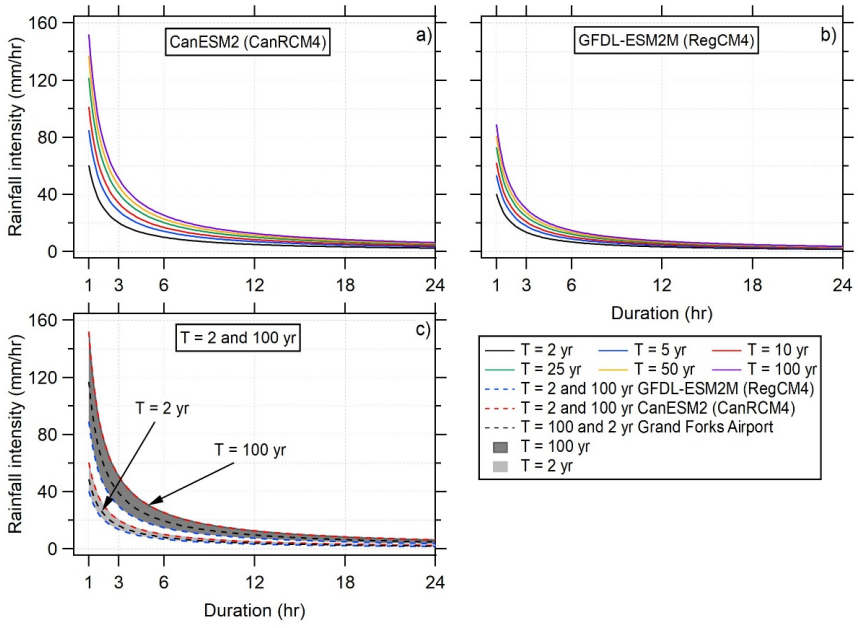

4 Conclusions and Implications for Future Research and Implementation

The main objective of this project was to investigate the timing and intensity of snow accumulation, snowmelt, and runoff for historical and future climate scenarios at regional and watershed scales. Additionally, the objective included producing flood return levels, investigating changes in hydrological extremes using trend analysis, and precipitation return levels and generating current and future IDF curves for our three study sites: YTC, Washington; Fort Carson, Colorado, and GFAFB, North Dakota.

We found that snow arrival, departure, and resultant runoff have been changing across the Western U.S. and within our three study areas since 1979. Changes have not been uniform in trajectory and magnitude, but many areas exhibit declines in snow's longevity and hydrological importance. The yearly and area-averaged 36-year snow duration, ROS, and snowmelt runoff all indicated a decreasing trend. We saw extreme changes in the Washington area where snow duration varied throughout the site, showing a decreasing trend at higher elevations and an increasing trend at lower elevations. The snowmelt runoff in the Washington area decreased drastically, especially at the higher elevations. Such a decreasing trend could result in a decline in water resources for the region. In Colorado, even though most of the area at lower elevations had an increasing snow-duration trend, our analysis indicated a decreasing snowmelt-runoff trend. The decreasing snow-duration trend of up to 16 days/decade in North Dakota could result in a drastic change, considering that the maximum number of snow-duration days in our 36-year historical simulations was 140 days. We detected no apparent change for ROS events in both Colorado and North Dakota, perhaps because of very few initial ROS events in these areas. For example, Washington averaged 50 days/year of ROS events for the 1979–2015 simulation, and Colorado had up to only 10 days/year. In North Dakota, this estimate is 1 day or less ROS event per year. Future projections for snow duration indicated a continuing decreasing snow trend in Washington and North Dakota. Colorado showed an alarming decrease at higher elevations.

We also observed changes in watershed streamflow. All three study areas exhibited flow changes in most seasons, especially winter, most likely due to a warming climate. In Washington, no statistically significant change in

maximum annual trend was found, but a statistically significant increase (>99th percentile) in minimum annual streamflow in the HUC 8 Upper Yakima Watershed was evident. In general, a stationary (S) response illustrated that conditions were not changing in terms of maximum streamflow trend, with two exceptions. An increase in maximum streamflow was exhibited within an upriver watershed of YTC, which was also illustrated by a linear nonstationary (LNS) GEV model in summer. The increase in this basin was also reflected in the statically significant trend analysis during the July–September (JAS) period. Additionally, an LNS GEV trend in maximum streamflow was minimized for the American River near the Nile Basin in winter, also reflected in a strongly increasing maximum streamflow trend during the winter. Colorado area flows were mixed, where statistically significant increases in both minimum and maximum flows were found across all seasons. The Fountain Creek near Fountain and Piñon watersheds that encompassed the east of Fort Carson showed statistically significant increasing trend (>90th percentile) in both annual maximum and minimum flow. In the spring, some basins were minimized by S and a few were minimized by LNS models. The Purgatoire River near Las Animas and Fountain Creek near Fountain and Piñon watersheds were minimized by a decreasing LNS model for the annual streamflow. The North Dakota study site experienced a statistically significant increase in both minimum and maximum flow during all seasons for most stations. The station in the HUC 8 Turtle watershed (upstream of GFAFB) showed no increase in maximum streamflow during any months. On the contrary, the other basins experienced a statistically significant increase in maximum streamflow during most months and an increase in minimum streamflow during all months. At this site, there was a mix of S and LNS models where the minimized fits for the annual streamflow was an S model. All seasons at the basin upstream of GFAFB fit the S model best.

When we performed the future annual maximum daily precipitation depths, we noticed that, out of the 16 climate models applied in the analysis, different climate models produced low and high confidence level for each site. The CanESM2 (CanRCM4) climate model produced the highest confidence level at all sites, implying that this model returns the wettest climate. The driest models (least precipitation) were the lowest-confidence-value climate models, and these varied between sites (GFDL-ESM2M [WRF] at Washington, MPI-ESM-LR [WRF] at Colorado, and GFDL-ESM2M [RegCM4] at North Dakota). Because of these results, we chose different climate models for each site when we performed the future

IDF curve analysis. We used the future rainfall from the lowest (and highest) confidence climate models and produced future IDF curves for each location. As a comparison, we looked at the current climate IDF curves from the closest meteorological station to YTC, Fort Carson, and GFAFB, respectively. At YTC, the future annual maximum daily precipitation was at a much higher value compared to the current climate (at Yakima Airport). In fact, at a return level of 100 years, the highest projected annual maximum daily precipitation (at the upper 95% confidence level) doubled from the current climate levels. In comparison, the future annual maximum daily precipitation (and future IDF curves) for Fort Carson and GFAFB were similar to the current climate (Colorado Springs Municipal Airport and Grand Forks International Airport, respectively). The projected rainfall intensity at a return period of 100 years and a duration of 1 hr was at Fort Carson about 2.5 times more than the lowest projected rainfall intensity by a different climate model. At GFAFB, this difference between climate model outputs was slightly less (1.5 times). These results indicated a wide variation between climate models at all sites, and we recommend using an ensemble of models for future analysis.

Since YTC, Washington, is in an area heavily relying on snow for water resources, we also want to provide some additional notes about some of the specific implications reported for this area. Water stress is looming at YTC because recharge from natural sources (e.g., snowmelt) is greatly reduced while enhanced water demands have grown at YTC and from adjacent land development and agricultural needs. Wells are YTC's only source of potable water, and wells also provide a significant portion of nonpotable needs. Over the past few years, two wells have gone dry, and multiple wells are experiencing significant static water-level decline. Our snow-model results indicated a historical decreasing trend for snowmelt runoff, which could possibly explain this. Surface waters have also declined by an estimated 50% since the year 2000; and crucial riparian zones are drying and showing evidence of vegetation transition to upland and dryland species (P. Nissen, U.S. Army Yakima Training Center, pers. comm., 15 January 2020). Concerns are that water supplies deemed currently ample will not be sufficient in the coming decades. Moreover, YTC is embedded in a heavily productive agricultural region of Washington, where groundwater tables are dropping within the Yakima River Basin watershed. Assuming ground- and surface-water declines continue, which is a possible outcome

considering the declining trends in snow duration, the Army may face potential water shortages for mission-critical needs (e.g., potable and nonpotable) at YTC.

The observation and modeling approach used worked well for Washington and demonstrated impacts of shifting snow; Colorado and North Dakota areas were more of a modeling challenge. Namely, in areas dominated by winter precipitation, where few meteorological stations can be used for validation and snow is unevenly distributed, estimating snow water content and its distribution over different landscapes remains a formidable challenge with substantial physical and ecosystem implications. A sizeable modeling gap remains in linking snow processes and watershed models. Increasingly, models are used to identify precipitation patterns since there was no long-term record available from remote sensing or an accepted remote-sensing technique to measure snow in all environments. Realistic snow distributions can be developed by combining terrain, meteorological data, models, remote sensing, and ground observations, which proved successful in the Washington site but was more difficult in the Colorado and North Dakota sites where snow was intermittent (Colorado) or impacted by landscape management, infrastructure, and crop rotation practices (North Dakota). Ditches and waterways are linear features in North Dakota that are not resolved by most topographic and vegetation datasets. Therefore, models struggled to accurately represent those processes in that landscape.

Field-measurement validation of models was labor intensive, and there was a great need to develop more streamlined methods. To improve our modeling results, we explored several other methods that were outside the scope of our initial project. These methods included using remote-sensing imagery, snow patterns, and photogrammetry analysis; and we found that they have a great potential to improve modeling output. We identify these as research gaps that future efforts should address. Appendix A.5 presents some initial results from these methods.

The YTC landscape is dominated by sagebrush steppe and is increasingly exposed to natural and human-caused fires that kill sagebrush, shifting areas of the landscape toward annual and perennial grasslands. As an additional task from an In-Progress-Review meeting, we were asked to provide a white paper, “Interactions among Snow, Sagebrush, and Greater Sage-

Grouse" (see a summary of this in Appendix A.7). This white paper explores impacts of snow on sagebrush (*Artemisia tridentata*) and greater sage-grouse (*Centrocercus urophasianus*) and their interactions. That paper also identified crucial research gaps linking fire, snow, and loss of sagebrush on greater sage-grouse. A summary of that white paper is in Appendix A.6. In short, our recommendation was to better understand snow, sagebrush, and sage-grouse interactions to identify range vulnerabilities, to develop management tools, and to aid best management practices that prevent deleterious sage-grouse impacts on DoD-managed landscapes.

This study presents both a historical perspective and a forecast of snow and river discharge climatology in the Western U.S. at selected military installations. Moreover, this work provides insight into trends in streamflow and IDF curves and the importance of addressing a changing climate in the designs of future infrastructure. Our field and modeling methods are transferable to a myriad of locations where snowmelt and its subsequent runoff present a challenge to infrastructure planning and maintenance. This will help DoD to further define the impacts from a changing climate, thus allowing for development of mitigation or adaptation strategies, leading to lowered operational costs.

References

Barnett, T. P., J. C. Adam, and D. P. Lettenmaier. 2005. "Potential Impacts of a Warming Climate on Water Availability in Snow-Dominated Regions." *Nature* 438, no. 7066 (November): 303–09. https://doi.org/10.1038/nature04141.

Berghuijs, Wouter R., Ross A. Woods, Christopher J. Hutton, and M. Sivapalan. 2016. "Dominant Flood Generating Mechanisms across the United States." *Geophysical Research Letters* 43 (9): 4382–90. https://doi.org/10.1002/2016GL068070.

Bormann, Kat J., Ross D. Brown, Chris Derksen, and Thomas H. Painter. 2018. "Estimating Snow-Cover Trends from Space." *Nature Climate Change* 8 (11): 924–28. https://doi.org/10.1038/s41558-018-0318-3.

Bradford, John B., Daniel R. Schlaepfer, and William K. Lauenroth. 2014. "Ecohydrology of Adjacent Sagebrush and Lodgepole Pine Ecosystems: The Consequences of Climate Change and Disturbance." *Ecosystems* 17 (4): 590–605. https://doi.org/10.1007/s10021-013-9745-1.

Brown, R. D., and D. A. Robinson. 2011. "Northern Hemisphere Spring Snow Cover Variability and Change over 1922–2010 Including an Assessment of Uncertainty." *Cryosphere* 5 (1): 219–29. https://doi.org/10.5194/tc-5-219-2011.

Brown, Ross D., and Philip W. Mote. 2009. "The Response of Northern Hemisphere Snow Cover to a Changing Climate." *Journal of Climate* 22 (8): 2124–45. https://doi.org/10.1175/2008JCLI2665.1.

Cannon, Alex J. 2010. "A Flexible Nonlinear Modelling Framework for Nonstationary Generalized Extreme Value Analysis in Hydroclimatology." *Hydrological Processes: An International Journal* 24 (6): 673–85. https://doi.org/10.1002/hyp.7506.

Cayan, Daniel R., Susan A. Kammerdiener, Michael D. Dettinger, Joseph M. Caprio, and David H. Peterson. 2001. "Changes in the Onset of Spring in the Western United States." *Bulletin of the American Meteorological Society* 82 (3): 399–416. https://doi.org/10.1175/1520-0477(2001)082<0399:CITOOS>2.3.CO;2.

Clow, David W. 2010. "Changes in the Timing of Snowmelt and Streamflow in Colorado: A Response to Recent Warming." *Journal of Climate* 23 (9): 2293–306. https://doi.org/10.1175/2009JCLI2951.1.

Connelly, John W., Michael A. Schroeder, Alan R. Sands, and Clait E. Braun. 2000. "Guidelines to Manage Sage Grouse Populations and their Habitats." *Wildlife Society Bulletin* 28, no. 4 (Winter): 967–85. https://www.jstor.org/stable/3783856.

Dai, Aiguo, Roy M. Rasmussen, Changhai Liu, Kyoko Ikeda, and Andreas F. Prein. 2017. "A New Mechanism for Warm-Season Precipitation Response to Global Warming Based on Convection-Permitting Simulations." *Climate Dynamics* 55 (1): 343–68. https://doi.org/10.1007/s00382-017-3787-6.

Derksen, C., and R. Brown. 2012. "Spring Snow Cover Extent Reductions in the 2008–2012 Period Exceeding Climate Model Projections." *Geophysical Research Letters* 39 (19): L19504. https://doi.org/10.1029/2012GL053387.

Deschamps-Berger, César, Simon Gascoin, Etienne Berthier, Jeffrey Deems, Ethan Gutmann, Amaury Dehecq, David Shean, and Marie Dumont. 2020. "Snow Depth Mapping from Stereo Satellite Imagery in Mountainous Terrain: Evaluation Using Airborne Laser-Scanning Data." *The Cryosphere* 14 (9): 2925–40. https://doi.org/10.5194/tc-14-2925-2020.

Dettinger, Michael D., Daniel R. Cayan, Mary K. Meyer, and Anne E. Jeton. 2004. "Simulated Hydrologic Responses to Climate Variations and Change in the Merced, Carson, and American River Basins, Sierra Nevada, California, 1900–2099." *Climatic Change* 62 (1–3): 283–317. https://doi.org/10.1023/B:CLIM.0000013683.13346.4f.

Dickerson-Lange, Susan E., James A. Lutz, Kael A. Martin, Mark S. Raleigh, Rolf Gersonde, and Jessica D. Lundquist. 2015. "Evaluating Observational Methods to Quantify Snow Duration under Diverse Forest Canopies." *Water Resources Research* 51 (2): 1203–24. https://doi.org/10.1002/2014WR015744.

Edwards, Anthony C., Riccardo Scalenghe, and Michele Freppaz. 2007. "Changes in the Seasonal Snow Cover of Alpine Regions and Its Effect on Soil Processes: A Review." *Quaternary International* 162:172–81. https://doi.org/10.1016/j.quaint.2006.10.027.

Elsner, Marketa M., Lan Cuo, Nathalie Voisin, Jeffrey S. Deems, Alan F. Hamlet, Julie A. Vano, Kristian E. B. Mickelson, Se-Yeun Lee, and Dennis P. Lettenmaier. 2010. "Implications of 21st Century Climate Change for the Hydrology of Washington State." *Climatic Change* 102 (1–2): 225–60. doi:10.7915/CIG3610W9.

Gan, Thian Yew, Roger G. Barry, Mesgana Gizaw, Adam Gobena, and Rajagopalan Balaji. 2013. "Changes in North American Snowpacks for 1979–2007 Detected from the Snow Water Equivalent Data of SMMR and SSM/I Passive Microwave and Related Climatic Factors." *Journal of Geophysical Research: Atmospheres* 118 (14): 7682–97. https://doi.org/10.1002/jgrd.50507.

Gergel, Diana R., Bart Nijssen, John T. Abatzoglou, Dennis P. Lettenmaier, and Matt R. Stumbaugh. 2017. "Effects of Climate Change on Snowpack and Fire Potential in the Western USA." *Climatic Change* 141 (2): 287–99. https://doi.org/10.1007/s10584-017-1899-y.

Gleick, Peter H. 1987. "The Development and Testing of a Water Balance Model for Climate Impact Assessment: Modeling the Sacramento Basin." *Water Resources Research* 23 (6): 1049–61. https://doi.org/10.1029/WR023i006p01049.

Groisman, Pavel Ya, Richard W. Knight, David R. Easterling, Thomas R. Karl, Gabriele C. Hegerl, and Vyacheslav N. Razuvaev. 2005. "Trends in Intense Precipitation in the Climate Record." *Journal of Climate* 18 (9): 1326–50. https://doi.org/10.1175/JCLI3339.1.

Gumbel, Emil Julius. 1941. "The Return Period of Flood Flows." *The Annals of Mathematical Statistics* 12 (2): 163–90. https://www.jstor.org/stable/2235766.

Hall, Dorothy K., Christopher J. Crawford, Nicolo E. DiGirolamo, George A. Riggs, and James L. Foster. 2015. "Detection of Earlier Snowmelt in the Wind River Range, Wyoming, Using Landsat Imagery, 1972–2013." *Remote Sensing of Environment* 162 (June): 45–54. https://doi.org/10.1016/j.rse.2015.01.032.

Homer, C., J. Dewitz, J. Fry, M. Coan, N. Hossain, C. Larson, N. Herold, et al. 2007. "Completion of the 2001 National Land Cover Database for the Conterminous United States.". *Photogrammetric Engineering and Remote Sensing* 73, no. 4 (April): 337–41. https://www.academia.edu/download/43228714/Completion_of_the_2001_National_Land_Cov20160301-16896-zq4sut.pdf.

Jeong, Dae Il, and Laxmi Sushama. 2018. "Rain-on-Snow Events over North America Based on Two Canadian Regional Climate Models." *Climate Dynamics* 50 (1): 303–16. https://doi.org/10.1007/s00382-017-3609-x.

Judson, A., and N. Doesken. 2000. "Density of Freshly Fallen Snow in the Central Rocky Mountains." *Bulletin of the American Meteorological Society* 81, no. 7 (July): 1577–87. https://doi.org/10.1175/1520-0477(2000)081<1577:DOFFSI>2.3.CO;2.

Klos, P. Zion, Timothy E. Link, and John T. Abatzoglou. 2014. "Extent of the Rain-Snow Transition Zone in the Western US under Historic and Projected Climate." *Geophysical Research Letters* 41 (13): 4560–8. https://doi.org/10.1002/2014GL060500.

Knight, Dennis H., George P. Jones, William A. Reiners, and William H. Romme. 2014. *Mountains and Plains: The Ecology of Wyoming Landscapes*. New Haven, CT: Yale University Press.

Knowles, Noah. 2015. "Trends in Snow Cover and Related Quantities at Weather Stations in the Conterminous United States." *Journal of Climate* 28 (19): 7518–28. https://doi.org/10.1175/JCLI-D-15-0051.1.

Knowles, Noah, and Daniel R. Cayan. 2004. "Elevational Dependence of Projected Hydrologic Changes in the San Francisco Estuary and Watershed." *Climatic Change* 62 (1–3): 319–36. https://doi.org/10.1023/B:CLIM.0000013696.14308.b9.

Lemke, P., J. Ren, R. B. Alley, I. Allison, J. Carrasco, G. Flato, Y. Fujii, et al. 2007. "Observations: Changes in Snow, Ice and Frozen Ground." In *Climate Change 2007: The Physical Science Basis. Contribution of Working Group I to the Fourth Assessment Report of the Intergovernmental Panel on Climate Change*, edited by S. Solomon, D. Qin, M. Manning, Z. Chen, M. Marquis, K. B. Averyt, M. Tignor, and H. L. Miller. New York: Cambridge University Press. http://www.ipcc.ch/pdf/assessment-report/ar4/wg1/ar4-wg1-chapter4.pdf.

Lettenmaier, Dennis P., and Thian Yew Gan. 1990. "Hydrologic Sensitivities of the Sacramento-San Joaquin River Basin, California, to Global Warming." *Water Resources Research* 26 (1): 69–86. https://doi.org/10.1029/WR026i001p00069.

Leung, L. Ruby, Yun Qian, Xindi Bian, Warren M. Washington, Jongil Han, and John O. Roads. 2004. "Mid-Century Ensemble Regional Climate Change Scenarios for the Western United States." *Climatic Change* 62 (1): 75–113. https://doi.org/10.1023/B:CLIM.0000013692.50640.55.

Li, Dongyue, Dennis P. Lettenmaier, Steven A. Margulis, and Konstantinos Andreadis. 2019. "The Role of Rain-on-Snow in Flooding over the Conterminous United States." *Water Resources Research* 55 (11): 8492–513. https://doi.org/10.1029/2019WR024950.

Li, Dongyue, Melissa L. Wrzesien, Michael Durand, Jennifer Adam, and Dennis P. Lettenmaier. 2017. "How Much Runoff Originates as Snow in the Western United States, and How Will That Change in the Future?" *Geophysical Research Letters* 44 (12): 6163–72. https://doi.org/10.1002/2017GL073551.

Liang, Xu, Dennis P. Lettenmaier, Eric F. Wood, and Stephen J. Burges. 1994. "A Simple Hydrologically Based Model of Land Surface Water and Energy Fluxes for General Circulation Models." *Journal of Geophysical Research: Atmospheres* 99 (D7): 14415–28. https://doi.org/10.1029/94JD00483.

Liang, Xu, Eric F. Wood, and Dennis P. Lettenmaier. 1996. "Surface Soil Moisture Parameterization of the VIC-2L Model: Evaluation and Modification." *Global and Planetary Change* 13 (1–4): 195–206. https://doi.org/10.1016/0921-8181(95)00046-1.

Liston, Glen E., and Kelly Elder. 2006. "A Distributed Snow-Evolution Modeling System (SnowModel)." *Journal of Hydrometeorology* 7:1259–76. https://doi.org/10.1175/JHM548.1.

Liston, Glen E., and Christopher. A. Hiemstra. 2011a. "Representing Grass- and Shrub-Snow-Atmosphere Interactions in Climate System Models." *Journal of Climate* 24, no. 8 (April): 2061–79. https://doi.org/10.1175/2010JCLI4028.1.

———.. 2011b. "The Changing Cryosphere: Pan-Arctic Snow Trends (1979–2009)." *Journal of Climate* 24, no. 21 (November): 5691–712. https://doi.org/10.1175/JCLI-D-11-00081.1.

Liston, Glen E., Polona Itkin, Julienne Stroeve, Mark Tschudi, J. Scott Stewart, Stine H. Pedersen, Adele K. Reinking, and Kelly Elder. 2020. "A Lagrangian Snow-Evolution System for Sea-Ice Applications (SnowModel-LG): Part I—Model Description." *Journal of Geophysical Research: Oceans* 125 (10):e2019JC015913. https://doi.org/10.1029/2019JC015913.

Liston, Glen E., and Sebastian H. Mernild. 2012. "Greenland Freshwater Runoff. Part I: A Runoff Routing Model for Glaciated and Nonglaciated Landscapes (HydroFlow)." *Journal of Climate* 25, no. 17 (September): 5997–6014. https://doi.org/10.1175/JCLI-D-11-00591.1.

Liu, Changhai, Kyoko Ikeda, Roy Rasmussen, Mike Barlage, Andrew J. Newman, Andreas F. Prein, Fei Chen, et al. 2017. "Continental-Scale Convection-Permitting Modeling of the Current and Future Climate of North America." *Climate Dynamics* 49 (1): 71–95. https://doi.org/10.1007/s00382-016-3327-9.

Livneh, Ben, Eric A. Rosenberg, Chiyu Lin, Bart Nijssen, Vimal Mishra, Kostas M. Andreadis, Edwin P. Maurer, and Dennis P. Lettenmaier. 2013. "A Long-Term Hydrologically Based Dataset of Land Surface Fluxes and States for the Conterminous United States: Update and Extensions." *Journal of Climate* 26 (23): 9384–92. https://doi.org/10.1175/JCLI-D-12-00508.1.

Lute, A. C., J. T. Abatzoglou, and K. C. Hegewisch. 2015. "Projected Changes in Snowfall Extremes and Interannual Variability of Snowfall in the Western United States." *Water Resources Research* 51 (2): 960–72. https://doi.org/10.1002/2014WR016267.

Mahrt, Larry, and Dean Vickers. 2005. "Moisture Fluxes over Snow with and without Protruding Vegetation." *Quarterly Journal of the Royal Meteorological Society: A Journal of the Atmospheric Sciences, Applied Meteorology and Physical Oceanography* 131 (607): 1251–70. https://doi.org/10.1256/qj.04.66.

Mearns, L., S. McGinnis, D. Korytina, R. Arritt, S. Biner, M. Bukovsky, H. I. Chang, et al. 2017. *The NA-CORDEX Dataset*. Version 1.0. Boulder, CO: NCAR Climate Data Gateway. https://doi.org/10.5065/D6SJ1JCH.

Meyer, S. E. 2008. "*Artemisia* L.: Sagebrush." In *The Woody Plant Seed Manual*," edited by F. T. Bonner, 274–280. Agriculture Handbook 727. Washington, D.C.: Government Printing Office. https://www.fs.fed.us/rm/pubs_series/wo/wo_ah727.pdf.

Miller, Richard F., Steven T. Knick, David A. Pyke, Cara W. Meinke, Steven E. Hanser, Michael J. Wisdom, and Ann L. Hild. 2011. "Chapter Ten. Characteristics of Sagebrush Habitats and Limitations to Long-Term Conservation." In *Greater Sage-Grouse*, 145–184. Berkeley: University of California Press. https://doi.org/10.1525/9780520948686-014.

Mote, P. W., A. F. Hamlet, M. P. Clark, and D. P. Lettenmaier. 2005. "Declining Mountain Snowpack in Western North America.". *Bulletin of the American Meteorological Society* 86, no. 1 (January): 39–49. https://doi.org/10.1175/BAMS-86-1-39.

Mote, Philip W., Sihan Li, Dennis P. Lettenmaier, Mu Xiao, and Ruth Engel. 2018. "Dramatic Declines in Snowpack in the Western US." *npj Climate and Atmospheric Science* 1 (1): 1–6. https://doi.org/10.1038/s41612-018-0012-1.

Musselman, Keith N., Flavio Lehner, Kyoko Ikeda, Martyn P. Clark, Andreas F. Prein, Changhai Liu, Mike Barlage, and Roy Rasmussen. 2018. "Projected Increases and Shifts in Rain-on-Snow Flood Risk over Western North America." *Nature Climate Change* 8 (9): 808–12. https://doi.org/10.1038/s41558-018-0236-4.

Nolan, Matt, Chris Larsen, and Matthew Sturm. 2015. "Mapping Snow Depth from Manned Aircraft on Landscape Scales at Centimeter Resolution Using Structure-from-Motion Photogrammetry." *The Cryosphere* 9 (4): 1445–63. https://doi.org/10.5194/tc-9-1445-2015.

Pederson, G. T., S. T. Gray, T. Ault, W. Marsh, D. B. Fagre, A. G. Bunn, C. A. Woodhouse, and L. J. Graumlich. 2011. "Climatic Controls on the Snowmelt Hydrology of the Northern Rocky Mountains." *Journal of Climate* 24, no. 6 (March): 1666–87. https://doi.org/10.1175/2010JCLI3729.1.

Prein, Andreas F., Changhai Liu, Kyoko Ikeda, Randy Bullock, Roy M. Rasmussen, Greg J. Holland, and Martyn Clark. 2017. "Simulating North American Mesoscale Convective Systems with a Convection-Permitting Climate Model." *Climate Dynamics* 5:1–16. https://doi.org/10.1007/s00382-017-3993-2.

Prein, Andreas F., Roy M. Rasmussen, Kyoko Ikeda, Changhai Liu, Martyn P. Clark, and Greg J. Holland. 2017. "The Future Intensification of Hourly Precipitation Extremes." *Nature Climate Change* 7 (1): 48–52. https://doi.org/10.1038/nclimate3168.

Pyke, David A., Jeanne C. Chambers, Mike Pellant, Steven T. Knick, Richard F. Miller, Jeffrey L. Beck, Paul S. Doescher, et al. 2015. *Restoration Handbook for Sagebrush Steppe Ecosystems with Emphasis on Greater Sage-Grouse Habitat-Part 1*. Circular 1416. Reston, VA: U.S. Geological Survey. http://dx.doi.org/10.3133/cir1416.

Raghavendra, Ajay, Aiguo Dai, Shawn M. Milrad, and Shealynn R. Cloutier-Bisbee. 2019. "Floridian Heatwaves and Extreme Precipitation: Future Climate Projections." *Climate Dynamics* 52 (1): 495–508. https://doi.org/10.1007/s00382-018-4148-9.

Räisänen, Jouni. "Warmer Climate: Less or More Snow?" 2008. *Climate Dynamics* 30 (2): 307–19. https://doi.org/10.1007/s00382-007-0289-y.

Rasmussen, Roy, Bruce Baker, John Kochendorfer, Tilden Meyers, Scott Landolt, Alexandre P. Fischer, Jenny Black, et al. 2012. "How Well Are We Measuring Snow: The NOAA/FAA/NCAR Winter Precipitation Test Bed." *Bulletin of the American Meteorological Society* 93 (6): 811–29. https://doi.org/10.1175/BAMS-D-11-00052.1.

Rasmussen, Roy, and Changhai Liu. 2017. "High Resolution WRF Simulations of the Current and Future Climate of North America." Boulder, CO: Research Data Archive at the National Center for Atmospheric Research, Computational and Information Systems Laboratory. https://doi.org/10.5065/D6V40SXP.

Rhoades, Alan M., Paul A. Ullrich, and Colin M. Zarzycki. 2018. "Projecting 21st Century Snowpack Trends in Western USA Mountains Using Variable-Resolution CESM." *Climate Dynamics* 50 (1): 261–88. https://doi.org/10.1007/s00382-017-3606-0.

Robertson, Joseph H. 1947. "Responses of Range Grasses to Different Intensities of Competition with Sagebrush (Artemisia Tridentata Nutt.)." *Ecology* 28 (1): 1–16. https://doi.org/10.2307/1932913.

Rupp, David E., Philip W. Mote, Nathaniel L. Bindoff, Peter A. Stott, and David A. Robinson. 2013. "Detection and Attribution of Observed Changes in Northern Hemisphere Spring Snow Cover." *Journal of Climate* 26 (18): 6904–14. https://doi.org/10.1175/JCLI-D-12-00563.1.

SERDP (Strategic Environmental Research and Development Program). 2013. *Adapting to Changes in the Hydrologic Cycle under Non-Stationary Climate Conditions*. FY 2015 Statement of Need—Resource Conservation and Climate Change (RC) Program Area. RCSON-15-02. Alexandria, VA: Strategic Environmental Research and Development Program.

Stewart, I. T. 2009. "Changes in Snowpack and Snowmelt Runoff for Key Mountain Regions." *Hydrological Processes* 23, no. 1 (January): 78–94. https://doi.org/10.1002/hyp.7128.

Stewart, Iris T., Daniel R. Cayan, and Michael D. Dettinger. 2004. "Changes in Snowmelt Runoff Timing in Western North America under A 'Business as Usual' Climate Change Scenario." *Climatic Change* 62 (1–3): 217–32. https://doi.org/10.1023/B:CLIM.0000013702.22656.e8.

———. 2005. "Changes toward Earlier Streamflow Timing across Western North America." *Journal of Climate* 18 (8): 1136–55. https://doi.org/10.1175/JCLI3321.1.

Sturm, M., J. Holmgren, and G. E. Liston. 1995. "A Seasonal Snow Cover Classification System for Local to Global Applications." *Journal of Climate* 8, no. 5 (May): 1261–83. https://doi.org/10.1175/1520-0442(1995)008<1261:ASSCCS>2.0.CO;2.

Sturm, M., B. Taras, G. E. Liston, C. Derksen, T. Jonas, and J. Lea. 2010. "Estimating Snow Water Equivalent Using Snow Depth Data and Climate Classes." *Journal of Hydrometeorology* 11, no. 6 (December): 1380–94. https://doi.org/10.1175/2010JHM1202.1.

Sturm, M., and A. M. Wagner. 2010. "Using Repeated Patterns in Snow Distribution Modeling: An Arctic Example." *Water Resources Research* 46, no. 12 (December). https://doi.org/10.1029/2010WR009434.

Sturm, Matthew. 2009. "Field Techniques for Snow Observations on Sea Ice." In *Field Techniques for Sea Ice Research,* edited by H. Eicken, R. R. Gradinger, M. Salganek, K. Shirasawa, D. K. Perovich and M. Leppäranta, 25–47. https://hdl.handle.net/10013/epic.47809.

Sturm, Matthew, and Jon Holmgren. 2018. "An Automatic Snow Depth Probe for Field Validation Campaigns." *Water Resources Research* 54 (11): 9695–701. https://doi.org/10.1029/2018WR023559.

Villarini, Gabriele. 2016. "On the Seasonality of Flooding across the Continental United States." *Advances in Water Resources* 87 (January): 80–91. https://doi.org/10.1016/j.advwatres.2015.11.009.

Wigmosta, Mark S., Leonard J. Lane, Jerry D. Tagestad, and Andre M. Coleman. 2009. "Hydrologic and Erosion Models to Assess Land Use and Management Practices Affecting Soil Erosion." *Journal of Hydrologic Engineering* 14 (1): 27–41. https://doi.org/10.1061/(ASCE)1084-0699(2009)14:1(27).

Yang, D. Q., Y. Y. Zhao, R. Armstrong, D. Robinson, and M. J. Brodzik. 2007. "Streamflow Response to Seasonal Snow Cover Mass Changes over Large Siberian Watersheds.". *Journal of Geophysical Research-Earth Surface* 112, no. F2 (May). https://doi.org/10.1029/2006JF000518.

Appendix A: Supplementary Material

A.1 Technical Approach

Table A-1. SNOTEL stations used in the snow-model validation of SWE for the Washington site.

Site Name	SNOTEL Number	Latitude	Longitude	Elevation (m)
Blewett Pass	352	47.35	−120.68	1,292
Bumping Ridge	375	46.81	−121.33	1,405
Cayuse Pass	1085	46.87	−121.53	1,597
Fish Lake	478	47.54	−121.09	1,045
Green Lake	502	46.55	−121.17	1,804
Grouse Camp	507	47.28	−120.49	1,643
Morse Lake	642	46.91	−121.48	1,649
Olallie Meadows	672	47.37	−121.44	1,228
Sasse Ridge	734	47.38	−121.06	1,323
Sawmill Ridge	1068	47.16	−121.42	1,414
Stampede Pass	788	47.27	−121.34	1,173
Tinkham Creek	899	47.33	−121.47	911
Trough	832	47.23	−120.29	1,670
White Pass E.S.	863	46.64	−121.38	1,353

Table A-2. SNOTEL and meteorological stations used in the snow-model validation of SWE for the Colorado site.

Site Name	Latitude	Longitude	Elevation (m)
Canon City	38.46	−105.23	1,639
Colorado Springs Airport	38.81	−104.69	1,884
Eastonville 2 NNW	39.11	−104.60	2,198
Fowler 1 SE	38.12	−104.01	1,320
Glen Cove (SNOTEL station #1057)	38.88	−105.07	3,493
Karval	38.74	−103.54	1,547
La Junta 20S	37.75	−103.48	1,283
Lake George 8 SW	38.91	−105.47	2,606
Las Animas	38.06	−103.22	1,186
Limon Hass Ranch	39	−103.74	1,678
Pueblo Memorial Airport	38.29	−104.50	1,439
Rocky Ford 2 SE	38.04	−103.69	1,271
Ruxton Park	38.84	−104.97	2,758
Trinidad	37.18	−104.49	1,838
Walsenburg 1 NW	37.63	−104.80	1,920
Westcliffe	38.13	−105.47	2,396
Whiskey Creek	37.21	−105.12	3,115

Table A-3. Meteorological stations used in the snow-model validation of SWE for the North Dakota site.

Site Name	Latitude	Longitude	Elevation (m)
Adams 7 SSW	48.33	−98.12	476
Agassiz Refuge	48.30	−95.98	348
Crookston NW Exp Station	47.80	−96.60	271
Grand Forks Air Force Base	47.97	−97.40	278
Grand Forks International Airport	47.94	−97.18	257
Larimore 4SW	47.87	−97.71	351
Mahnomen	47.31	−95.97	369
Mayville	47.50	−97.35	300
McVille	47.76	−98.18	447
Grand Forks 0.6 SW	47.91	−97.08	254
Thorhult	48.21	−95.25	377

Table A-4. Station name/code for analysis, station number, latitude (lat.), longitude (long.), length of gage record, number of years, and drainage basin size for the Washington site. The time period and number of years are for the peak flow analysis.

Station Name (Code for Analysis)	Station Number	Lat.	Long.	Time Period	Length (yr)	Basin Size (km^2)
Yakima River at Cle Elum	12479500	47.19	−120.95	1907–1990	67[a]	1,300
Naneum Creek near Ellensburg	12483800	47.13	−120.48	1957–1977	19[b]	178
Yakima River at Umtanum (YAKUM)	12484500	46.86	−120.48	1906–2019	97[c]	4,128
American River near Nile (AME)	12488500	46.98	−121.17	1909–2019	71[d]	205
Tieton River at Canal Headworks near Naches	12492500	46.67	−121.00	1908–1977	65[e]	622
Naches River near North Yakima	12499000	46.63	−120.52	1900–1990	16[f]	2,865
Yakima River above Ahtanum Creek at Union Gap (YAKUN)	12500450	46.53	−120.47	1967–2019	44[g]	9,011
North Fork Ahtanum Creek near Tampico	12500500	46.56	−120.92	1908–1979	55[h]	180
SF Ahtanum Creek at Conrad Ranch near Tampico	12501000	46.51	−120.92	1915–1977	42[i]	65
Ahtanum Creek at Union Gap (AHTUN)	12502500	46.54	−120.47	1908–2019	61[j]	446

[a] Missing years: 1907, 1912, 1918, 1922, 1934, 1960, 1976, 1978–1987.
[b] Missing years: 1963, 1973.
[c] Missing years: 1907, 1912, 1918, 1922, 1924, 1928, 1934, 1947, 1960, 1963, 1973, 1976, 1978, 1981, 1987, 1991, 2000.
[d] Missing years: 1910–1939, 1942, 1950, 1973, 1976, 1978, 1981, 1991, 2000, 2007, 2016.
[e] Missing years: 1910, 1922, 1925, 1934, 1976.
[f] Missing years: 1907, 1910–1911, 1915–1986.
[g] Missing years: 1973, 1976, 1978, 1981, 1987, 1991, 1997, 2000, 2016.
[h] Missing years: 1909, 1922–1931, 1934, 1947, 1963, 1973, 1976, 1978.
[i] Missing years: 1925–1930, 1934, 1947, 1963, 1973, 1976.
[j] Missing years: 1909, 1911, 1915–1951, 1953–1959, 1973, 1978, 1981, 1988, 2018.

Table A-5. Station names/code for analysis, station number, regulated streamflow (i.e., percentage for flow management) in percentage of area basin, latitude (lat.), longitude (long.), length of gage record, number of years, and drainage basin size for the Colorado site. The time period and number of years are for the peak flow analysis.

Station Name (Code for Analysis)	Station Number	Regulated (%)	Lat.	Long.	Time Period	Length (yr)	Basin Size (km^2)
Beaver Creek above Highway 115	07099060	0	38.49	−104.00	1991–2019	27[a]	357
Beaver Creek near Portland	07099100	0	38.37	−104.96	1971–1981	11	554
Turkey Creek above Teller Reservoir near Stone City (TURK)	07099230	0	38.47	−104.83	1978–2017	37[b]	161
Fountain Creek near Colorado Springs (FNCS)	07103700	0	38.85	−104.88	1958–2019	61[c]	264
Monument Creek above North Gate Blvd. at USAF Academy (MCUSAF)	07103780	0	39.03	−104.85	1985–2019	35	212
Monument Creek at Bijou St. at Colorado Springs (MCCS)	07104905	2.5	38.84	−104.83	2003–2019	17	609
Fountain Creek at Colorado Springs (FCCS)	07105500	1.5	38.82	−104.82	1976–2019	44	1,015
Fountain Creek near Fountain (FCF)	07106000	1.3	38.60	−104.67	1939–2019	52[d]	1,740
Fountain Creek near Piñon (FCF)	07106300	1.0	38.44	−104.59	1973–2019	47	2,240
Purgatoire River near Thatcher (PURT)	07126300	37.2	37.36	−103.90	1965–2019	53[e]	5,012
Purgatoire River at Rock Crossing near Timpas (PRRCT)	07126485	25.8	37.62	−103.59	1984–2019	36[f]	6,825
Purgatoire River near Las Animas (PTLA)	07128500	20.7	38.03	−103.20	1922–2019	71[g]	9,073

[a] Missing year: 2016.
[b] Missing years: 2013–2015.
[c] Missing year: 1995.
[d] Missing years: 1956–1984.
[e] Missing years: 2009, 2016.
[f] Missing years: 2009, 2016.
[g] Missing years: 1924, 1931–1948, 2016.

Table A-6. Station name/code for analysis, station number, latitude (lat.), longitude (long.), length of gage record, number of years, and drainage basin size for the North Dakota site. The time period and number of years are for the peak flow analysis.

Station Name (Code for Analysis)	Station Number	Lat.	Long.	Time Period	Length (yr)	Basin Size (km^2)
Turtle River at Turtle River State Park near Arvilla (TUR)	05082625	47.93	−97.51	1993–2019	27	805
Salt Water Coulee tributary near Emerado	05082680	47.88	−97.37	1955–1973	18[a]	57
Salt Water Coulee near Emerado	05082700	47.93	−97.26	1950–1973	20[b]	285
Freshwater Coulee near Emerado	05082900	47.93	−97.23	1955–1973	19	80
Turtle River at Manvel	05083000	48.08	−97.18	1945–1970	25	1,588
Middle branch Forest River near Whitman	05083600	48.25	−98.12	1961–1990	30	124
Forest River near Fordville (FOR)	05084000	48.20	−97.73	1940–2019	80	1,181
Forest River at Minto (MIN)	05085000	48.29	−97.37	1882–2019	80[c]	1,917
South branch Park River below Homme Dam	05089000	48.40	−97.78	1950–1994	45	585
Park River at Grafton (PAR)	05090000	48.42	−97.41	1931–2003	90[d]	1,801

[a] Missing years: 1968.
[b] Missing years: 1951–1954.
[c] Missing years: 1883–1896, 1898–1906, 1908–1915, 1917–1943.
[d] Missing years: 1883–1897, 1898–1931.

Table A-7. Station name, station number, latitude (lat.), longitude (long.), length of meteorological record, and number of years for the Washington site.

Station	Station number.	Lat.	Long.	Elevation (m)	Start–End	Length (yr)
Cle Elum	USC00451504	47.19	−120.91	579	1899–2019	102[a]
Ellensburg Bowers Field	USW00024220	47.03	−120.53	538	1941–2019	39[b]
Ellensburg	USC00452505	46.97	−120.54	451	1894–2019	107[c]
Moxee City	USC00455688	46.51	−120.17	472	1947–2014	64[d]
Priest Rapids Dam	USC00456747	46.65	−119.91	131	1957–2019	54[e]
Quincy	USC00456880	47.22	−119.85	392	1943–2018	70[f]
Selah 2	USC00457522	46.67	−120.50	341	1999–2019	21
Smyrna	USC00457727	46.84	−119.66	171	1952–2007	50[g]
Stampede Pass	USW00024237	47.28	−121.34	1,207	1944–2019	64[h]
Wapato	USC00458959	46.44	−120.42	256	1916–2011	87[i]
Yakima Airport	USW00024243	46.57	−120.54	324	1947–2019	73

[a] Missing years: 1935, 1941, 1946, 1954–1956, 1959, 1969, 1989, 2000, 2002–2009, 2015.
[b] Missing years: 1959–1998.
[c] Missing years: 1938, 1941–1953, 1972–1973, 2003–2005.
[d] Missing years: 1948, 1981–1983, 2015–2017.
[e] Missing years: 1987, 1997–1998, 2002–2005, 2007–2008.
[f] Missing years: 1945, 1965, 1982, 2006–2008.
[g] Missing years: 1966–1970, 1992.
[h] Missing years: 1989–1991, 1994–1997, 2014–2017.
[i] Missing years: 1922–1923, 1925, 1928–1931, 1935–1940, 1989, 1998–1999, 2005–2006, 2008–2009.

Table A-8. Station names, station number, latitude (lat.), longitude (long.), length of meteorological record, and number of years for the Colorado site.

Station	Station Number	Lat.	Long.	Elevation (m)	Start–End	Length (yr)
Canon City	USC00051294	38.46	−105.23	1,639	1894–2019	1,12[a]
Cheesman	USC00051528	39.22	−105.28	2,097	1903–2019	117
Colorado Springs Municipal Airport	USW00093037	38.81	−104.69	1,884	1948–2019	72
Florissant Fossil Bed	USC00052965	38.91	−105.28	2,561	1989–2019	31
Guffey 10 SE	USC00053656	38.68	−105.39	2,620	1951–2006	54[b]
Palmer Lake	USC00056280	39.12	−104.92	2,195	1966–2019	21[c]
Pueblo Memorial Airport	USW00093058	38.29	−104.51	1,441	1954–2019	66[d]
Pueblo Reservoir	USC00056765	38.26	−104.72	1,482	1976–2019	44
Ruxton Park	USC00057309	38.84	−104.97	2,762	1960–2019	60
La Junta	USC00054724	37.98	−103.54	1,246	1996–2019	24
La Junta 20 S	USC00054726	37.75	−103.48	1,283	1983–2019	37
La Junta Municipal Airport	USW00023067	38.05	−103.51	1,278	1946–2019	72[e]
Las Animas	USC00054834	38.06	−103.22	1,186	1893–2019	127
Rocky Ford 2 SE	USC00057167	38.04	−103.69	1,271	1893–2019	125[f]
Trinidad Airport	USW00023070	37.26	−104.34	1,750	1948–2019	72

[a] Gap between years: 1921–1922, 1933, 1976–1978, 1982, 1984, 1987, 1994–1995, 2000–2001, 2006.
[b] Gap between years: 1953–1954.
[c] Gap between years: 1977, 1983, 1986–2007, 2010–2017.
[d] Gap between years: 1973.
[e] Gap between years: 1982, 1996.
[f] Gap between years: 1897, 1899.

Table A-9. Station names, station number, latitude (lat.), longitude (long.), length of meteorological record, and number of years for the North Dakota site.

Station	Station Number	Lat.	Long.	Elevation (m)	Start–End	Length (yr)
Argyle	USC00210252	48.33	−96.83	258	1949–2016	68
Adams 7 SSW	USC00320022	48.33	−98.12	476	1949–2015	67
Cavalier	USC00321435	48.86	−97.70	274	1935–2019	85
Drayton	USC00322312	48.56	−97.18	244	1968–2000	25[a]
Edmore 4 NW	USC00322525	48.46	−98.52	469	1906–2013	88[b]
Grafton	USC00323594	48.42	−97.42	252	1893–2004	112
Grand Forks International Airport	USW00014916	47.94	−97.18	257	1942–2019	78
Grand Forks University NWS	USC00323621	47.92	−97.10	253	1893–2019	127
Hallock	USC00213455	48.77	−96.94	248	1900–2019	103[c]
Langdon Experimental Farm	USC00324958	48.76	−98.34	492	1914–2012	99
Larimore	USC003245013	47.87	−97.71	351	1897–2004	85[d]
Petersburg 2 N	USC00327027	48.04	−98.01	467	1933–2019	85[e]

[a] Gap between years: 1984–1991.
[b] Gap between years : 1912–1931, 1994.
[c] Gap between years: 1996–2013.
[d] Gap between years: 1906–1909, 1911, 1944–1945, 1949–1951, 1970–1971, 1973–1976, 1978–1979, 1982–1986.
[e] Gap between years: 1932–1943, 2016–2017.

A.2 Results and Discussion for Washington

Figure A-1. VIC and SnowModel SWE model output compared to SNOTEL stations from 1979 to 2015, Washington.

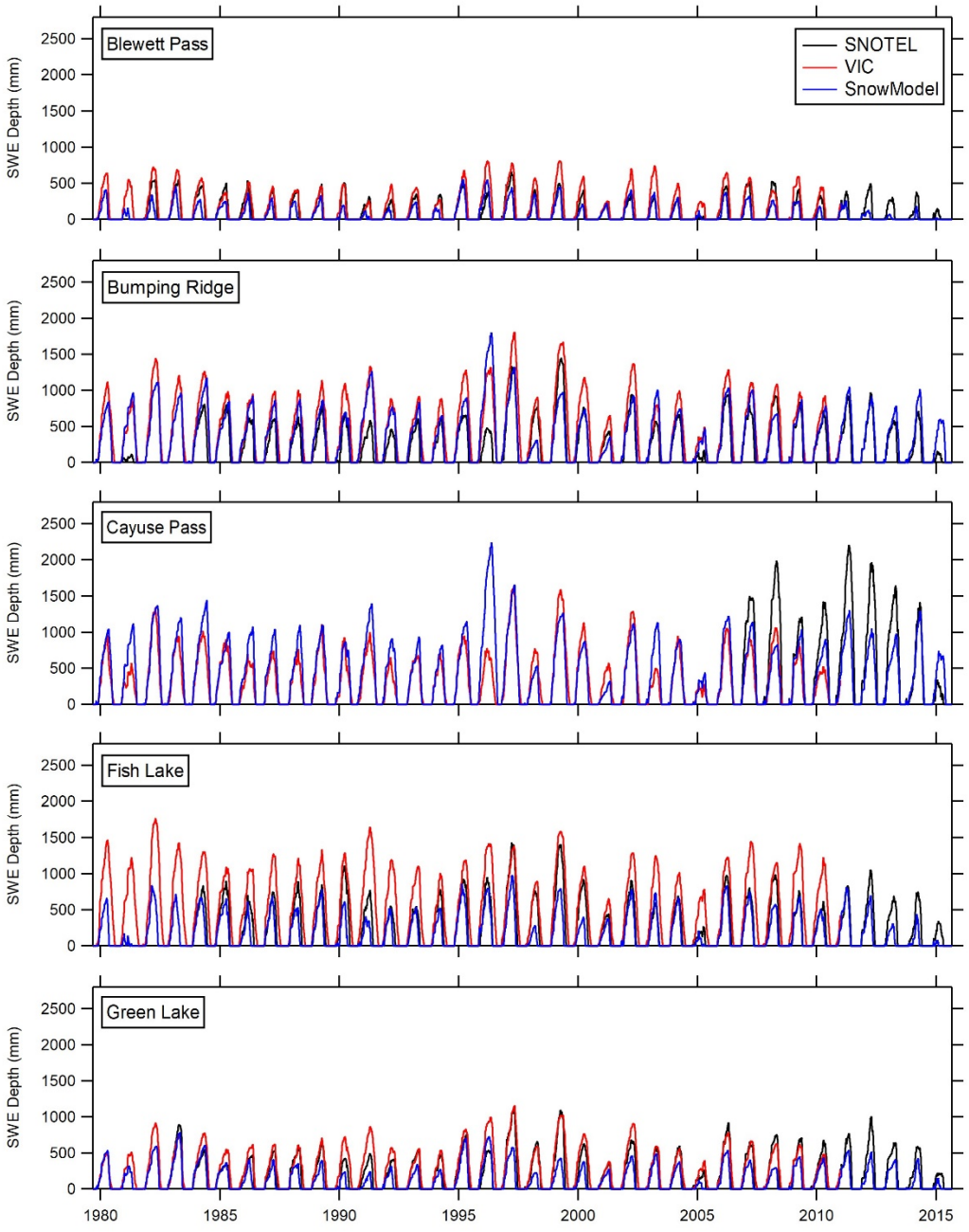

Figure A-1 (cont.). VIC and SnowModel SWE model output compared to SNOTEL stations from 1979 to 2015, Washington.

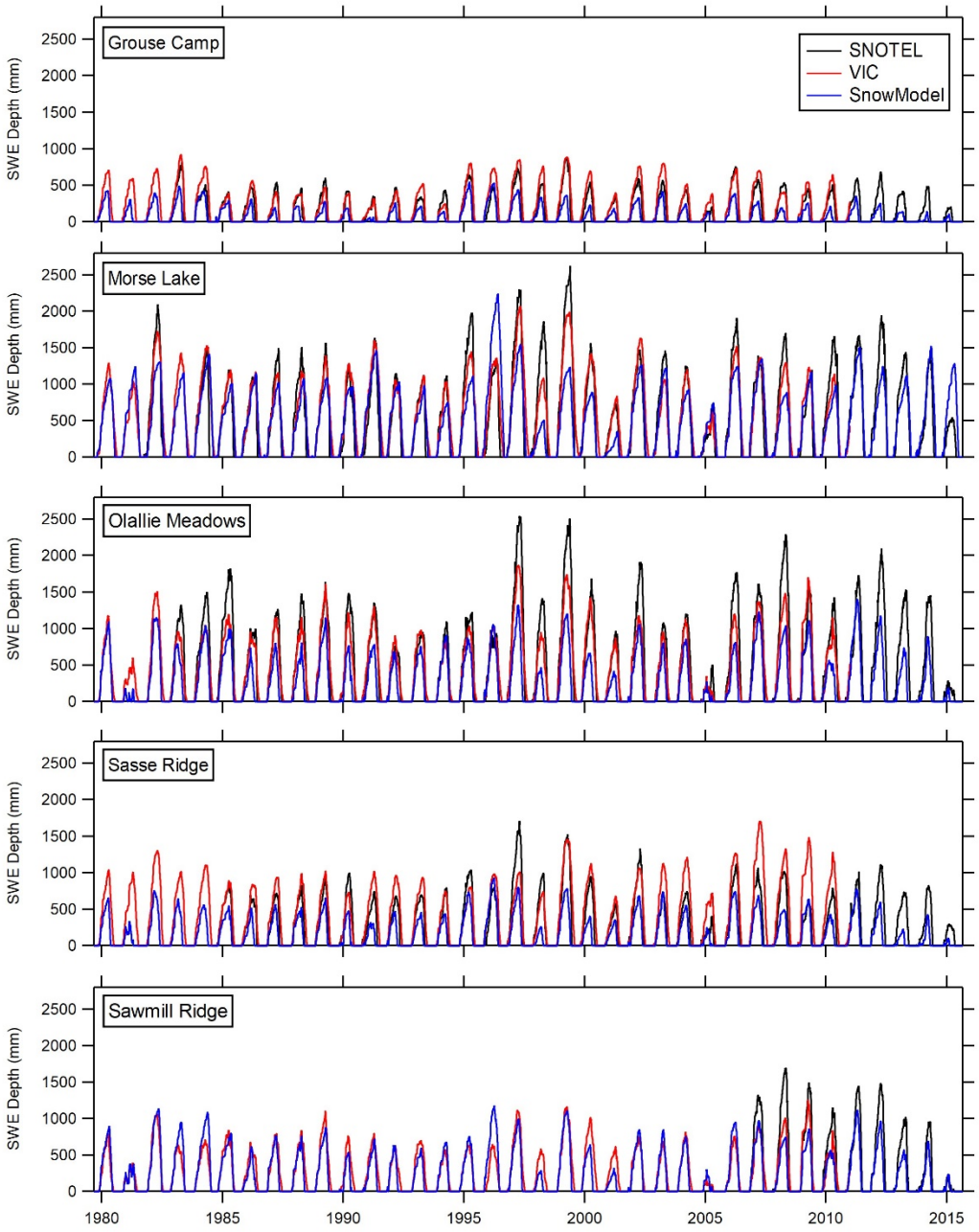

Figure A-1 (cont.). VIC and SnowModel SWE model output compared to SNOTEL stations from 1979 to 2015, Washington.

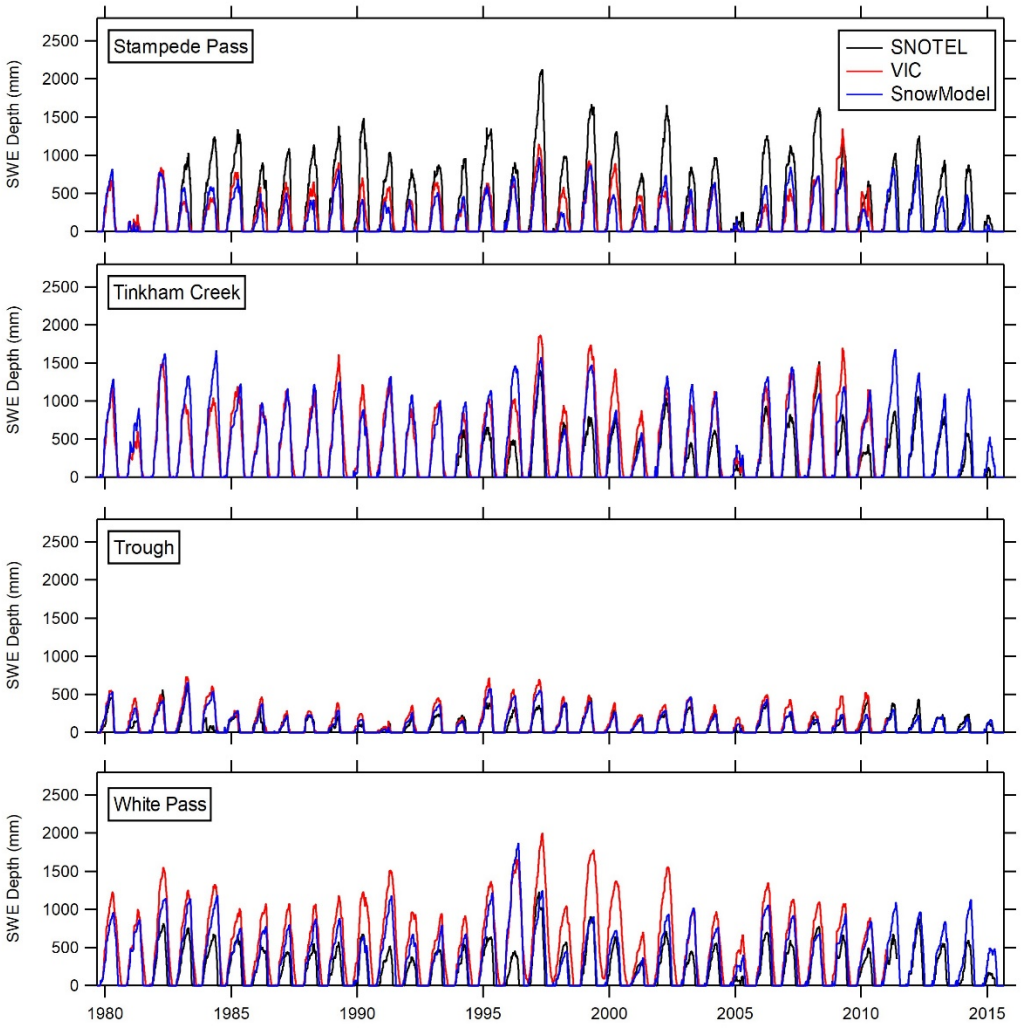

Figure A-2. Return period of annual peak flow and upper- and lower-boundary 95% CL for the USGS gages in the Washington site.

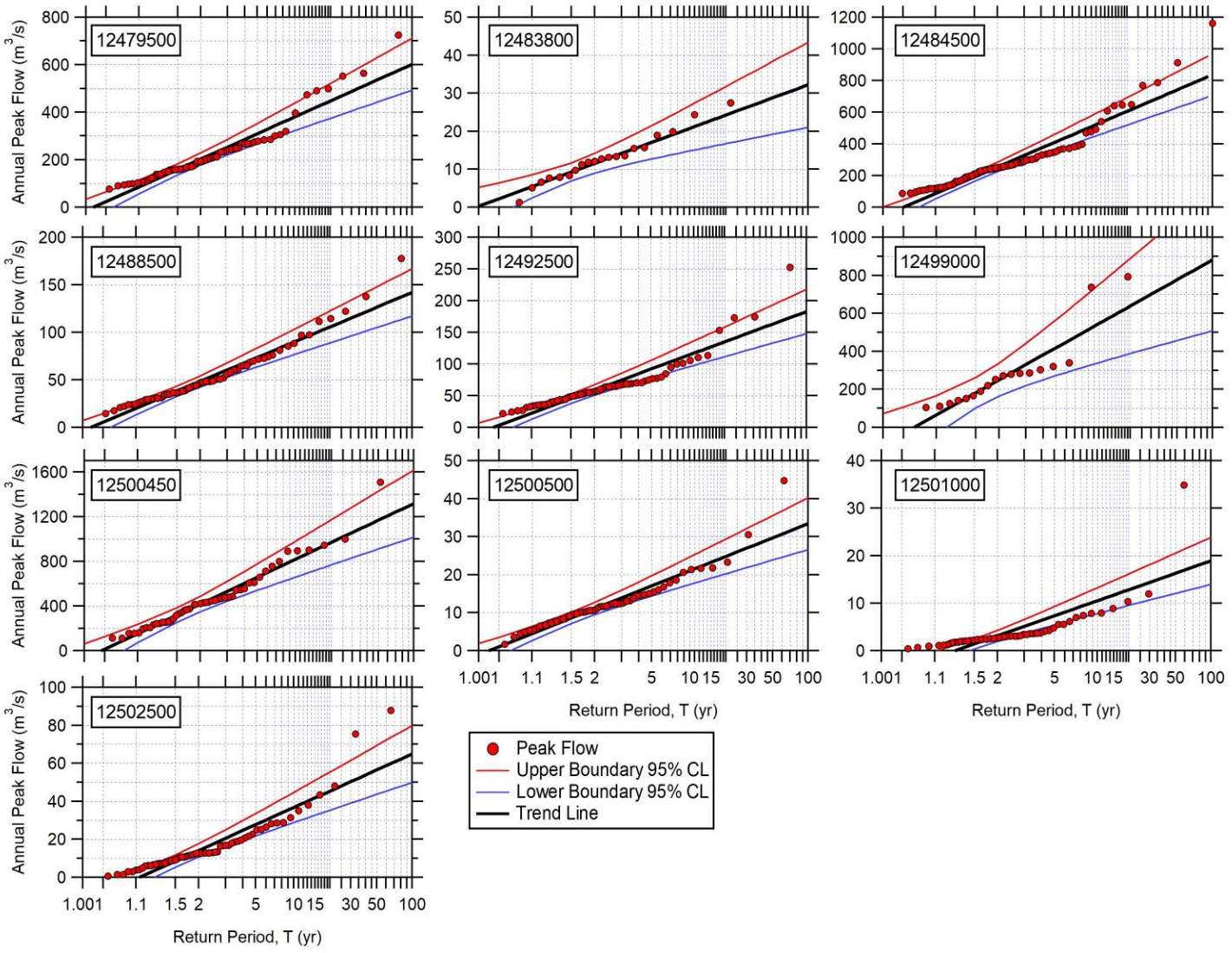

Table A-10. Streamflow trends (maximum and minimum) for the Washington site. Percentile interval values are in *parentheses,* and the >90th percentile intervals are *bolded*.

Station Name (Code for Analysis, USGS Number)	Jan (%)	Feb (%)	Mar (%)	Apr (%)	May (%)	Jun (%)	Jul (%)	Aug (%)	Sep (%)	Oct (%)	Nov (%)	Dec (%)	JFM (%)	AMJ (%)	JAS (%)	OND (%)	Year (%)
Maximum Streamflow Difference																	
Yakima River at Umtanum (YAKUM, 12484500)	19 (0.32)	16 (0.19)	17 (0.13)	−13 (0.43)	−27 (0.19)	−19 (0.38)	**34 (0.00)**	**39 (0.00)**	8 (0.59)	−21 (0.16)	**26 (0.03)**	3 (0.68)	**25 (0.09)**	−28 (0.11)	**30 (0.00)**	4 (0.43)	−12 (0.70)
American River near Nile (AME; 12488500)	**39 (0.03)**	17 (0.35)	**31 (0.03)**	16 (0.42)	−3 (0.82)	−24 (0.15)	**−33 (0.10)**	−17 (0.21)	**−19 (0.09)**	6 (0.59)	27 (0.08)	2 (0.91)	**68 (0.01)**	−3 (0.57)	−32 (0.11)	25 (0.22)	10 (0.52)
Yakima River above Ahtanum Creek at Union Gap (YAKUN, 12500450)	−23 (0.35)	−18 (0.40)	15 (0.73)	31 (0.27)	6 (0.83)	−29 (0.29)	−10 (0.42)	−3 (0.49)	**−15 (0.03)**	**16 (0.03)**	**26 (0.02)**	9 (0.89)	10 (0.79)	5 (0.82)	−7 (0.55)	10 (0.56)	0 (0.97)
Ahtanum Creek at Union Gap (AHTUN, 12502500)	−17 (0.41)	−25 (0.65)	10 (0.72)	28 (0.28)	39 (0.12)	−13 (0.87)	−16 (0.53)	8 (0.67)	5 (0.71)	32 (0.43)	23 (0.33)	−2 (0.60)	−9 (0.85)	22 (0.40)	−11 (0.66)	10 (0.87)	−2 (0.97)
Minimum Streamflow Difference																	
Yakima River at Umtanum (YAKUM, 12484500)	**45 (0.01)**	**42 (0.01)**	**22 (0.06)**	7 (0.50)	−16 (0.41)	0 (0.93)	**39 (0.00)**	**23 (0.00)**	**−49 (0.00)**	**60 (0.00)**	**68 (0.00)**	**33 (0.01)**	**54 (0.00)**	12 (0.27)	**−46 (0.00)**	**74 (0.00)**	**80 (0.00)**
American River near Nile (AME; 12488500)	23 (0.17)	**23 (0.04)**	**20 (0.10)**	**27 (0.03)**	3 (0.55)	−17 (0.32)	−20 (0.14)	−13 (0.18)	−6 (0.32)	−14 (0.18)	2 (1.00)	−21 (0.19)	21 (0.12)	**25 (0.05)**	−6 (0.40)	−13 (0.12)	−8 (0.25)
Yakima River above Ahtanum Creek at Union Gap (YAKUN, 12500450)	**25 (0.10)**	9 (0.69)	15 (0.60)	31 (0.14)	1 (0.89)	−8 (0.75)	0 (0.96)	**−10 (0.09)**	**−13 (0.04)**	**25 (0.05)**	**32 (0.02)**	**34 (0.01)**	**36 (0.07)**	20 (0.39)	−13 (0.04)	**38 (0.01)**	**45 (0.00)**
Ahtanum Creek at Union Gap (AHTUN, 12502500)	**−46 (0.04)**	−41 (0.14)	−27 (0.56)	1 (0.74)	7 (0.57)	−16 (0.71)	−11 (0.64)	16 (0.65)	8 (0.59)	14 (0.64)	−7 (1.00)	**−48 (0.04)**	**−47 (0.07)**	−15 (0.64)	11 (0.79)	−11 (0.67)	0 (0.92)

Figure A-3. Maximum streamflow (*top* = JFM; *second row* = AMJ; *third row* = JAS; *fourth row* = OND; *fifth row* = year [YR]) GEV results for Washington sites. Return intervals (T = 2, 5, 10, 20, 50, and 100 years) from the GEV fits are shown in *dashed lines*.

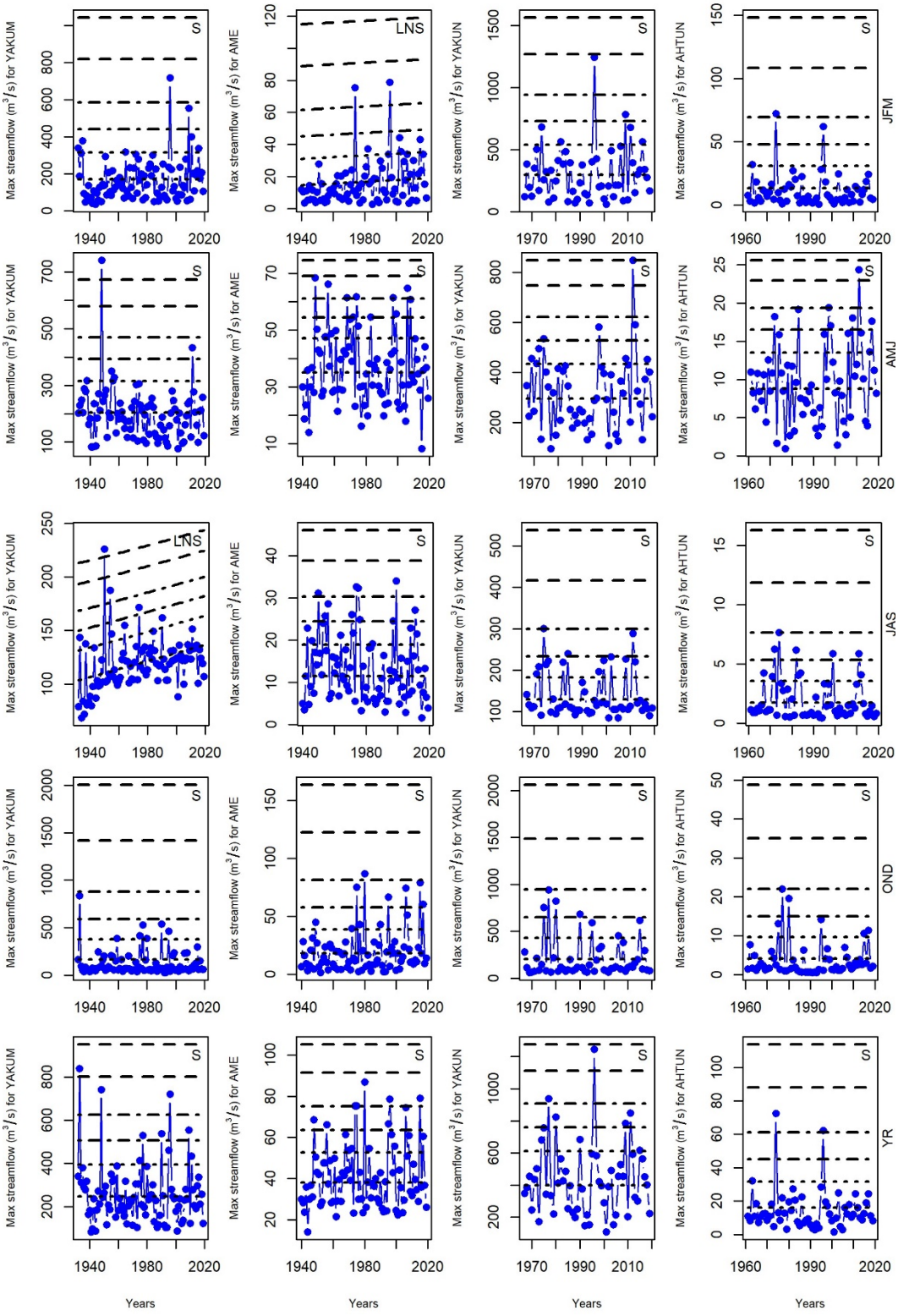

Figure A-4. Annual maximum daily precipitation depths for meteorological stations in the Washington site.

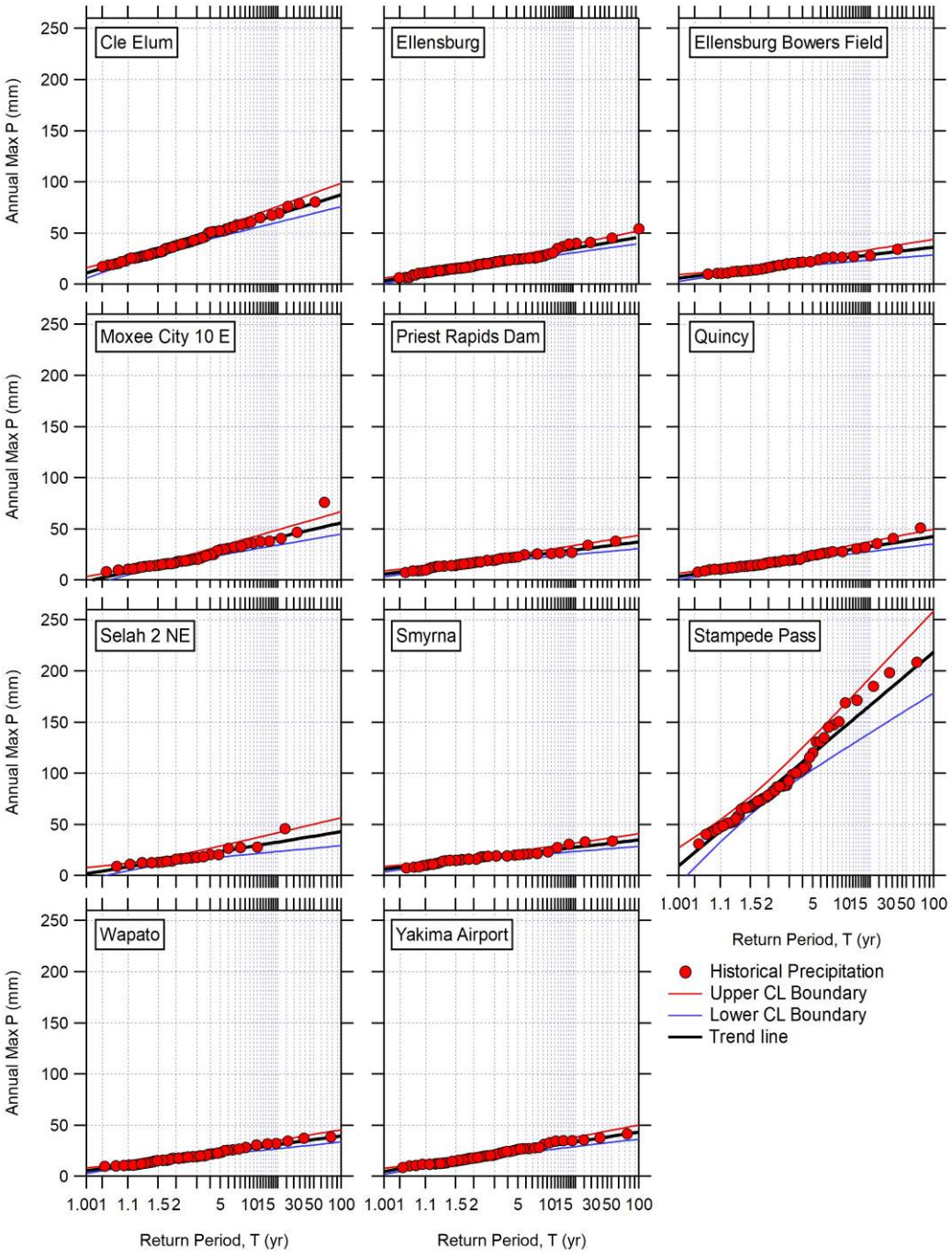

A.3 Results and Discussion for Colorado

Figure A-5. VIC and SnowModel SWE output compared to SNOTEL and meteorological stations from 1979 to 2015, Colorado.

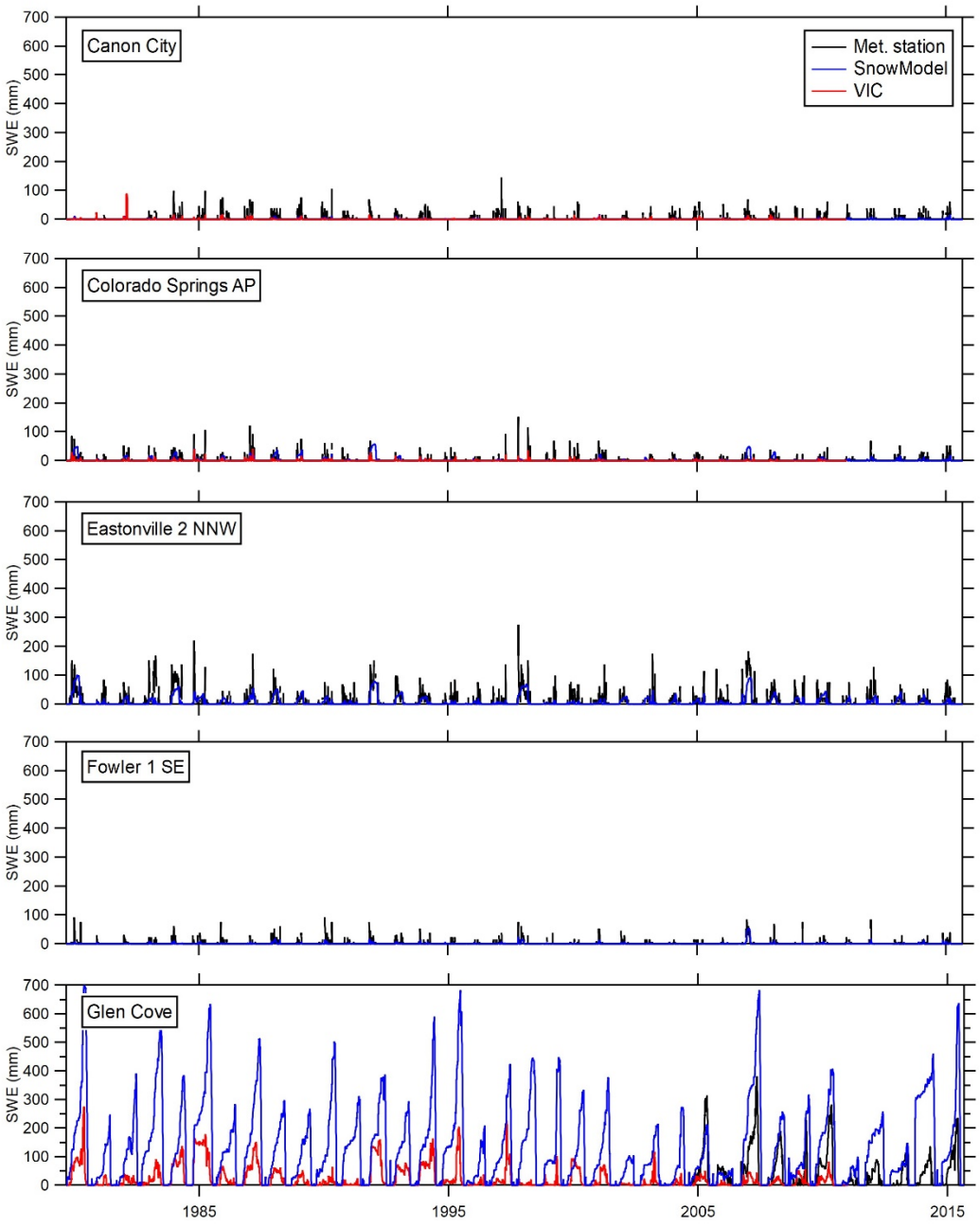

Figure A-5 (cont.). VIC and SnowModel SWE output compared to SNOTEL and meteorological stations from 1979 to 2015, Colorado.

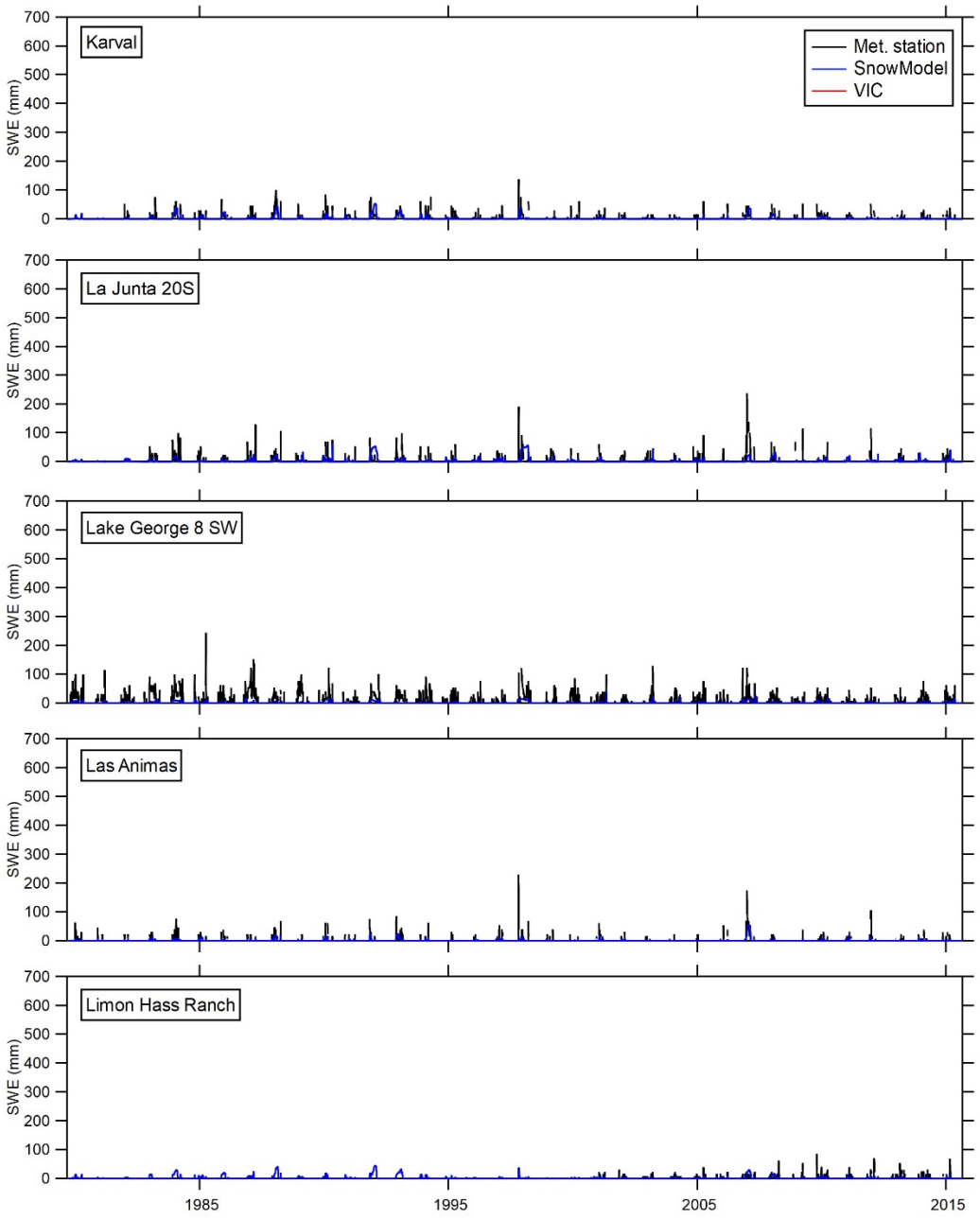

Figure A-5 (cont.). VIC and SnowModel SWE output compared to SNOTEL and meteorological stations from 1979 to 2015, Colorado.

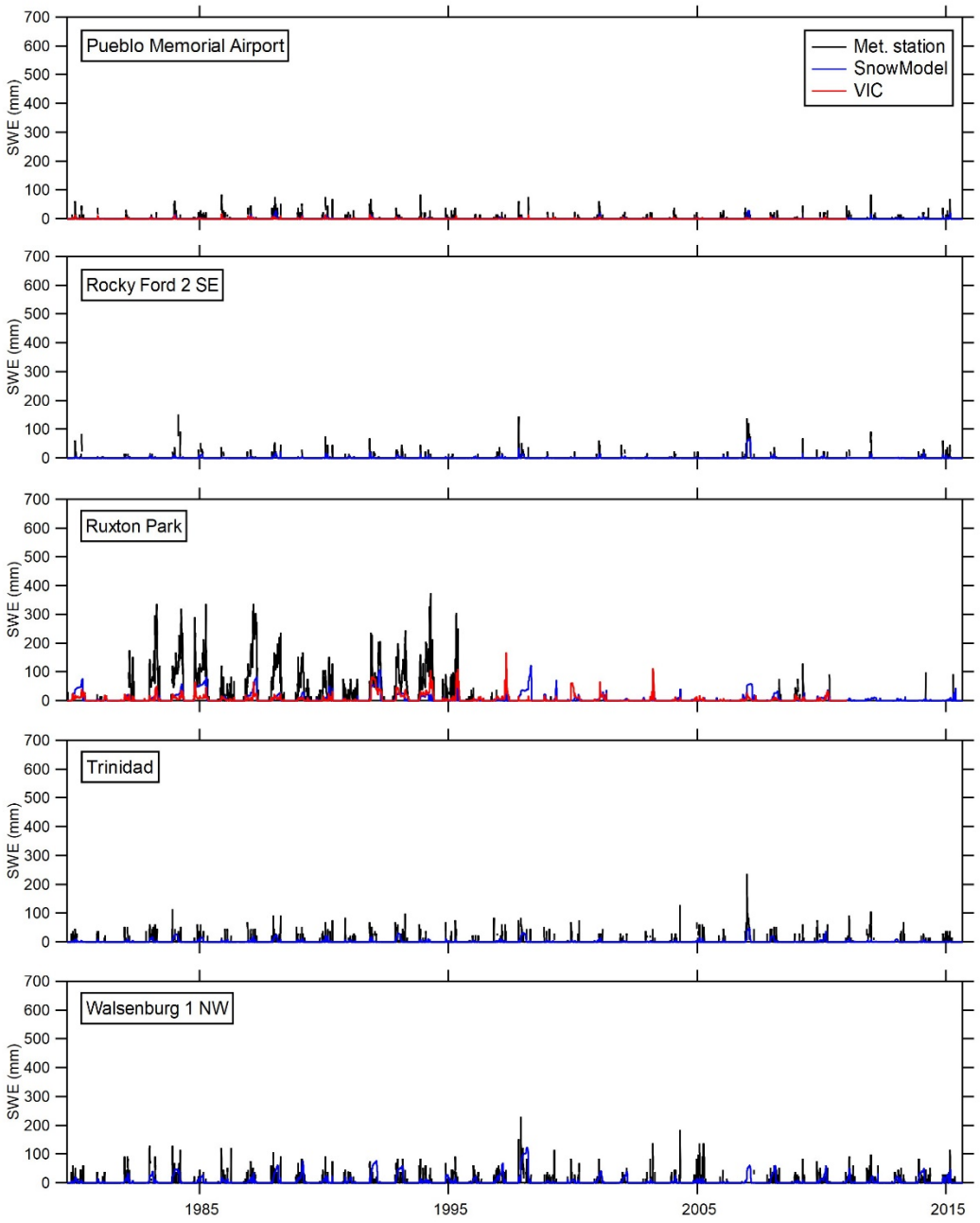

Figure A-5 (cont.). VIC and SnowModel SWE output compared to SNOTEL and meteorological stations from 1979 to 2015, Colorado.

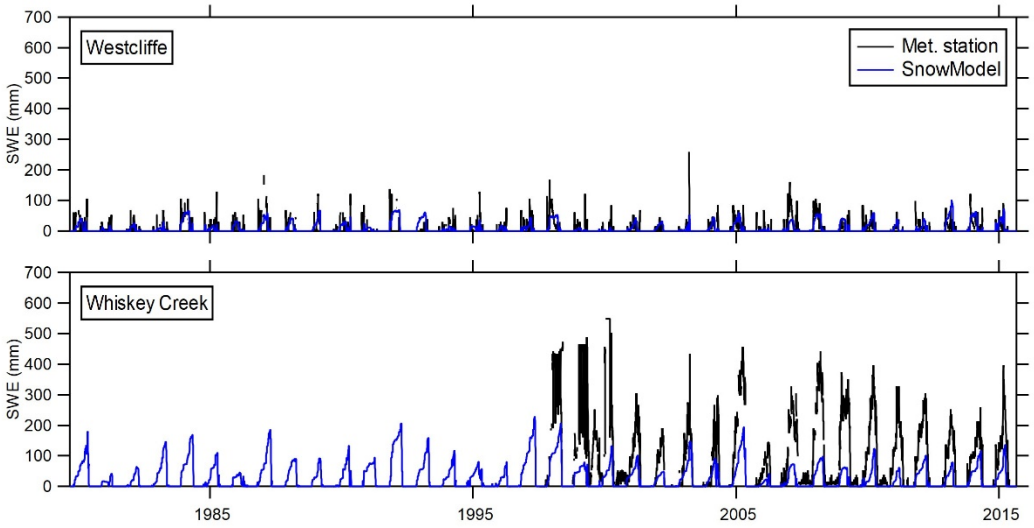

Figure A-6. Return period of annual peak flow and upper- and lower-boundary 95% CL for the USGS gaged rivers in the Colorado site.

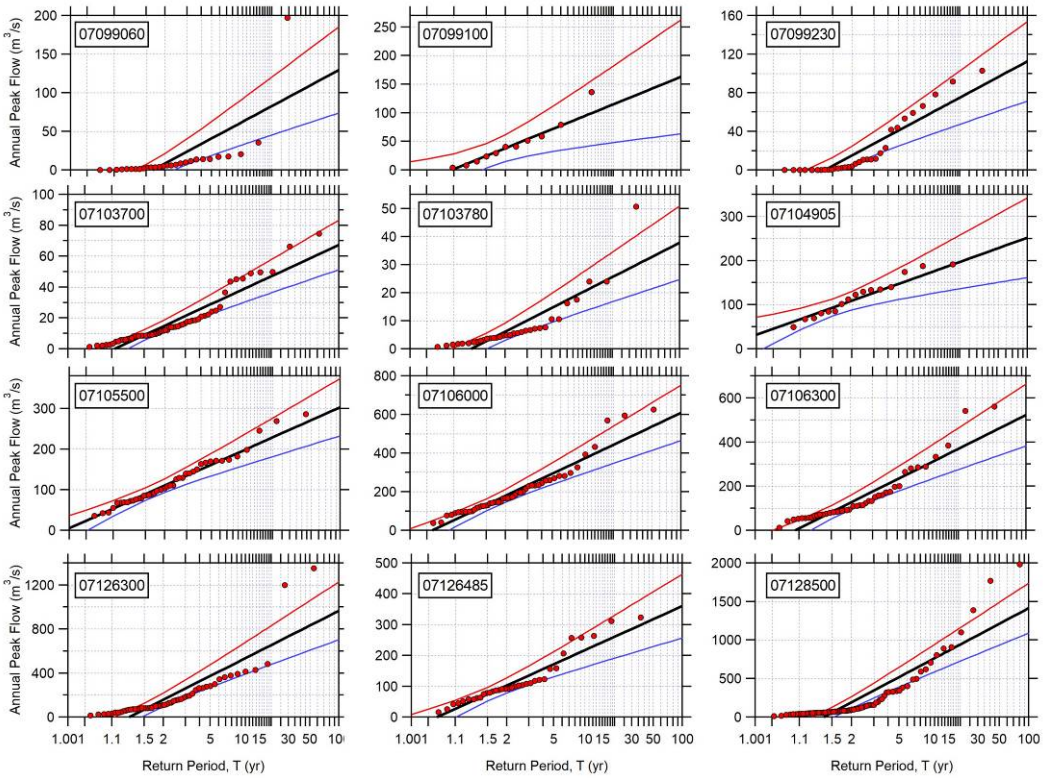

Figure A-7. (*a*) Maximum and (*b*) Minimum streamflow (*Q*) trends (%) for the USGS stations in Colorado. *Circles* indicate the trends for 12 days, *rectangles* indicate seasonal results, and the annual trend is given in the *lower left box*. Statistical significance is shown: the 99th percentile (*dark gray*), the 95th percentile (*light gray*), and nonsignificant results (*white*). Midmonth dates are shown on the x-axis. Sites are ordered by basin size.

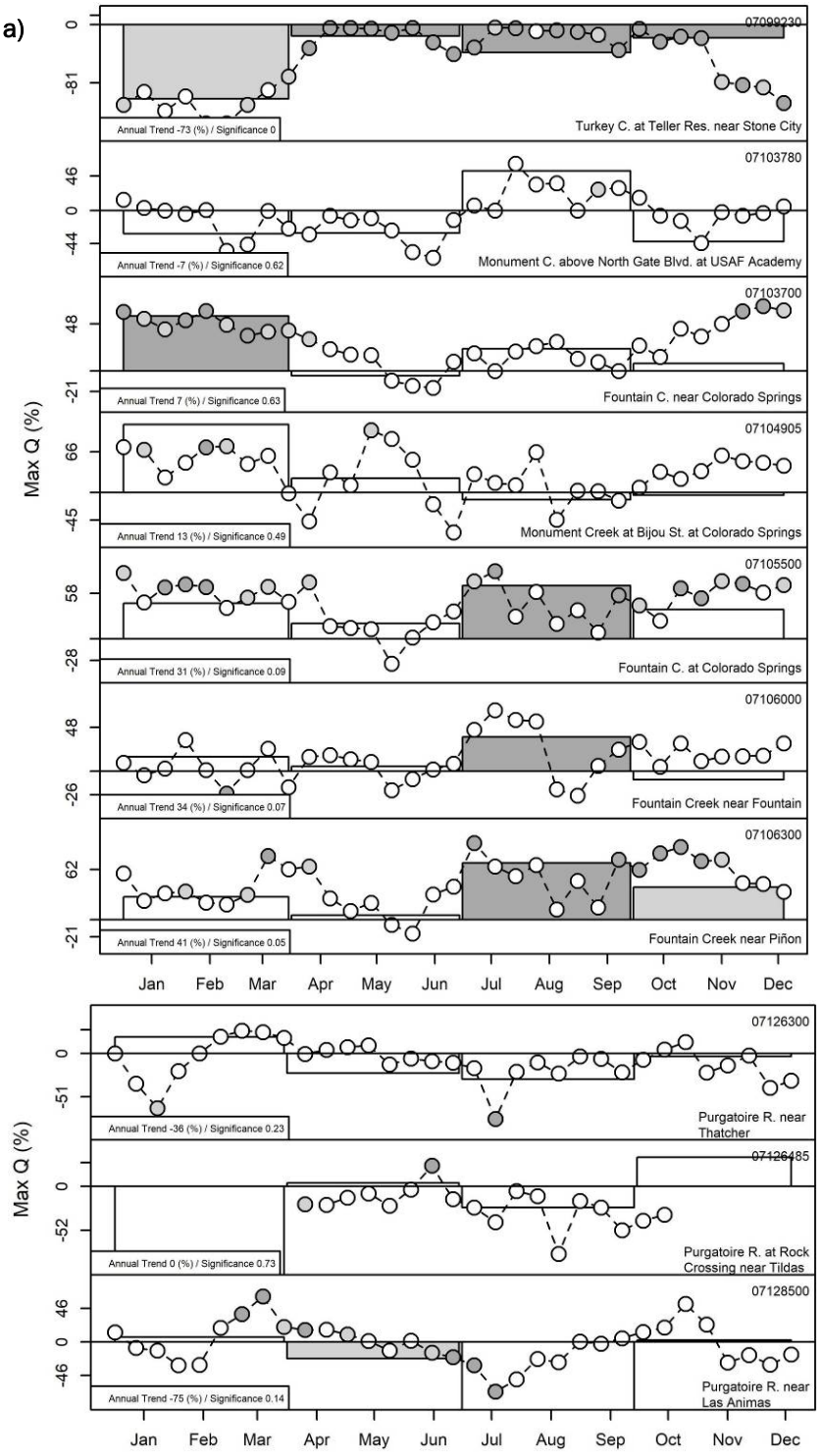

Figure A-7 (cont.). (*a*) Maximum and (*b*) Minimum streamflow (*Q*) trends (%) for the USGS stations in Colorado. *Circles* indicate the trends for 12 days, *rectangles* indicate seasonal results, and the annual trend is given in the *lower left box*. Statistical significance is shown: the 99th percentile (*dark gray*), the 95th percentile (*light gray*), and nonsignificant results (*white*). Midmonth dates are shown on the x-axis. Sites are ordered by basin size.

b)

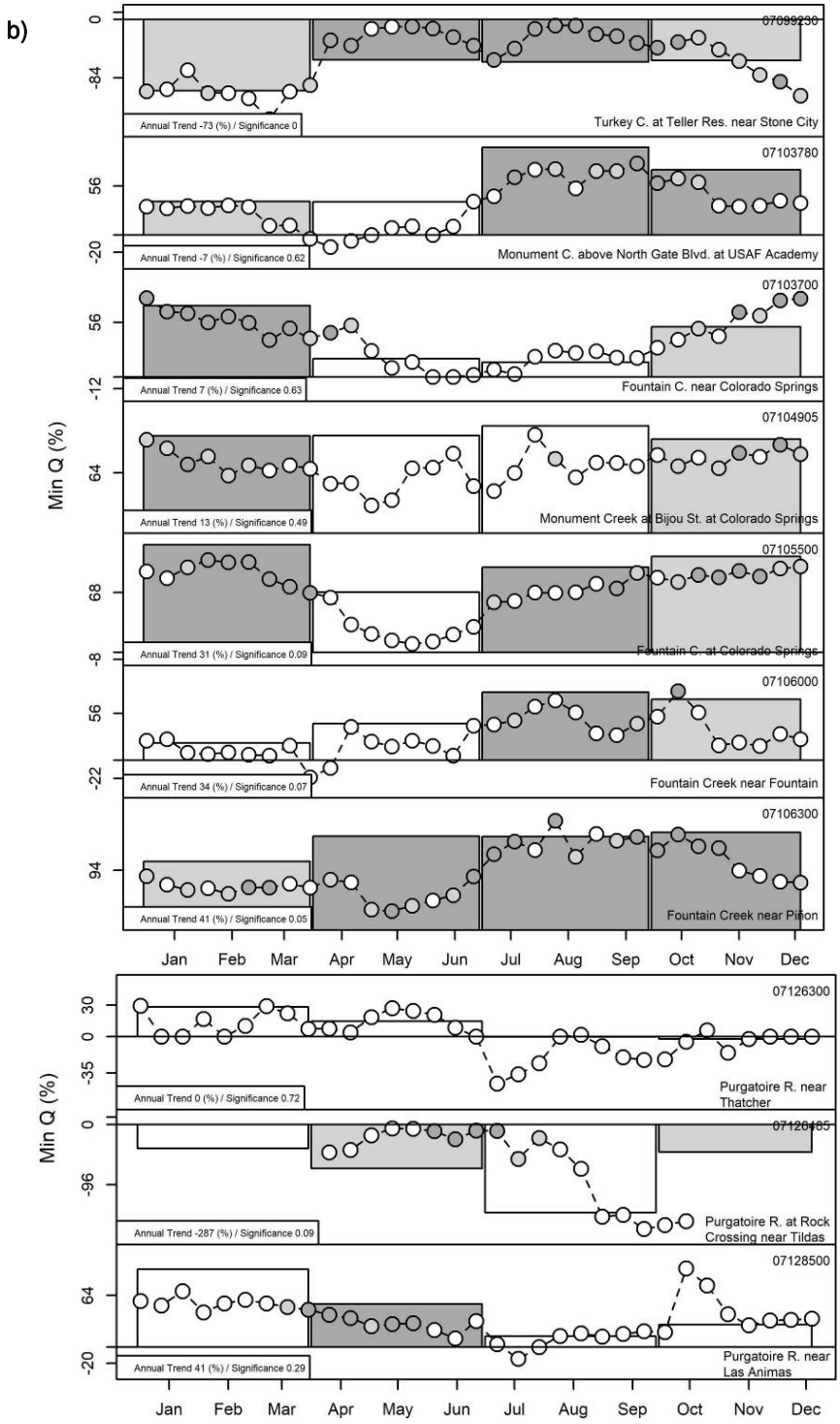

Table A-11. Streamflow trends (maximum and minimum) for the Colorado site. Percentile interval values are in *parentheses,* and the >90th percentile intervals are *bolded*.

Station Name (Code for Analysis, USGS Number)	Jan (%)	Feb (%)	Mar (%)	Apr (%)	May (%)	Jun (%)	Jul (%)	Aug (%)	Sep (%)	Oct (%)	Nov (%)	Dec (%)	JFM (%)	AMJ (%)	JAS (%)	OND (%)	Year (%)
Maximum Streamflow Difference																	
Turkey Creek at Teller Res. near Stone City (TURK, 07099230)	**−117 (0.05)**	**−129 (0.09)**	**−91 (0.04)**	**−5 (0.01)**	**−5 (0.00)**	**−9 (0.00)**	**−21 (0.03)**	**−13 (0.00)**	**−28 (0.00)**	**−10 (0.01)**	**−21 (0.00)**	**−97 (0.01)**	**−103 (0.03)**	**−16 (0.00)**	**−39 (0.00)**	**−18 (0.00)**	**−1 (0.03)**
Fountain Creek near Colorado Springs (FNCS, 07103700)	**48 (0.01)**	**56 (0.00)**	**55 (0.00)**	24 (0.11)	12 (0.40)	−25 (0.17)	22 (0.48)	25 (0.37)	20 (0.17)	10 (0.47)	**40 (0.09)**	**66 (0.01)**	**56 (0.00)**	−5 (0.75)	23 (0.43)	7 (0.60)	7 (0.63)
Monument Creek above North Gate Blvd. at USAF Academy (MCUSAF, 07103780)	0 (0.72)	−22 (0.64)	−24 (0.38)	−13 (0.36)	−12 (0.41)	**−61 (0.06)**	12 (0.84)	37 (0.13)	23 (0.13)	−11 (0.91)	−41 (0.14)	−24 (0.44)	−31 (0.27)	−30 (0.16)	53 (0.13)	**−41 (0.10)**	−7 (0.62)
Monument Creek at Bijou Street at Colorado Springs (MCCS, 07104905)	46 (0.77)	**66 (0.02)**	121 (0.17)	−17 (0.84)	**87 (0.03)**	−41 (0.69)	**45 (0.09)**	−12 (0.49)	3 (0.84)	8 (0.69)	22 (0.37)	42 (0.20)	111 (0.14)	23 (0.55)	−12 (0.77)	−5 (0.92)	13 (0.49)
Fountain Creek at Colorado Springs (FCCS, 07105500)	**56 (0.05)**	**60 (0.01)**	**60 (0.04)**	28 (0.26)	16 (0.71)	9 (0.98)	**64 (0.01)**	**65 (0.00)**	**32 (0.01)**	34 (0.20)	**55 (0.03)**	**58 (0.07)**	**45 (0.10)**	19 (0.45)	**68 (0.00)**	37 (0.16)	**31 (0.09)**
Fountain Creek near Fountain (FCF, 07106000)	−2 (0.79)	8 (0.59)	15 (0.91)	23 (0.33)	7 (0.89)	−17 (0.22)	63 (0.14)	28 (0.33)	17 (0.15)	13 (0.70)	9 (0.19)	24 (0.31)	16 (0.96)	5 (0.55)	**38 (0.00)**	−9 (1.00)	**34 (0.07)**
Fountain Creek near Piñon (FCP, 07106300)	21 (0.13)	**27 (0.03)**	**42 (0.04)**	30 (0.14)	20 (0.60)	−1 (0.70)	**100 (0.01)**	36 (0.41)	**38 (0.00)**	**54 (0.01)**	**64 (0.06)**	28 (0.17)	**28 (0.08)**	6 (1.00)	**70 (0.00)**	**40 (0.02)**	**41 (0.05)**
Purgatoire River near Thatcher (PURT, 07126300)	**−58 (0.05)**	−11 (0.37)	**33 (0.01)**	5 (0.77)	−6 (0.62)	−18 (0.38)	−33 (0.11)	−33 (0.36)	−8 (0.98)	4 (0.47)	−6 (0.98)	−31 (0.19)	19 (0.25)	−23 (0.29)	−30 (0.54)	−3 (0.66)	−36 (0.23)
Purgatoire River at Rock Crossing near Tildas (PRRCT, 07126485)	−125 (0.32)	−436 (0.26)	7 (0.93)	−38 (0.61)	−51 (0.41)	−8 (0.32)	−6 (0.61)	−6 (0.32)	−59 (0.26)	6 (0.93)	−199 (0.61)	−1002 (0.41)	−203 (0.50)	4 (0.93)	−25 (0.50)	35 (0.93)	−16 (0.50)
Purgatoire River near Las Animas (PTLA, 07128500)	−18 (0.35)	−48 (0.17)	**43 (0.00)**	**15 (0.01)**	−9 (0.22)	**−29 (0.02)**	**−110 (0.01)**	**−83 (0.02)**	−4 (0.62)	14 (0.22)	15 (0.48)	−41 (0.16)	7 (0.58)	**−23 (0.03)**	−101 (0.26)	3 (0.58)	−75 (0.14)

Table A-11 (cont.). Streamflow trends (maximum and minimum) for the Colorado site. Percentile interval values are in *parentheses,* and the >90th percentile intervals are ***bolded***.

Station Name (Code for Analysis, USGS Number)	Jan (%)	Feb (%)	Mar (%)	Apr (%)	May (%)	Jun (%)	Jul (%)	Aug (%)	Sep (%)	Oct (%)	Nov (%)	Dec (%)	JFM (%)	AMJ (%)	JAS (%)	OND (%)	Year (%)
Minimum Streamflow Difference																	
Turkey Creek at Teller Res. near Stone City (TURK, 07099230)	**−92** **(0.07)**	**−115** **(0.05)**	**−130** **(0.05)**	**−32** **(0.04)**	−15 (0.45)	**−20** **(0.00)**	**−34** **(0.00)**	**−16** **(0.00)**	**−28** **(0.00)**	**−48** **(0.01)**	**−45** **(0.02)**	**−98** **(0.02)**	**−103** **(0.04)**	**−58** **(0.00)**	**−61** **(0.00)**	**−59** **(0.03)**	**−321** **(0.04)**
Fountain Creek near Colorado Springs (FNCS, 07103700)	**69** **(0.01)**	**61** **(0.00)**	**44** **(0.01)**	**37** **(0.05)**	15 (0.36)	9 (0.63)	11 (0.51)	17 (0.93)	19 (0.54)	**39** **(0.10)**	**64** **(0.01)**	**73** **(0.01)**	**73** **(0.00)**	19 (0.44)	15 (0.41)	**52** **(0.04)**	**41** **(0.08)**
Monument Creek above North Gate Blvd. at USAF Academy (MCUSAF, 07103780)	**37** **(0.07)**	**38** **(0.01)**	22 (0.28)	4 (0.91)	14 (0.79)	19 (0.33)	**86** **(0.00)**	**81** **(0.02)**	**82** **(0.01)**	**80** **(0.00)**	50 (0.16)	50 (0.15)	**38** **(0.03)**	38 (0.33)	**100** **(0.00)**	**74** **(0.01)**	**110** **(0.01)**
Monument Creek at Bijou Street at Colorado Springs (MCCS, 07104905)	**90** **(0.01)**	**85** **(0.00)**	**80** **(0.06)**	76 (0.20)	53 (0.43)	82 (0.23)	**96** **(0.07)**	**76** **(0.03)**	**89** **(0.09)**	**108** **(0.02)**	**94** **(0.01)**	**92** **(0.01)**	**97** **(0.00)**	97 (0.28)	106 (0.14)	**94** **(0.04)**	111 (0.14)
Fountain Creek at Colorado Springs (FCCS, 07105500)	**101** **(0.06)**	**118** **(0.00)**	**98** **(0.00)**	**70** **(0.02)**	27 (0.26)	20 (0.57)	**70** **(0.01)**	**83** **(0.02)**	**89** **(0.02)**	**90** **(0.03)**	**99** **(0.01)**	**98** **(0.01)**	**122** **(0.00)**	**68** **(0.07)**	**97** **(0.01)**	**109** **(0.02)**	**121** **(0.07)**
Fountain Creek near Fountain (FCF, 07106000)	31 (0.51)	19 (0.96)	0 (0.41)	24 (0.33)	22 (0.27)	31 (0.39)	**69** **(0.00)**	96 (0.29)	43 (0.33)	**69** **(0.02)**	25 (0.53)	26 (0.12)	21 (0.47)	44 (0.18)	**81** **(0.01)**	**73** **(0.03)**	**92** **(0.01)**
Fountain Creek near Piñon (FCP, 07106300)	**99** **(0.01)**	**87** **(0.01)**	**80** **(0.05)**	**87** **(0.01)**	**54** **(0.00)**	**68** **(0.00)**	**119** **(0.00)**	**157** **(0.03)**	**160** **(0.01)**	**136** **(0.00)**	**124** **(0.01)**	**89** **(0.08)**	**106** **(0.01)**	**139** **(0.00)**	**138** **(0.00)**	**143** **(0.00)**	**170** **(0.00)**
Purgatoire River near Thatcher (PURT, 07126300)	34 (0.61)	21 (0.79)	27 (0.75)	6 (0.93)	24 (0.40)	24 (0.42)	−8 (0.77)	−8 (0.70)	−1 (0.98)	−10 (0.64)	7 (0.65)	11 (0.91)	28 (0.64)	15 (0.69)	0 (0.95)	−2 (0.79)	0 (0.72)
Purgatoire River at Rock Crossing near Tildas (PRRCT, 07126485)	**−75** **(0.03)**	−27 (0.55)	−15 (0.82)	−15 (0.31)	**−49** **(0.08)**	**−74** **(0.02)**	**−413** **(0.00)**	**−149** **(0.03)**	−63 (0.55)	−22 (0.82)	−14 (0.31)	**−46** **(0.08)**	−38 (0.21)	**−70** **(0.04)**	−141 (0.21)	**−44** **(0.04)**	−120 (0.21)
Purgatoire River near Las Animas (PTLA, 07128500)	**72** **(0.05)**	**85** **(0.05)**	71 (0.21)	**54** **(0.00)**	**52** **(0.00)**	**35** **(0.01)**	17 (0.44)	15 (0.79)	26 (0.32)	35 (0.51)	51 (0.36)	46 (0.35)	96 (0.18)	**53** **(0.00)**	13 (0.66)	28 (0.52)	41 (0.29)

Figure A-8. Maximum streamflow (*top* = JFM; *second row* = AMJ; *third row* = JAS; *fourth row* = OND; *fifth row* = YR) GEV results for Colorado stations. Return intervals (T = 2, 5, 10, 20, 50, and 100 years) from the GEV fits are shown in *dashed lines*.

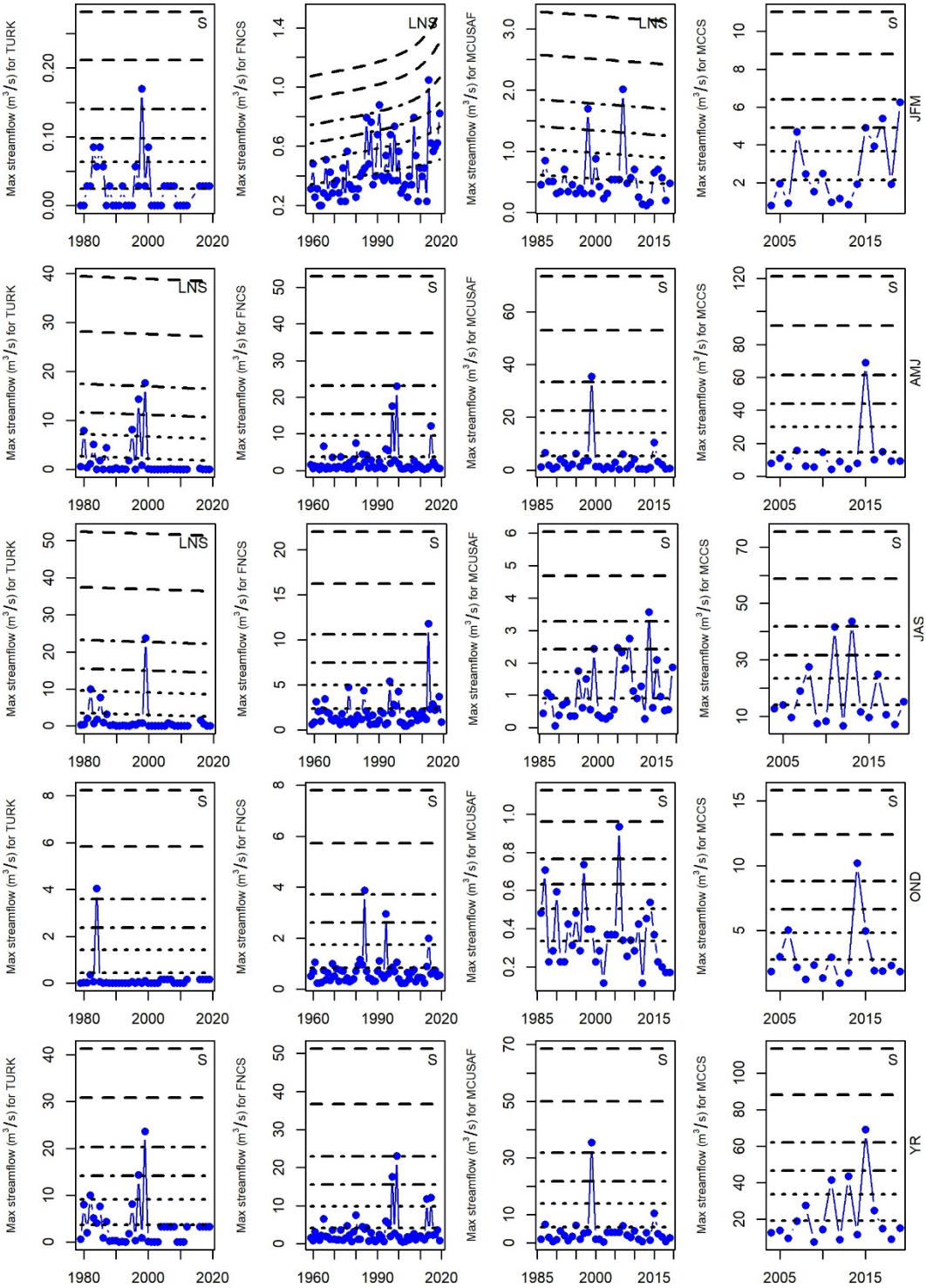

Figure A-8 (cont.). Maximum streamflow (*top* = JFM; *second row* = AMJ; *third row* = JAS; *fourth row* = OND; *fifth row* = YR) GEV results for Colorado stations. Return intervals (T = 2, 5, 10, 20, 50, and 100 years) from the GEV fits are shown in *dashed lines*.

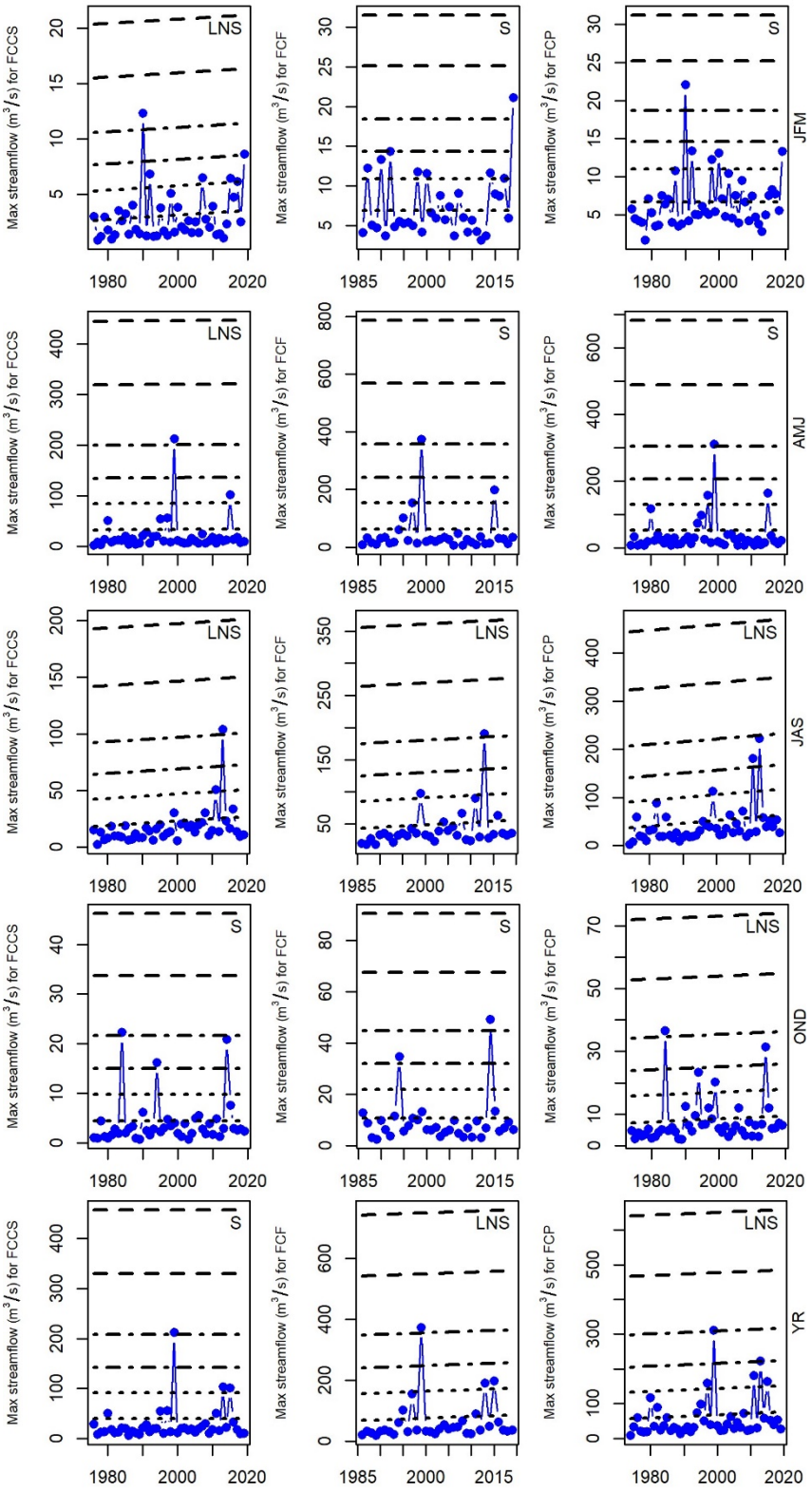

Figure A-8 (cont.). Maximum streamflow (*top* = JFM; *second row* = AMJ; *third row* = JAS; *fourth row* = OND; *fifth row* = YR) GEV results for Colorado stations. Return intervals (T = 2, 5, 10, 20, 50, and 100 years) from the GEV fits are shown in *dashed lines*.

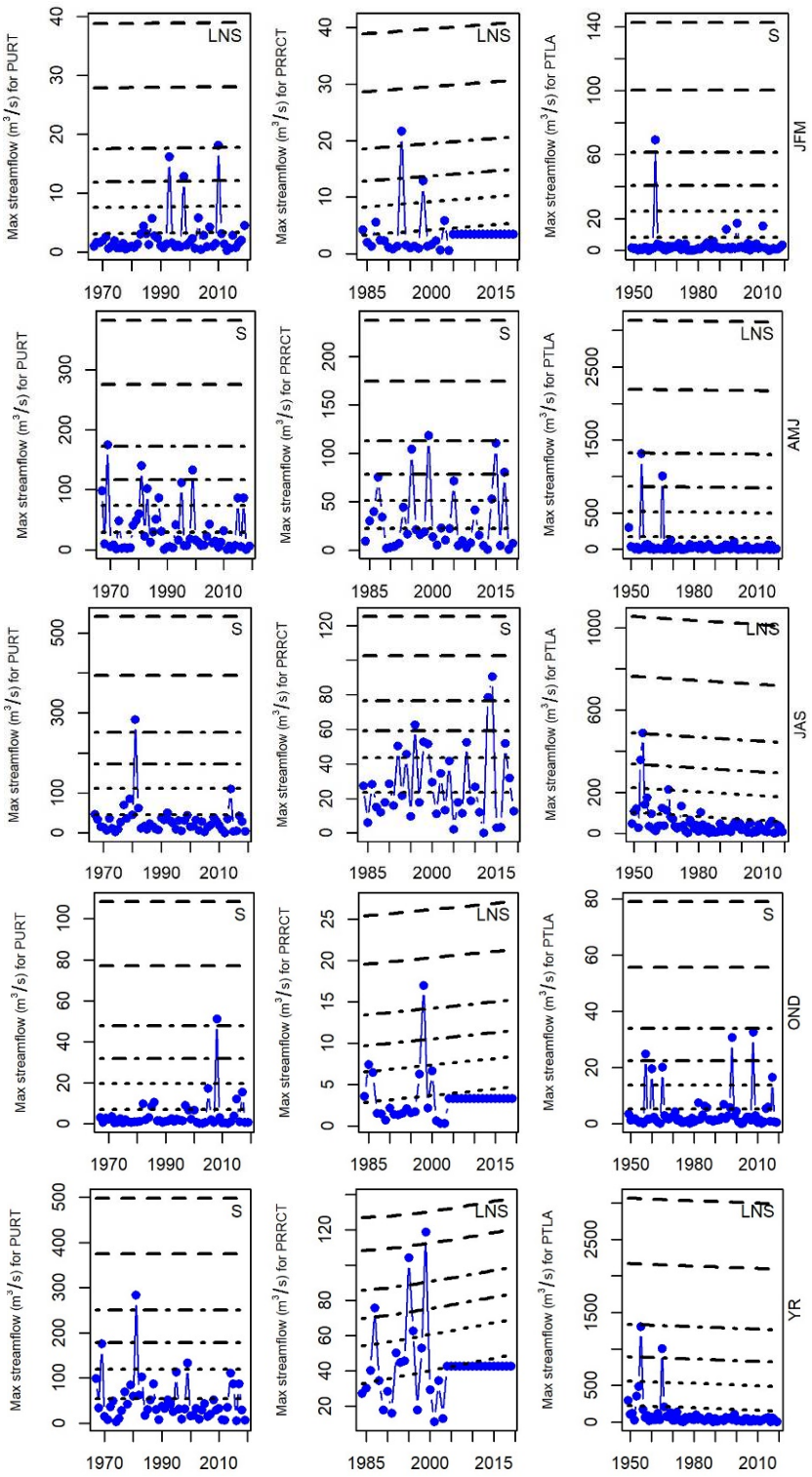

Figure A-9. Annual maximum precipitation depths for meteorological stations in the Colorado site. The site for this analysis was split up into the stations included in the vicinity of (*a*) Fort Carson and (*b*) the Piñon Canyon Maneuver Site.

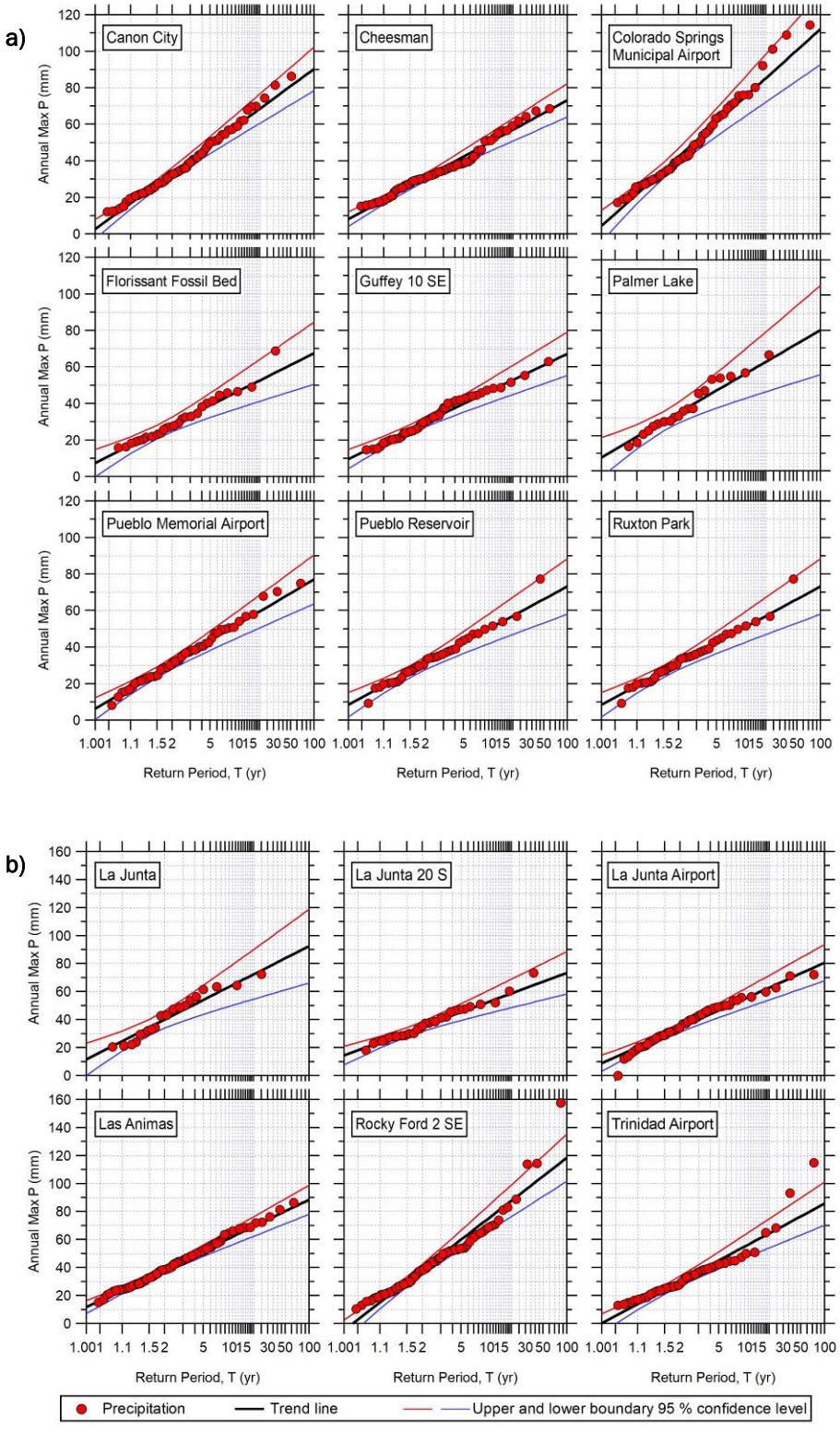

A.4 Results and Discussion for North Dakota

Figure A-10. VIC and SnowModel SWE output compared to meteorological stations from 1979 to 2015, North Dakota.

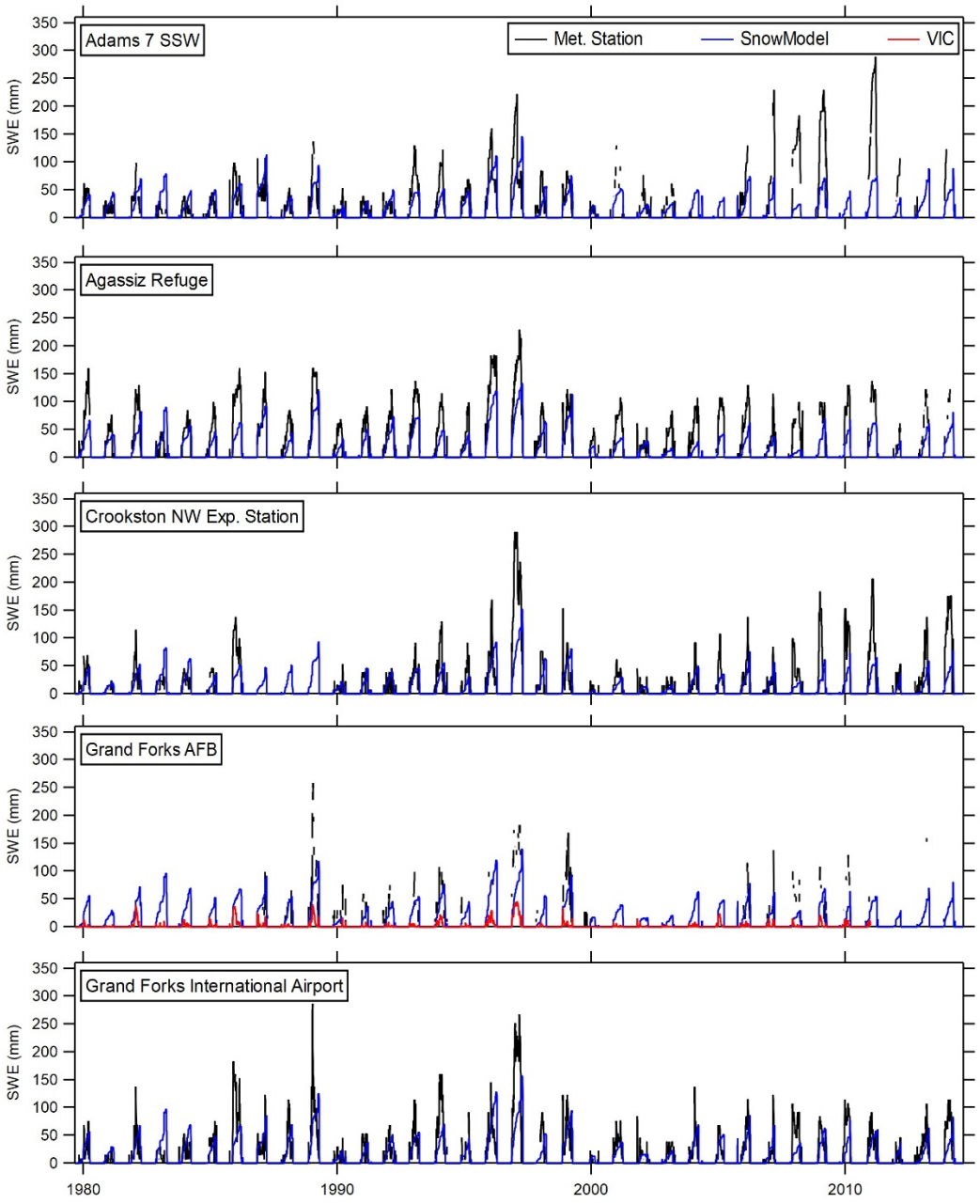

Figure A-10 (cont.). VIC and SnowModel SWE output compared to meteorological stations from 1979 to 2015, North Dakota.

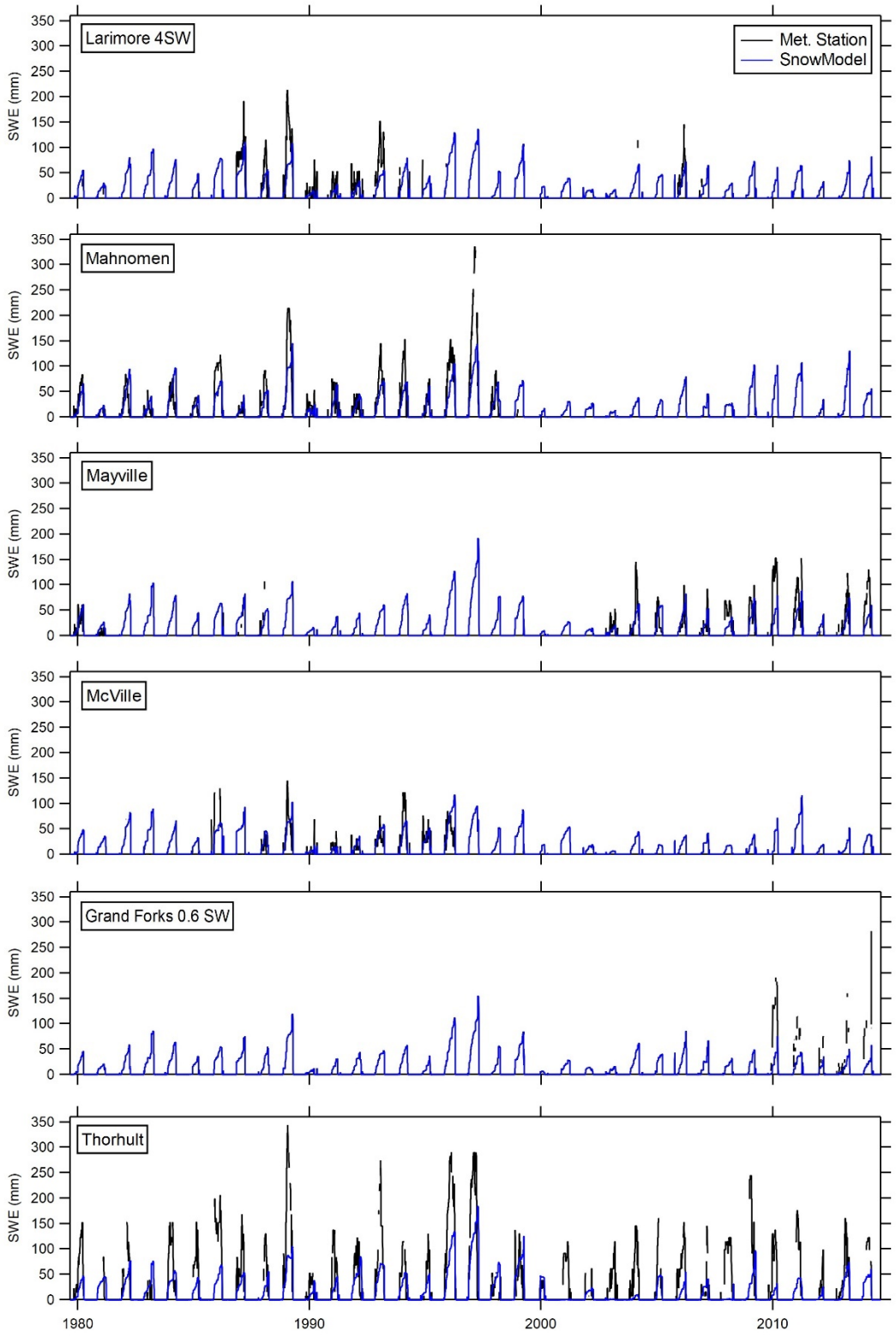

Figure A-11. Return period of annual peak flow for the gaged rivers in the North Dakota site.

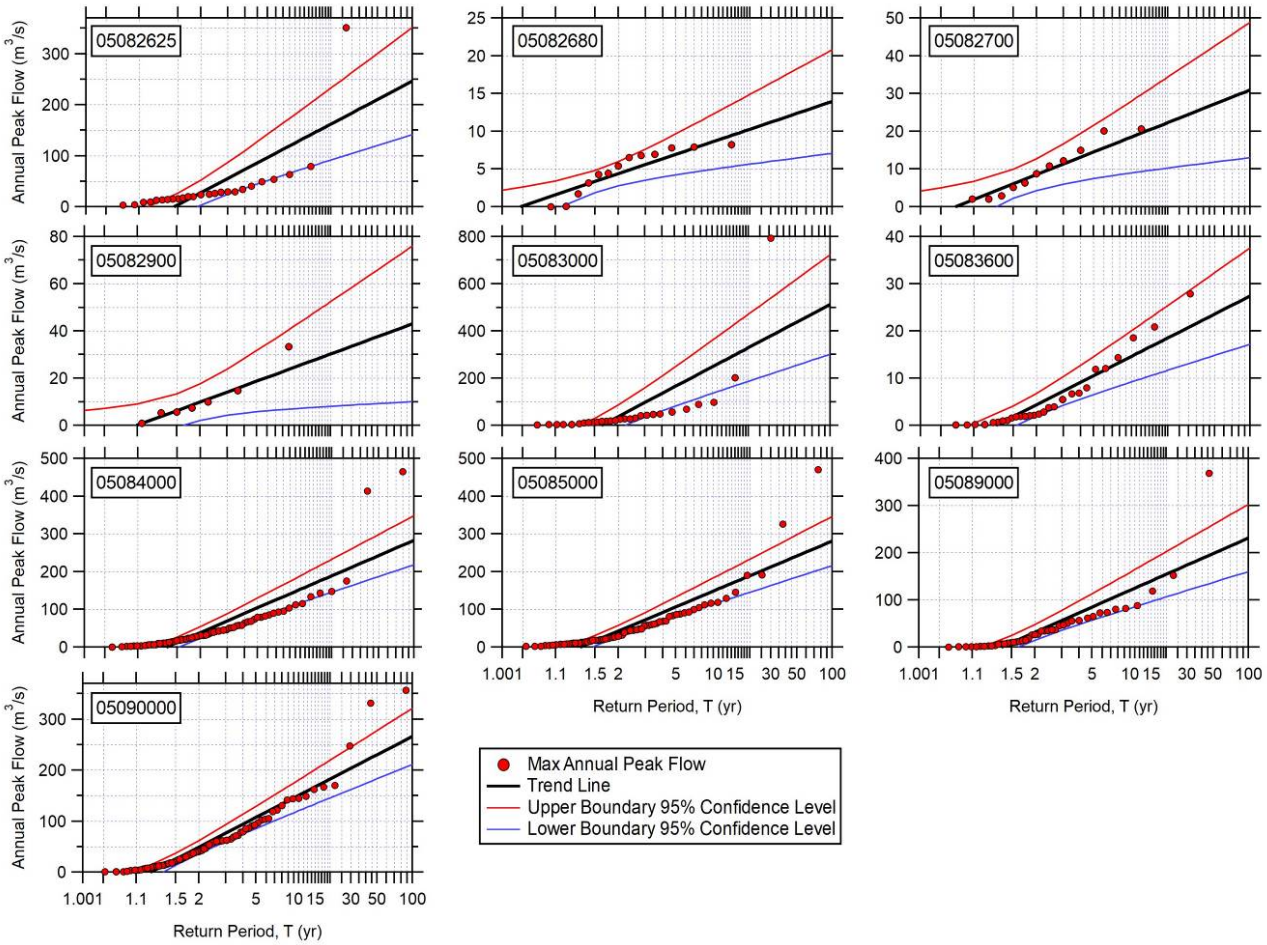

Table A-12. Streamflow trends (maximum and minimum) for the North Dakota site. Percentile interval values are in *parentheses,* and the >90th percentile intervals are ***bolded***.

Station Name (Code for Analysis; USGS Number)	Jan (%)	Feb (%)	Mar (%)	Apr (%)	May (%)	Jun (%)	Jul (%)	Aug (%)	Sep (%)	Oct (%)	Nov (%)	Dec (%)	JFM (%)	AMJ (%)	JAS (%)	OND (%)	Year(%)
Maximum Streamflow Difference																	
Turtle River at Turtle River State Park near Arvilla (TUR)/ 50862625	20 (0.89)	−2 (0.79)	−43 (0.35)	9 (1.00)	41 (0.40)	11 (0.66)	7 (0.60)	−6 (0.96)	14 (0.66)	5 (0.33)	17 (0.63)	28 (0.19)	−43 (0.35)	9 (0.89)	−3 (0.79)	4 (0.86)	−18 (0.23)
Forest River near Fordville (FOR, 5084000)	**104 (0.00)**	**57 (0.00)**	15 (0.32)	−3 (0.87)	**33 (0.00)**	**30 (0.00)**	**34 (0.00)**	**77 (0.00)**	**60 (0.00)**	**87 (0.00)**	**74 (0.00)**	**94 (0.00)**	15 (0.31)	−2 (0.94)	**35 (0.01)**	**74 (0.00)**	−8 (0.80)
Forest River at Minto (MIN, 5085000)	**199 (0.00)**	**93 (0.00)**	19 (0.34)	2 (0.99)	**38 (0.00)**	**42 (0.01)**	**55 (0.00)**	**82 (0.00)**	**72 (0.00)**	**87 (0.00)**	**92 (0.00)**	**133 (0.00)**	19 (0.37)	12 (0.72)	**47 (0.00)**	**77 (0.00)**	10 (0.79)
Park River at Grafton (PAR, 5090000)	**141 (0.00)**	**45 (0.00)**	**25 (0.03)**	20 (0.32)	**50 (0.00)**	**64 (0.00)**	**37 (0.00)**	**23 (0.00)**	**11 (0.00)**	**28 (0.00)**	**93 (0.00)**	**100 (0.00)**	**25 (0.03)**	34 (0.15)	**39 (0.00)**	**68 (0.00)**	**42 (0.09)**
Minimum Streamflow Difference																	
Turtle River at Turtle River State Park near Arvilla (TUR, 50862625)	10 (0.96)	27 (0.54)	29 (0.27)	−2 (0.51)	61 (0.13)	**98 (0.05)**	15 (0.77)	−9 (0.63)	**34 (0.08)**	**33 (0.07)**	18 (0.28)	**28 (0.09)**	22 (0.54)	**68 (0.03)**	**45 (0.07)**	**48 (0.03)**	34 (0.31)
Forest River near Fordville (FOR, 5084000)	**127 (0.00)**	**117 (0.00)**	**77 (0.00)**	**93 (0.00)**	**89 (0.00)**	**113 (0.00)**	**121 (0.00)**	**114 (0.00)**	**113 (0.00)**	**116 (0.00)**	**127 (0.00)**	**121 (0.00)**	**117 (0.00)**	**126 (0.00)**	**119 (0.00)**	**127 (0.00)**	**134 (0.00)**
Forest River at Minto (MIN, 5085000)	**198 (0.00)**	**207 (0.00)**	**151 (0.00)**	**108 (0.00)**	**67 (0.02)**	**102 (0.01)**	**143 (0.00)**	**145 (0.00)**	**147 (0.00)**	**164 (0.00)**	**134 (0.00)**	**204 (0.00)**	**180 (0.00)**	**144 (0.00)**	**148 (0.01)**	**210 (0.00)**	**195 (0.00)**
Park River at Grafton (PAR, 5090000)	**101 (0.00)**	**115 (0.00)**	**84 (0.00)**	**66 (0.00)**	**89 (0.00)**	**114 (0.00)**	**92 (0.00)**	**24 (0.00)**	**20 (0.00)**	**8 (0.01)**	**56 (0.00)**	**128 (0.00)**	**97 (0.00)**	**116 (0.00)**	**27 (0.00)**	**17 (0.01)**	**9 (0.08)**

Figure A-12. Maximum streamflow (*top* = JFM; *second row* = AMJ; *third row* = JAS; *fourth row* = OND; *fifth row* = YR) GEV results for North Dakota stations. Return intervals (T = 2, 5, 10, 20, 50, and 100 years) from the GEV fits are shown in *dashed lines*.

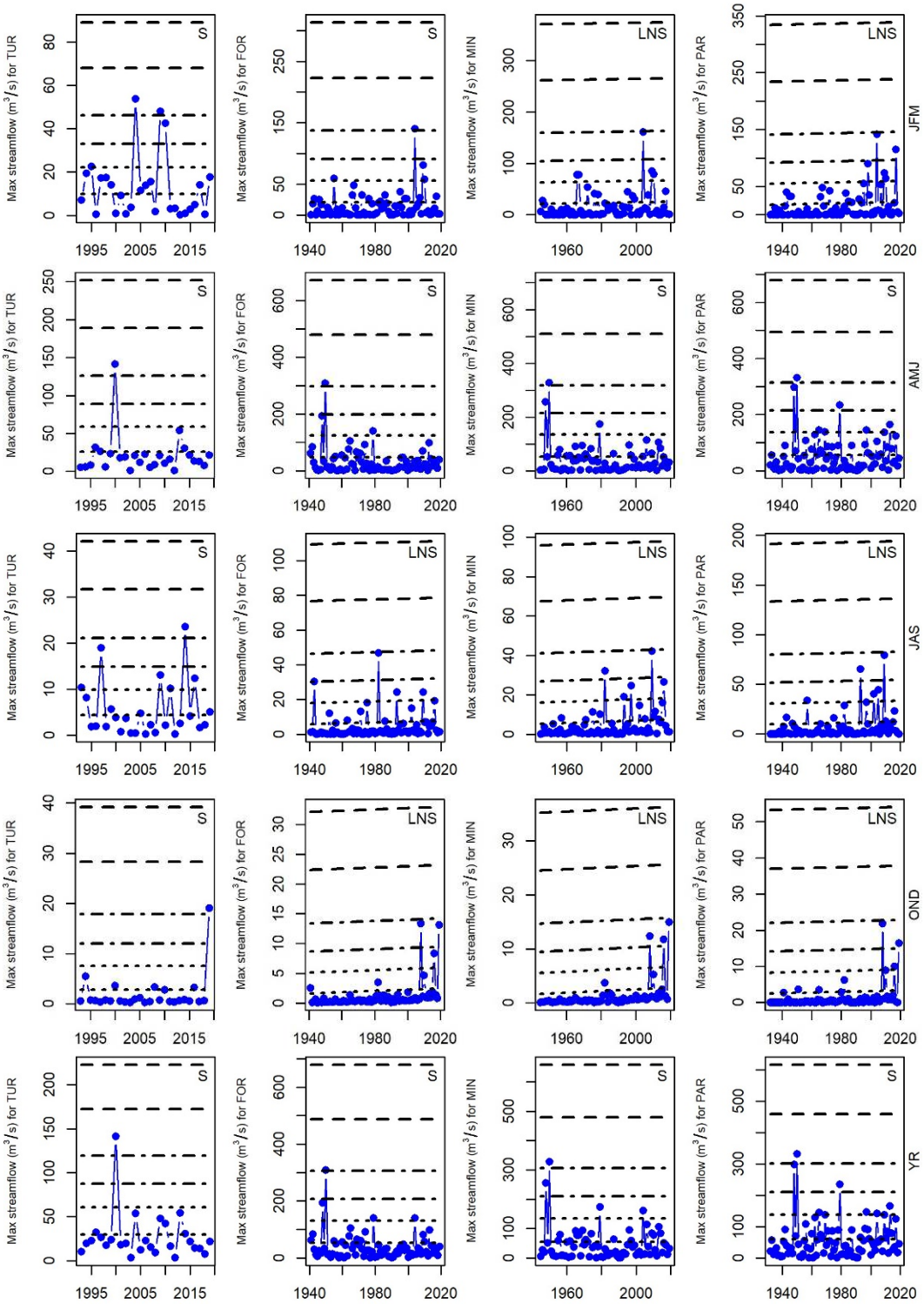

Figure A-13. Annual maximum precipitation depths for meteorological stations in the North Dakota site.

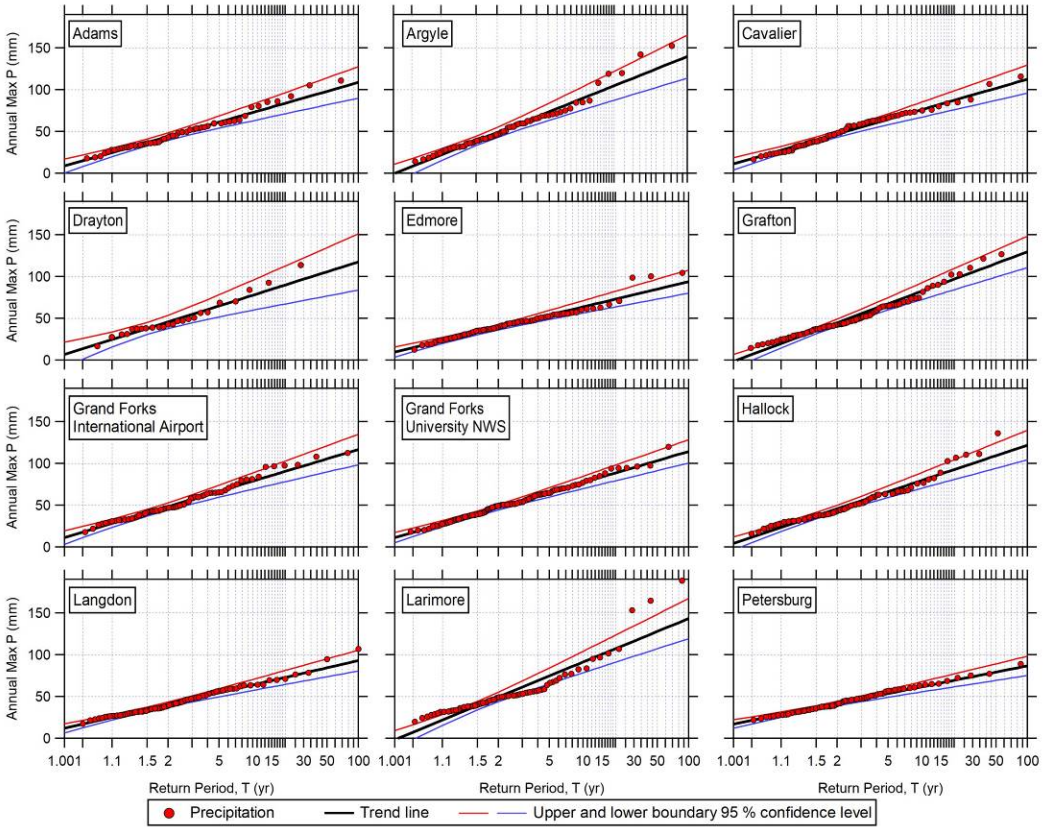

A.5 Geospatial Snow Analyses

A substantial validation gap exists in measured snow depths and SWE calculations. This gap cannot be filled with week-long field campaigns and a handful of cameras, and lidar or photogrammetry flights are expensive to conduct. We sought to partially fill that validation gap with snow-pattern analyses and high-resolution imagery to map snow distributions.

A method that has shown success in previous research studies is using snow patterns for snow-model validation or to produce snow-depth maps (Sturm and Wagner 2010). To normalize snow-depth patterns from year to year, a standardized value (STD) can be derived from the following equation:

$$\mathrm{STD} = \frac{(\mathrm{SD}_i - \mu)}{\sigma}, \tag{A.1}$$

where

SD_i = the snow depth (or SWE) at cell i,
μ = the mean, and
σ = the standard deviation used in the pattern comparison.

We explored this method where we used snow-pattern recognition between the coarse (grid cell = 300 m) and fine-scale (grid cell = 30 m) snow modeling for the YTC, Washington, site (see subsection 3.2.2).

Figure A-14 compares the coarse grid simulations for the highest SWE (3 March 1997) and 1 March 2017 for the finer-resolution grid cell simulations. A striking similarity of the snow patterns between the two different dates are shown and indicates that the snow models perform similarly for a larger- and finer-scale grid cell (300 m vs. 30 m).

Figure A-14. Snow-pattern comparison at YTC, Washington, between (*a*) coarse grid cell (300 m) simulation (3 March 1997) and (*b*) fine grid cell (30 m) simulation (1 March 2017). *Solid black line* outlines YTC.

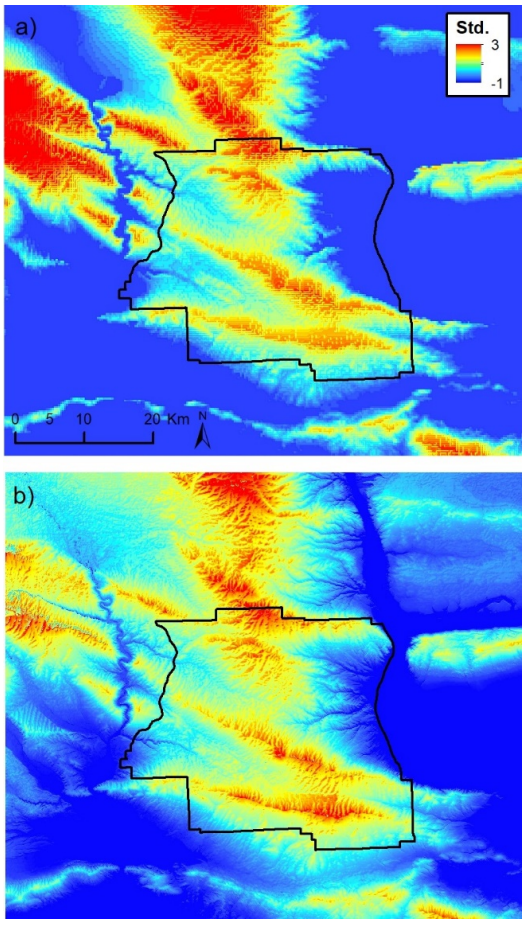

Satellite-imagery analysis consisted of two approaches. In the first, snow extents of available high-resolution images were compared with snow-model outputs. Unfortunately, this approach is limited by available imagery. Not all sites had imagery collected when there was snow present. In fact, the Colorado site had zero stereo image collections with snow. The second entailed using stereo photogrammetry, or structure from motion (Deschamps-Berger et al. 2020; Nolan, Larsen, and Sturm 2015), to calculate snow depths. This requires stereo data collections during satellite tasking.

Modeled snow depths were compared with coincident high-resolution satellite imagery at the Washington site (Figure A-15). The 2 February 2016, 12 January 2017, and 24 January 2017 comparisons show excellent agreement for snow-covered and snow-free areas. The 12 January and 24 January 2017 dates show abundant protruding shrubs (20–80 cm high) underlain by snow. The image from 1 March 2017 looks mismatched, but snow in agricultural clearings east and south of YTC betray the influence of taller shrubs obscuring snow in the 30 m image. The 2 April 2017 image shows modeled shallow snow lingering at higher elevations; but the snow model shows a solid shallow patch, and the image has snow distributed in ravines. In all, this comparison shows that general snow-on and snow-off trends were represented in snow-model simulations.

Stereo photogrammetry has been used for over a century to map terrain. As software has improved and high-resolution imagery has been available to process stereo satellite images, an emerging application of this mapping is the development of snow-depth maps (Nolan, Larsen, and Sturm 2015; Deschamps-Berger et al. 2020). At a minimum, this approach requires overlapping satellite-image collections of coincident snow-on and snow-off areas whereby elevations can be differenced (Figure A-16).

Stereo pairs were available for our Washington and North Dakota study sites. The Washington site was a larger area (360 km^2) that encompassed mountain topography and included shrubland and grasslands (Figure A-17). At this location, snow is redistributed by wind and deposited into drifts in ravines and swales. Analysis of stereo-pair imagery from 8 March 2017 produced a snow-depth map of this site that illustrated the snow-depth features evident in the aerial image (Figure A-18). Unfortunately, no field observations were available to make comparisons, and depths are

likely biased toward being too deep; but with some corrections and analysis with higher-resolution digital elevation models (e.g., derived from lidar), this effort's accuracy could be improved greatly.

Figure A-15. Snow model and imagery comparison for the Washington site. *Solid white line* outlines the YTC boundary.

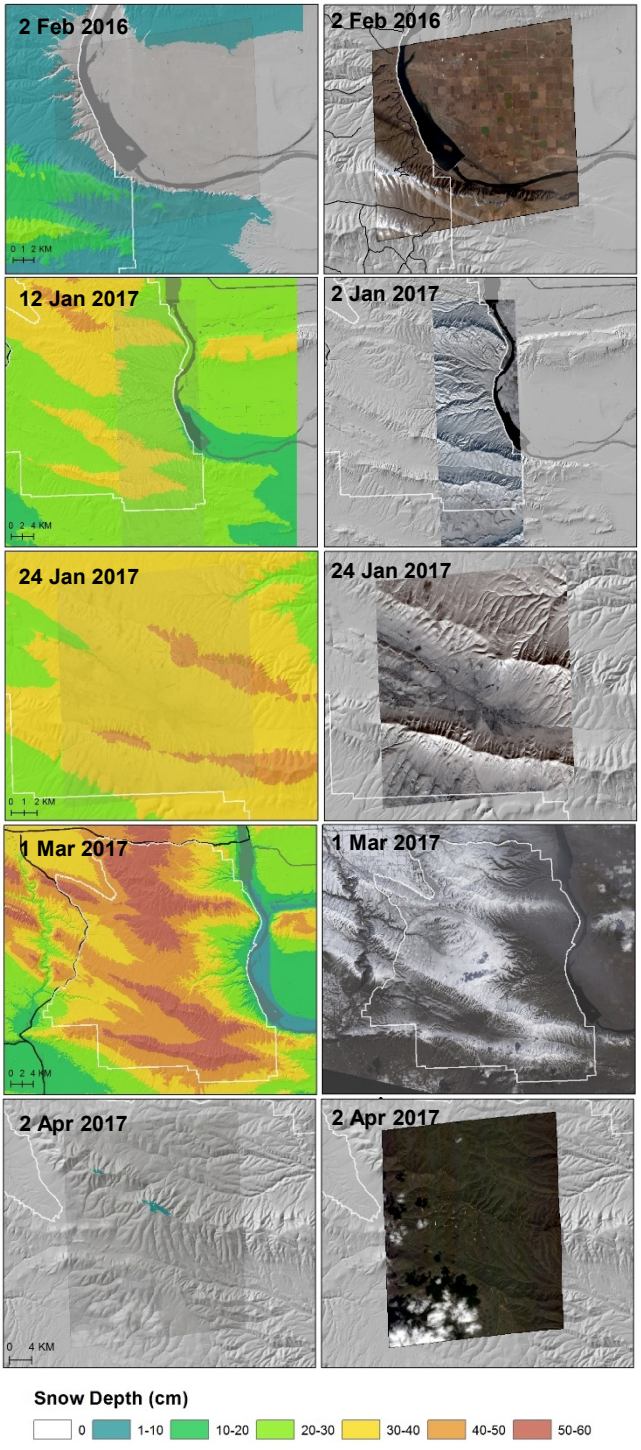

Figure A-16. Flow map of photogrammetry analysis.

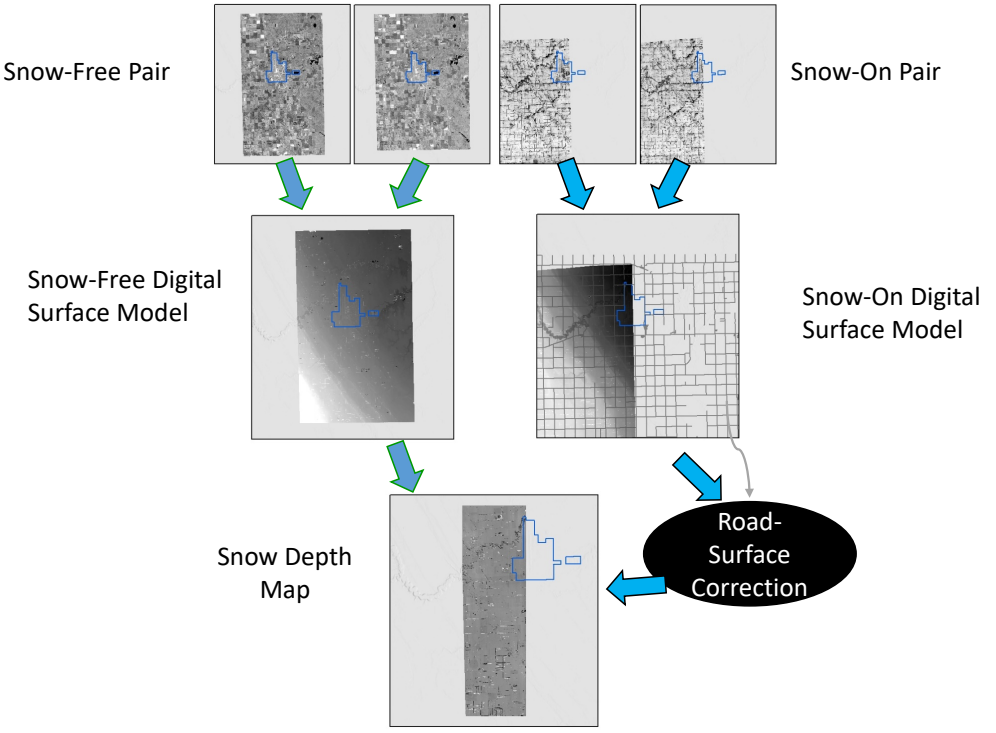

Figure A-17. Photogrammetry analysis area for the Washington domain. *Solid red line* outlines the YTC boundary.

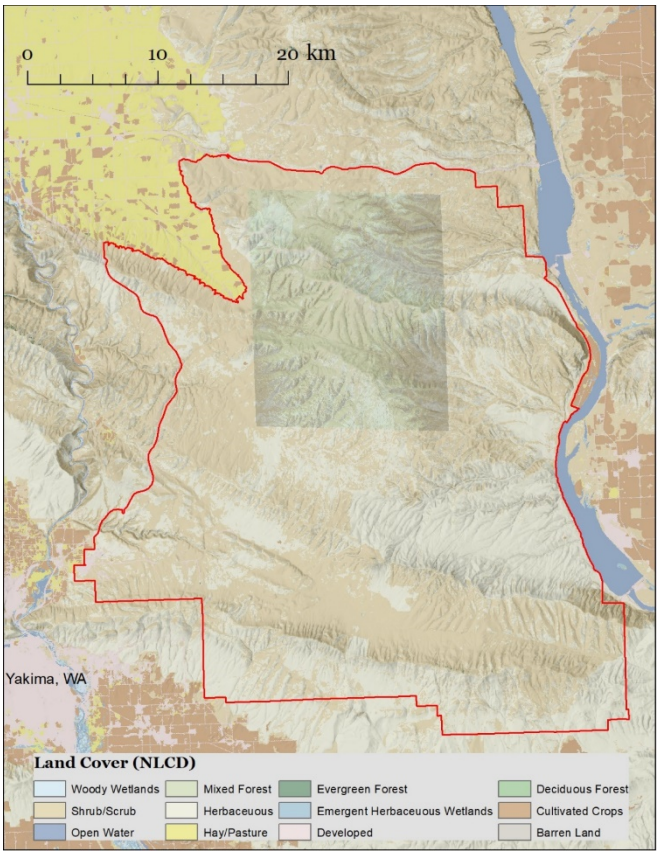

Figure A-18. Snow-depth map from the photogrammetry analysis, YTC, Washington.

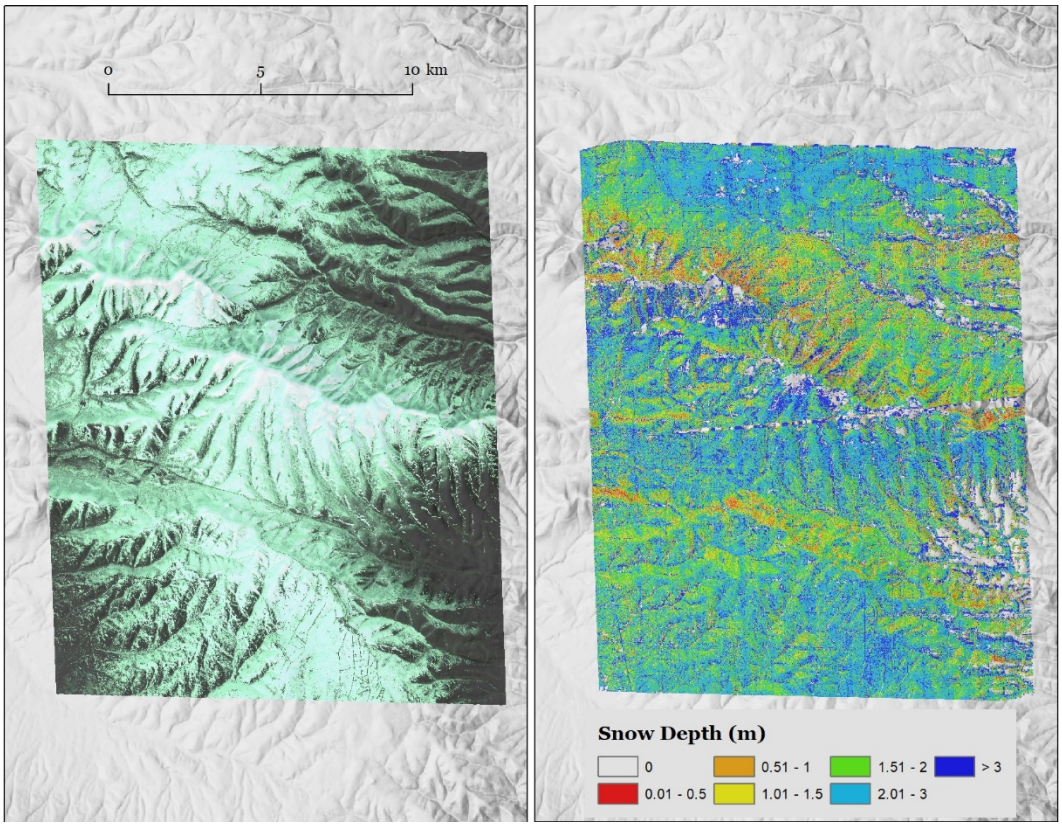

The analysis for the North Dakota site included GFAFB, and the total area was smaller than YTC (50 km² compared to 360 km²). This site is flat terrain that included agricultural and managed landscape (Figure A-19). This environment is typically windy, where snow is redistributed into drifts and on lee sides of shelterbelts, buildings, and obstacles. We produced snow-depth maps from this area in which landscape features such as runway snow piles and land cover shifts among crop types were identified (Figure A-20). The depths appear to be more realistic for the terrain compared with the YTC, Washington, effort, likely due to topography. Again, lidar-derived terrain information and additional stereo collections would likely improve this result.

This preliminary analysis shows promise in using this method for producing detailed snow-depth maps for these locations. Because no field data were collected or available for the dates analyzed, we could not perform a direct validation of snow depths, but results indicate that accuracy decreases with increased topographic relief and X, Y, and Z errors. To improve results, future research is needed to decrease errors from shadows and their impacts in the winter. Moreover, filtering changes in topography

(e.g., plant stature in croplands) from snow differences would increase accuracy in snow-depth estimation.

Figure A-19. Photogrammetry analysis site, North Dakota. *Solid blue line* outlines GFAFB.

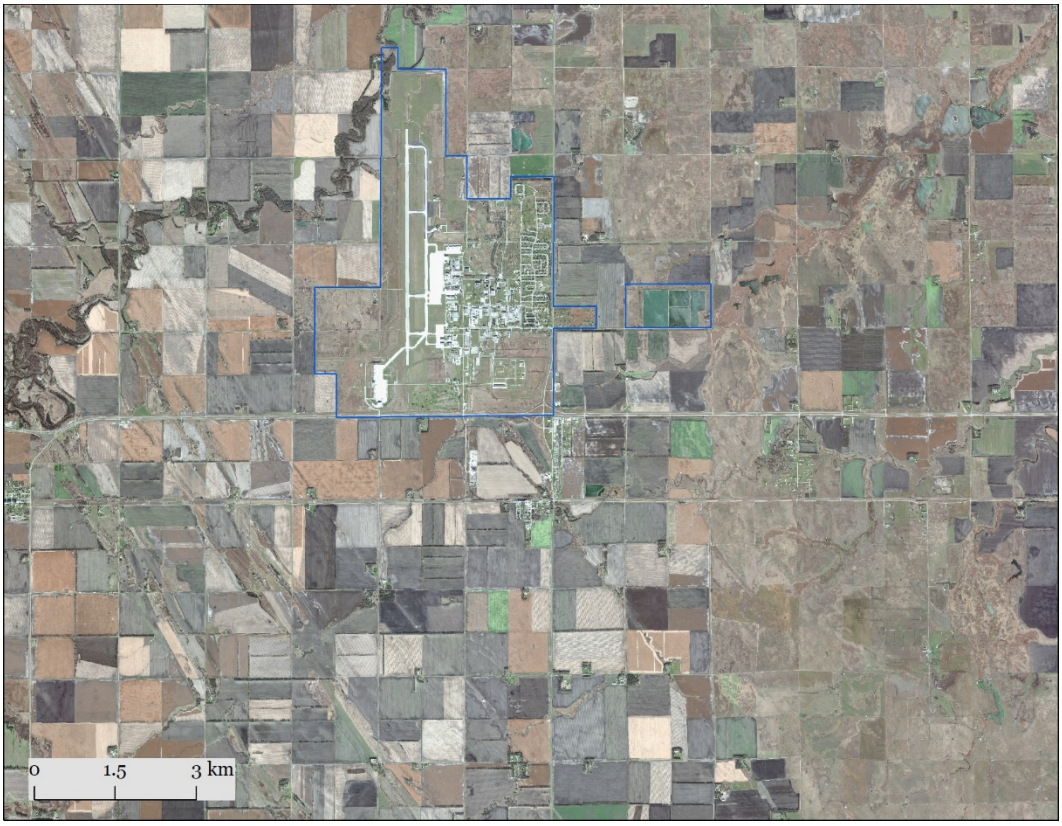

Figure A-20. Snow-depth maps from the photogrammetry analysis at the (*a*) western boundary of GFAFB and (*b*) airport at the GFAFB, North Dakota. *Blue line* outlines GFAFB, and the *purple box* is the zoomed figure to the right.

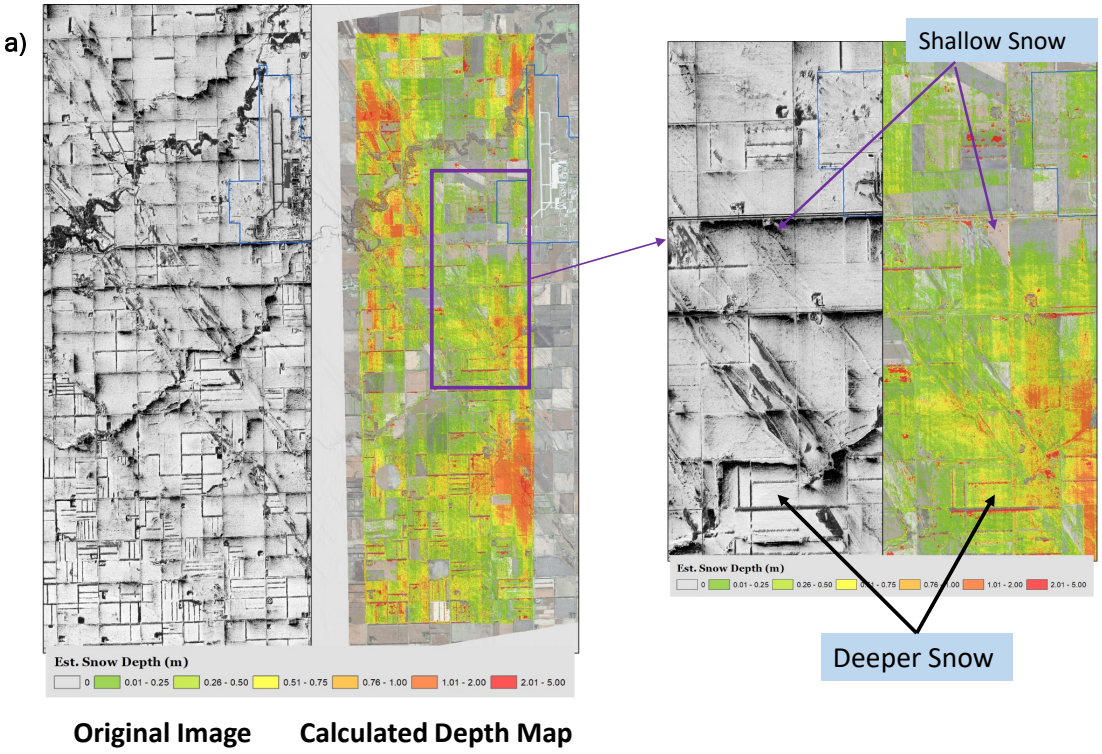

A.6 Summary of white paper *Interactions among Snow, Sagebrush, and Greater Sage-Grouse*

Snow, sagebrush, and sage-grouse are strongly intertwined, and future prospects for all three are dire. Over 60 million hectares of the contiguous United States is dominated by *Artemisia tridentata*'s six subspecies (Meyer 2008), which currently inhabit landscapes characterized by warm, dry summers and cold, snowy winters. Since sagebrush steppe occupies relatively low-elevation basins, temperatures are warming and the precipitation arriving as snow has declined (Brown and Mote 2009); this trend is expected to continue (Klos et al. 2014). Sagebrush rangelands, which were once expansive and uninterrupted, have been broken up, reduced, or otherwise altered, thanks to fires, drought, development, grazing, and winter-annual grass invasion (Miller et al. 2011). As a result, sage-grouse populations have also declined, and their range has been markedly reduced and isolated over the last 65 years (Connelly et al. 2000; Pyke et al. 2015). Sage-grouse are sagebrush obligates, requiring uninterrupted tracts of sagebrush for their habitat, nesting, and winter survival.

In arid sagebrush steppe, snow deposition is the primary mechanism for deep-soil water infiltration and storage (Bradford, Schlaepfer, and Lauenroth 2014; Knight et al. 2014). Summer storms may bring greater precipitation amounts, but they tend to be quickly used or lost from surface soils in the warm, dry environment. Since protruding canopies can also be warmed by solar radiation (Mahrt and Vickers 2005; Liston and Hiemstra 2011a) between storms, midwinter snowmelt adjacent to sagebrush creates local voids that can be filled by the next blowing-snow event (Robertson 1947); repeated cycles of this accumulation and melt sequence create local-scale soil moisture increases that are crucial to sagebrush habitat (Liston and Hiemstra 2011a). Snow is expected to play a smaller role in future shrubland winters, and whether increased winter rain will still yield deep water infiltration is unknown. Growing evidence points to an increasing proportion of precipitation arriving as rain instead of snow, potentially resulting in fewer voids filled with snow from blowing snow events. The implications of that impact on sagebrush landscapes need to be assessed. With less precipitation becoming mobile (i.e., less deposition from blowing snow), do areas that receive more windblown snow encounter drought stress more easily? Are drifts shrinking in this environment? How does a decline in snow and its redistribution by wind alter groundwater and impact vital steppe riparian areas?

Sagebrush steppe is an environment where snow sublimation is likely underestimated. From the standpoint of sublimation, how has sagebrush area loss, with its pronounced decline in stature, impacted water budgets in these water-limited ecosystems? Is sublimation increasing in sagebrush steppe?

Sagebrush steppe exists on a number of Department of Defense lands, and key remote-sensing and lidar datasets are available for many of those areas. These datasets would allow improved snow estimates in this landscape and would produce scientific dividends required to address potential changes in sagebrush steppe.

A.7 List of Scientific and Technical Publications

Hiemstra, C. A., G. E. Liston, and A. M. Wagner. 2017. "Snow Observations and Modeling in Prairie, High Plains, and Intermountain Landscapes." Poster presented at the SERDP/ESTCP Symposium, Washington, DC, 28–30 November 2017.

Hiemstra, C. A., A. M. Wagner, and G. E. Liston. 2017 "Interactions among Snow, Sagebrush, and Greater Sage-Grouse." White Paper submitted to SERDP on 15 May 2017. Hanover, NH: U.S. Army Engineer Research and Development Center, Cold Regions Research and Engineering Laboratory.

Schlef, K. E., K. E. Kunkel, C. Brown, Y. Demissie, D. P. Lettenmaier, A. M. Wagner, M. S. Wigmosta, T. R. Karl, D. R. Easterling, K. J. Wang, B. François, and E. Yan. In review. "Best Practices for Incorporating Non-Stationarity in Intensity-Duration-Frequency (IDF) Curves." *Journal of Water Resources Planning and Management*.

Wagner, A. M., K. Bennett, C. A. Hiemstra, G. E. Liston, and D. Cooley. In review. "Multiple Indicators of Extreme Changes in Snow Dominated Regimes, Yakima River Basin Region, USA." *Water*, special issue "Hydrological Extremes in a Warming Climate: Nonstationarity, Uncertainties, and Impacts."

Wagner, A. M., K. Bennett, C. A. Hiemstra, and G. E. Liston. 2018. "Changes in the Timing of Historical and Future Runoff in Different Snow Regimes." Poster presented at the AGU Fall Meeting, Washington, DC, 10–14 December 2018.

Wagner, A. M., K. Bennett, C. A. Hiemstra, and G. E. Liston. 2019. "Intensity and Variability of Runoff Events in Different Snow Environments." Poster presented at the SERDP/ESTCP Symposium, Washington, DC, 3–5 December 2019.

Wagner, A. M., K. E. Bennett, C. A. Hiemstra, and G. E. Liston. 2018. "Statistical Analyses of Historical and Future Runoff Focused on Military Installations Located in Three Different Snow Environments." Poster presented at the SERDP/ESTCP Symposium, Washington, DC, 28–30 November 2018.

REPORT DOCUMENTATION PAGE

Form Approved
OMB No. 0704-0188

1. REPORT DATE (DD-MM-YYYY)	2. REPORT TYPE	3. DATES COVERED (From - To)
July 2021	Final Report	FY16–FY20

4. TITLE AND SUBTITLE
Changes in Climate and Its Effect on Timing of Snowmelt and Intensity-Duration-Frequency Curves

5a. CONTRACT NUMBER

5b. GRANT NUMBER

5c. PROGRAM ELEMENT

6. AUTHOR(S)
Anna M. Wagner, Christopher A. Hiemstra, Glen E. Liston, Katrina E. Bennett, Dan S. Cooley, and Arthur B. Gelvin

5d. PROJECT NUMBER

5e. TASK NUMBER

5f. WORK UNIT NUMBER

7. PERFORMING ORGANIZATION NAME(S) AND ADDRESS(ES)
U.S. Army Engineer Research and Development Center (ERDC)
Cold Regions Research and Engineering Laboratory (CRREL)
4070 9th, Street
Fort Wainwright, AK 99703

8. PERFORMING ORGANIZATION REPORT NUMBER
ERDC/CRREL TR-21-8

9. SPONSORING / MONITORING AGENCY NAME(S) AND ADDRESS(ES)
Strategic Environmental Research and Development Program (SERDP)
4800 Mark Center Drive, Suite 17D03
Alexandria, VA 22350-3605

10. SPONSOR/MONITOR'S ACRONYM(S)
SERDP

11. SPONSOR/MONITOR'S REPORT NUMBER(S)

12. DISTRIBUTION / AVAILABILITY STATEMENT
Approved for public release; distribution is unlimited.

13. SUPPLEMENTARY NOTES
Funded under SERDP Resource Conservation (RC) and Resilience Project RC-2515, "Changes in Climate and its Effect on Timing of Snowmelt and Intensity-Duration-Frequency Curves," MIPR W74RDV60835264.

14. ABSTRACT
Snow is a critical water resource for much of the U.S. and failure to account for changes in climate could deleteriously impact military assets. In this study, we produced historical and future snow trends through modeling at three military sites (in Washington, Colorado, and North Dakota) and the Western U.S. For selected rivers, we performed seasonal trend analysis of discharge extremes. We calculated flood frequency curves and estimated the probability of occurrence of future annual maximum daily rainfall depths. Additionally, we generated intensity-duration-frequency curves (IDF) to find rainfall intensities at several return levels. Generally, our results showed a decreasing trend in historical and future snow duration, rain-on-snow events, and snowmelt runoff. This decreasing trend in snowpack could reduce water resources. A statistically significant increase in maximum streamflow for most rivers at the Washington and North Dakota sites occurred for several months of the year. In Colorado, only a few months indicated such an increase. Future IDF curves for Colorado and North Dakota indicated a slight increase in rainfall intensity whereas the Washington site had about a twofold increase. This increase in rainfall intensity could result in major flood events, demonstrating the importance of accounting for climate changes in infrastructure planning.

15. SUBJECT TERMS
Climatic changes, Flood forecasting, Infrastructure (Economics)--Planning, Rain and rainfall--Measurement, Rainfall intensity, Runoff, Snow, Stream measurements

16. SECURITY CLASSIFICATION OF:			17. LIMITATION OF ABSTRACT	18. NUMBER OF PAGES	19a. NAME OF RESPONSIBLE PERSON
a. REPORT	b. ABSTRACT	c. THIS PAGE			19b. TELEPHONE NUMBER (include area code)
Unclassified	Unclassified	Unclassified	SAR	147	